PATTERNING AND STABILIZING THE ZEBRAFISH PHARYNGEAL ARCH INTERMEDIATE DOMAIN

by

JARED COFFIN TALBOT

A DISSERTATION

Presented to the Department of Biology
and the Graduate School of the University of Oregon
in partial fulfillment of the requirements
for the degree of
Doctor of Philosophy

September 2011

DISSERTATION APPROVAL PAGE

Student: Jared Coffin Talbot

Title: Patterning and Stabilizing the Zebrafish Pharyngeal Arch Intermediate Domain

This dissertation has been accepted and approved in partial fulfillment of the requirements for the Doctor of Philosophy degree in the Department of Biology by:

Judith S. Eisen	Chairperson
Charles B. Kimmel	Advisor
John H. Postlethwait	Member
Chris Q. Doe	Member
Kennith E. Prehoda	Outside Member

and

Kimberly Andrews Espy	Vice President for Research & Innovation/Dean of the Graduate School

Original approval signatures are on file with the University of Oregon Graduate School.

Degree awarded September 2011

DISSERTATION ABSTRACT

Jared Coffin Talbot

Doctor of Philosophy

Department of Biology

September 2011

Title: Patterning and Stabilizing the Zebrafish Pharyngeal Arch Intermediate Domain

Approved: _____
Charles B. Kimmel

Improved understanding of pharyngeal arch (PA) patterning and morphogenesis can reveal critical insights into the origins of craniofacial diseases, such as Fraser syndrome. PAs contain mesenchymal condensations, which give rise to most of the facial skeleton in vertebrates. Studies of Endothelin1 signaling reveal that the skeleton derived from the first two PAs are patterned into dorsal, intermediate, and ventral domains. Previous work has indicated that endothelin targets, including the *Dlx* genes, homeotically pattern dorsal versus ventral PA identity. I show that the *Dlx* gene family plays a vital role in PA intermediate-domain identity establishment. In WT fish, the PA intermediate domain is delineated by combined expression of all *Dlx* genes. Reduction of *Dlx* gene function results in loss of intermediate-domain identity. Conversely, ventral expansion of *Dlx* expression, seen in *hand2* mutants, results in ventral expansion of intermediate-domain identity. Hence, PA intermediate-domain identity is defined by co-expression of *Dlx* genes.

Epithelial-mesenchymal interactions play an important part in PA intermediate-domain morphogenesis. Zebrafish *fras1* (epithelially expressed) and *itga8* (mesenchymally expressed) mutants also show specific defects within intermediate-

domain skeleton and epithelia. Facial phenotypes in *fras1;itga8* double mutants look extremely similar to either single mutant, suggesting that *fras1* and *itga8* might participate in the same epithelial-mesenchymal interaction during PA intermediate-domain formation. Our developmental studies reveal that *fras1*- and *itga8*-dependent epithelial segmentation of the PA intermediate domain stabilizes developing skeletal elements. Lesions in human *FRAS1* underlie many cases of Fraser syndrome, and this work provides an excellent developmental model for the craniofacial defects found in Fraser syndrome.

Loss of either *Dlx* or *fras1* function produces defects in the PA intermediate domain, yet seemingly during different developmental periods. Nonetheless, combined reduction of both *Dlx* and *fras1* function synergistically increases skeletal defects, implying a molecular connection between early (*Dlx*-mediated) pattern formation and later (*fras1*-mediated) pattern stabilization. Elucidation of the *Dlx-fras1* interaction is an interesting topic which may unveil new molecules pertinent to Fraser syndrome.

Supplemental movies highlighting skeletal and epithelial morphogenesis accompany this dissertation.

This dissertation includes both previously published/unpublished and co-authored material.

CURRICULUM VITAE

NAME OF AUTHOR: Jared Coffin Talbot

GRADUATE AND UNDERGRADUATE SCHOOLS ATTENDED:

University of Oregon, Eugene
Cornell University, Ithaca, New York

DEGREES AWARDED:

Doctor of Philosophy, Biology, 2011, University of Oregon
Bachelor of Science, Biology, 2004, Cornell University

AREAS OF SPECIAL INTEREST:

Developmental biology
Genetics
Zebrafish

PROFESSIONAL EXPERIENCE:

Undergraduate research, Henry Lab, 2000-2004

GRANTS, AWARDS, AND HONORS:

Developmental Training Grant, 2005-2009

Graduate Teaching Fellowship, Biology, 2004-2005

Baccalaureate Service Award, Cornell University, 2004

PUBLICATIONS:

Coffin Talbot, J., Johnson, S. L. and Kimmel, C. B. (2010). hand2 and Dlx genes specify dorsal, intermediate and ventral domains within zebrafish pharyngeal arches. *Development* 137, 2507-17.

Carney, T. J., Feitosa, N. M., Sonntag, C., Slanchev, K., Kluger, J., Kiyozumi, D., Gebauer, J. M., **Coffin Talbot, J**., Kimmel, C. B., Sekiguchi, K. et al. (2010). Genetic analysis of fin development in zebrafish identifies furin and hemicentin1 as potential novel fraser syndrome disease genes. *PLoS Genet* 6, e1000907.

MacDonald, R. B., Debiais-Thibaud, M., **Coffin Talbot, J.** and Ekker, M. (2010). The relationship between dlx and gad1 expression indicates highly conserved genetic pathways in the zebrafish forebrain. *Dev Dyn* 239, 2298-306.

Walker, M. B., Miller, C. T., **Coffin Talbot, J.**, Stock, D. W. and Kimmel, C. B. (2006). Zebrafish furin mutants reveal intricacies in regulating Endothelin1 signaling in craniofacial patterning. *Dev Biol* 295, 194-205.

ACKNOWLEDGMENTS

I greatly appreciate the hard work that Chuck has put in to this project. He has brought my critical thinking to new heights, and helped me to see both the forest through the trees, or the trees through the forest at different times. The whole Kimmel lab has provided invaluable input and training. Bill Cresko taught me statistical tools critical to completing this work. My committee has also been very supportive in this longer-than-expected process; I've appreciated your enthusiasm for my project. On key occaisions, Judith Eisen has been available to listen when I needed to talk; thank you. April Delaurier has been a constant source of help in this project's intellectual development, as well as preserving my sanity. Thanks go to Gage Crump, who mentored me as a first year, and has been a continued colleague. Macie Walker trained me in the ways of genetic mapping, and other fun fish techniques. Macie and Gage helped me to kick off the *Dlx* and *fras1* projects respectively. Thanks to Ryan Macdonald for getting me involved with Dlx brain patterning; also to Sarah Hutchinson, Judith Eisen, and Leisl Van Ryswyk for continuing to plug away on Lhx genes in motor neurons. These side-steps from my central project have been quite fun. Tom Carney and Matthias Hammerschmidt have been an extremely helpful to my graduate work. Their willingness to collaborate, rather than compete, pretty much saved the *fras1* project. John Paul Allee did a rotation project trying to find phenotypes in *dlx3b;4b*-MO injected fish, before we knew any better. Thanks to Linda Gai and Joseph Okray who dedicated many volunteer hours to the *fras1* project. My family, the Eugene's dance community, the Episcopal Campus Ministries in Eugene, and St. Mary Episcopal church; each community has provided invaluable spiritual support for this project. Thanks go in particular to my parents, who encouraged and supported the strange journey I have taken towards my doctorate. The U of O zebrafish facility, in particular John Dowd, and the U of O histology department were invaluable to conducting this research. This work was supported by NIH grants DE13834, HD22486, and DTG GM007257.

This thesis is dedicated to Mom and Dad
thank you for listening, as I tried to explain
thank you for surprising me with understanding.
However, I have never been surprised by your support-
which has been so consistent,
that you never left me wondering.

Also: to the fish.
You never knew it,
but I couldn't have done this without you.

TABLE OF CONTENTS

Chapter Page

Chapter Page

LIST OF FIGURES

Figure Page

LIST OF TABLES

CHAPTER I

GENERAL INTRODUCTION

Developmental genetic perspective on shape

How does an organism reproducibly obtain a characteristic shape? This question has been posed in many ways, for many centuries. In the past century, it has become apparent that an organism obtains its shape through interactions of genes and environment. As a developmental geneticist, I focus my work on how genetic architecture influences cell behaviors over time, to generate structures in an organism. Genes are units of heredity, encoded by DNA; they are transcribed into messenger molecules (RNA), which are often translated into proteins for functional output, though in other cases the RNA is itself the business end. Another answer is: 'An organism obtains its shape through complex interplay of cell division, death, and movement.' While accurate, both answers are broad, and don't provide insight into any particular piece of development. However, they flow into the next logical question: "Which genes, what environment, and why do these genes create shapes." In this study, I use several tools to discover where genes are expressed. "RNA in situ hybridization" shows where in an embryo RNA for a particular gene is turned on. Transgenic" fish in this study express a gene from another organism, which fluoresces (which is to say 'glow', when excited by a certain wavelength of light), in a pattern similar to a native gene of interest. Since zebrafish don't normally fluoresce very much, these "transgenes" allow us to easily visualize gene expression patterns in living fish. I visualize protein localization using antibodies. To understand what a gene does, I disrupt gene function, using two techniques. A mutation is a change in DNA sequence; the mutants used in this study break gene function. By observing what happens when I remove a gene's functionality, I can generate inferences about what that gene normally does. A phenotype is an observable output of a genetic change. If disruption of a gene's function causes a phenotype in a particular structure, then I infer that the gene normally does something to make that structure develop.

Morpholinos are, allegedly, an easy and cheap way to reduce a gene's functionality if a mutant is not available. Phenotypes can be both molecular and physiological. Throughout this paper, but especially in chapter II, I combine gene-knockdown with gene expression studies, to understand how one gene can change the activity of another. Throughout this paper, but especially in chapter III, I examine how loss of gene functions can alter the way cells physically interact. The next step is to integrate changes in cell and tissue behavior over time. A "time-course" analysis, as used in this study, examines a bunch of separate fish as they develop. There are three basic kinds of time-course analyses used in this study. Some of our techniques require the fish to be euthanized and fixed (preserved). In this case, we (1) examine many fish at different points in time and make inferences about how the population changes. However, the transgenes used in this paper allow me to look at morphology while the fish are still alive ("in vivo"), so I can (2) directly determine how skeletal shape in individual fish changes over time. To determine these changes at even higher resolution, I can leave a fish under a microscope, and image it relatively frequently, to (3) generate a "time-lapse" movie of development. These in vivo imaging techniques are particularly used in chapter III. By understanding how genes influence both other genes and tissue shapes, and how these influences are integrated over time, I can create a more precise understanding of how an organism generates a characteristic shape. This process is both much easier, and much more difficult than its sounds.

Phenotypic variation and developmental stability

To understand phenotypic variability, I look at phenotypes in many fish. When possible, I look at both sides of many fish, at multiple time points. To separate environmental and genetic variation from developmental instability, I need to examine variation in a system with as little environmental and phenotypic variation as possible. I do this by comparing morphologies of left and right sides of individual fish. An extensive literature posits that if (1) measurement is reliable, (2) antisymmetry isn't present, and (3) side bias isn't prominent, then left right asymmetry is a sign of developmental instability (Polak, 2003b). Both chapter II and chapter III investigate mutants and morpholino

knockdowns causing highly variable phenotypes. In chapter III this becomes a central part of my understanding of how those genes function.

It turns out that even in fish bearing a single mutation in certain genes, not every phenotype looks the same; by comparison WT ("not carrying the mutation") fish look relatively homogenous. There's a biological explanation for this called "canalization" or "Developmental Stability", which may be synonymous, depending on who you ask (Leamy and Klingenberg, 2005; Polak, 2003a). I dislike semantic arguments, so I will use canalization only for illustration; developmental stability will be used elsewhere. A developmental stabilizer is something that makes more development more stable. If the developmental stabilizer is lost, than inherent developmental instability is revealed. Canalization suggests that evolution has buffered development to precisely produce a WT shape in separate environmental and genetic contexts. If a WT shape is not produced, then buffering is lost, and more variation is seen. Or, to steal an example from Bill Cresko, "when the referee is absent, the kids make up their own rules." The word canalization draws to mind an illustration of what canalization means. A river flowing through a canal (WT: buffered) will vary less in its course than a river diverted onto a plain (mutant: unbuffered).

I think that the work in chapter III provides another nice illustration of canalization. Mutants I study in chapter III are required to shape a skin-like tissue called "endoderm" into a physical canal; a mold surrounding developing skeletal tissues. These mutants all have endoderm defects, but show a remarkable degree of skeletal variation. We infer that without the endodermal canal, the skeleton is more free to move during development, resulting in the variation found in the mutants.

Shaping the intermediate domain of facial skeleton

My dissertation research is focused on the study of skeletal shape, in part because of the obvious connection between shape and function in the skeleton. Zebrafish facial skeleton is a complex lever system; even small deformations in skeletal shape can produce a profound impact on the forces applied during feeding, hence many of the subtle shape defects we study can be thought to have clear functional consequences. Likely for this reason, skeletal shapes are reliably formed into precise shapes in healthy

zebrafish. Previous work e.g. (Kimmel et al., 1998; Miller et al., 2000; Walker et al., 2006; Yanagisawa et al., 2003) has indicated that pharyngeal arches are divided into three major "domains" along the dorsal-ventral axis: dorsal, intermediate, and ventral. Both the *Dlx* genes and *hand2* are patterning genes (Depew et al., 2002; Qiu et al., 1997; Yanagisawa et al., 2003) activated by *edn1* (Miller et al., 2000; Walker et al., 2006), making them logical candidates for intermediate domain patterning. In chapter II of this thesis, I show that *hand2* and *Dlx* help pattern the intermediate domain. *fras1* and *itga8*, the focus of chapter III, have not previously been implicated in the formation of skeletal shape in the intermediate domain.

The development of shape in craniofacial skeleton is of particular interest, because over half the people born with birth defects show craniofacial abnormalities (https://www.facebase.org). It is my hope that this work will lend insight into the causes of craniofacial birth defects, by improving understanding the genes underlying craniofacial shape. For example, Fraser syndrome is a genetic disorder causing many variable birth defects, including craniofacial birth defects (Fraser, 1962). In the third chapter III of this thesis, I investigate why zebrafish homozygous for *fras1* mutation (Fraser syndrome 1) show facial defects. I propose a model for *fras1* function in zebrafish, which I hope will provide insight into the craniofacial variation endemic in Fraser syndrome, and possibly Fraser syndrome symptoms in other tissues.

Using zebrafish to study facial shape

Three decades ago, George Streisinger published his first paper using zebrafish to study developmental genetics (Streisinger et al., 1981), right here at the university of Oregon. Over the past three decades, the field of zebrafish developmental genetics has blossomed around the globe; 701 labs have now produced well over 14000 papers involving zebrafish (as of 6/25/11; www.ZFIN.org). Develomental study using zebrafish has come so far that many scientists (myself included) no longer feel the need to justify zebrafish work during presentations: to us the advantages are completely obvious. However, for a general introduction to a broader audience, it's worth dwelling on the advantages of fish for a moment. This project focuses on the genetic and developmental basis of shape. How is it that cells gain identity over time, and rearrange themselves

through time? In brief: I do research in zebrafish, because this organism allows me to answer developmental/genetic questions with unrivaled four dimensional and cellular clarity.

Zebrafish have many biological properties that make them particularly suited for these developmental studies of facial shape. Many of these properties are described elsewhere e.g. (Westerfield, 1995). Zebrafish lay eggs (rather than developing in a uterus), of about the size of a pinhead, which grow into embryos only 5 millimeters long at the end of a week. This allows us to easily place zebrafish embryos under a microscope for imaging throughout the first week of life, and watch the process of development in action. Zebrafish have maternally deposited yolk, which can nourish the embryo for several days. However, very soon these fish need to eat on their own; so zebrafish need to develop a functional jaw to eat with in only a few days (making experiments go quickly). Zebrafish somatic (body) cells are separate from their yolk, which renders the body relatively transparent, allowing us to image deep into the embryo (past the axial midline) with cellular resolution for that entire first week. Furthermore, the first two pharyngeal arches in zebrafish (jaw-forming cell structures) only contain a few hundred cells early in development (Mark Sasaki, unpublished), allowing us to view the first two pharyngeal arches with cellular resolution. Zebrafish can be raised in enormous numbers, and each fish can lay many eggs per week, a property vital to almost every experiment in this thesis. For instance, the ability to raise many fish in a small space, each of which can lay many eggs, has allowed us to perform large genetic screens. In genetic screens, we mutate fish and look for interesting phenotypes (a physical sign of a genetic defect). These screens allowed previous investigators (Yelon et al., 2000) to discover the *hand2* mutants discussed in chapter II and, during screens I participated in, the *fras1* and *itga8* mutants discussed in chapter III. Forward genetic screens allow researchers to identify unexpected genes that cause a given phenotype. For instance, it is unlikely that we would have intentionally created *fras1* or *itga8* mutants to study cartilage pattern, since neither gene is expressed in cartilages, and there isn't a strong precedent for either gene in skeletal patterning (see chapter III). Thus, the forward genetic approach facilitated truly novel conclusions about the function of two important genes.

In addition to these physical properties of zebrafish development, the fact that so many labs focus their research on zebrafish is itself an advantage. The shared efforts of many labs produces many reagents, both physical and intellectual, for the study of zebrafish. For instance, none of the morpholinos or probes used in chapter II of this thesis were designed in our lab; they are the output of previous research. As a second example, collaboration with an independent research group allowed us to learn the genetic identity of *fras1* mutants before our own cloning was completed. There are many more reasons that people study fish; however these factors have been particularly pertinent to my dissertation work. It would have been exceedingly difficult, at best, to do these experiments using any other developmental system.

Acknowledgement of co-authorship

Chapter II of this dissertation contains published material, co-authored with Stephen L. Johnson and Charles B. Kimmel. Chapter III of this dissertation contains unpublished material, of which I will share authorship with Macie B. Walker, Thomas J. Carney, Matthias Hammmerschmidt, Yi-Lin Yan, Ruth A. Bremiller, and Charles B. Kimmel.

CHAPTER II

hand2 AND *Dlx* GENES SPECIFY DORSAL, INTERMEDIATE, AND VENTRAL DOMAINS WITHIN ZEBRAFISH PHARYNGEAL ARCHES

The work described in this chapter has been previously published in volume 137 of the the journal *Development* in June 2010. Stephen L. Johnson's lab contributed the *trps1:GFP* transgenic, and commentary on drafts of the paper. Charles B. Kimmel contributed to writing, and was the principal investigator for this work.

Chapter summary

The ventrally expressed secreted polypeptide Endothelin1 (Edn1) patterns the skeleton derived from the first two pharyngeal arches into dorsal, intermediate, and ventral domains. Edn1 activates expression of many genes, including *hand2* and *Dlx* genes. We ask how *hand2*/*Dlx* might generate distinct domain identities. Here we show that differential expression of *hand2* and *Dlx* delineates domain boundaries before and during cartilage morphogenesis. Knockdown of the broadly expressed genes *dlx1a* and *dlx2a* results in both dorsal and intermediate defects, whereas knockdown of the intermediate-domain restricted genes *dlx3b*, *dlx4b*, with *dlx5a* results in intermediate-domain-specific defects. The ventrally expressed gene *hand2* patterns ventral identity, in part by repressing *dlx3b/4b/5a*. The jaw joint is an intermediate-domain structure, which expresses *nkx3.2*, and a more general joint marker, *trps1*. The jaw joint expression of *trps1* and *nkx3.2* requires *dlx3b/4b/5a* function, and expands in *hand2* mutants. Both *hand2* and *dlx3b/4b/5a* repress dorsal patterning markers. Collectively our work indicates that the expression and function of *hand2* and *Dlx* genes specify major patterning domains along the dorsal-ventral axis of zebrafish pharyngeal arches.

Introduction to *hand2/Dlx*

Specification of pharyngeal arch-derived facial skeleton by transcription factor-encoding genes is a topic of considerable recent interest. Pharyngeal arches are comprised of neural crest derived mesenchymal cells, with mesodermal derived cores, surrounded medially by endoderm, and laterally by ectoderm. Edn1 is a secreted protein important for dorsal-ventral jaw patterning: in mouse, mutations in *Edn1* and its receptor *EdnrA* cause homeotic transformations of lower jaw skeleton into upper jaw skeleton (Ozeki et al., 2004; Ruest et al., 2004). Studies of Edn1 signaling in zebrafish (*Danio rerio*) indicate that early pharyngeal arch patterning results in discrete dorsal, intermediate, and ventral domains (D-I-V) in pharyngeal arch mesenchyme and pharyngeal-arch-derived skeleton (Kimmel et al., 1998; Miller and Kimmel, 2001; Miller et al., 2000; Miller et al., 2003; Walker et al., 2006). Edn1 is known to activate expression of many genes proposed to mediate D-I-V patterning, including *hand2*, *gsc*, *nkx3.2* (formerly *bapx1*), and the *Dlx* genes (Miller et al., 2000; Miller et al., 2007; Walker et al., 2006). However, the boundaries of early D-I-V patterning genes had not yet been examined at later timepoints when the D-I-V skeletal regions are visible. In this study we propose a unified definition of D-I-V domains, and examine interactions between genes that pattern these domains. We place a particular focus on the patterning of intermediate-domain joints, and jointed skeleton. In this study, "joint" refers specifically to mesenchyme connecting early larval skeletal elements, whereas "joint region" includes both this joint mesenchyme, and connected skeleton. We refer to the joint between Meckel's and palatoquadrate cartilages as the "jaw joint" of larval zebrafish.

Dlx genes are homeodomain containing transcription factors, homologs of the single *Distal-less* gene in Drosophila (reviewed in (Panganiban and Rubenstein, 2002). Mammalian *Dlx* genes are found in three bi-gene clusters (Qiu et al., 1997). Zebrafish also have three *Dlx* bi-gene clusters, containing *dlx1a* and *dlx2a*, *dlx3b* and *dlx4b*, *dlx5a* and *dlx6a,* as well as two additional *Dlx* genes, *dlx2b* and *dlx4a* (Stock et al., 1996). The two genes in each *Dlx* bi-gene cluster are approximately co-expressed (Ellies et al., 1997; Qiu et al., 1997), likely due to shared enhancers (Ghanem et al., 2003; Park et al., 2004; Sumiyama et al., 2003). In mouse and zebrafish, functional redundancy is present both

within and between these bi-gene pairs (Depew et al., 2005; Jeong et al., 2008; Qiu et al., 1997; Sperber et al., 2008; Walker et al., 2006). Within mouse pharyngeal arches, *Dlx1* and *Dlx2* (collectively referred to as *Dlx1/2*) expression extends further dorsally than *Dlx5/6*, which themselves show expression further dorsal than *Dlx3/4* (Depew et al., 2002; Qiu et al., 1997). *Dlx1*$^{-}$*;Dlx2*$^{-}$ mice primarily show dorsal skeletal defects (Qiu et al., 1997), and loss of dorsal specific molecular markers (Jeong et al., 2008). Conversely, *Dlx5*$^{-}$*;Dlx6*$^{-}$ mice show homeotic transformations of lower jaw into upper jaw, corresponding to the exclusion of *Dlx5/6* expression from dorsal arch regions (Beverdam et al., 2002; Depew et al., 2002). The skeletal homeosis of *Dlx5*/6 loss is mirrored by a ventral expansion of dorsal molecular markers, while several ventral markers (including *Hand2*) are lost.

Hand2 encodes a basic-helix-loop-helix protein critical for ventral facial pattern. Mice carrying a deletion in the pharyngeal arch specific promoter of *Hand2* have dramatically shortened lower jaws, but relatively normal patterning in joint regions and the upper jaw (Yanagisawa et al., 2003). When *Hand2* is ectopically expressed throughout pharyngeal arches the upper jaw was partially transformed into an ectopic lower jaw (Sato et al., 2008). Thus in mouse, the Edn1 targets *hand2* and *Dlx* are directly implicated as homeotic selector genes along the pharyngeal arch dorsal-ventral axis.

In zebrafish, *dlx3b* and *dlx5a* are redundantly required for patterning specifically within intermediate domain-derived skeleton (Walker et al., 2006). In contrast, zebrafish *hand2* nulls exhibit loss of lower jaws, but not upper jaws (Miller et al., 2003). *Hand2* is expressed ventral to *nkx3.2,* a marker of the jaw joint region (Miller et al., 2003). In zebrafish *hand2* mutants, *nkx3.2* expands ventrally, indicating that *hand2* patterns lower jaw identity in part by repressing jaw joint identity (Miller et al., 2003). However, it was unclear whether *hand2* represses intermediate domain identity, because *hand2* mutants consistently lose jointed-jaw-skeleton (Miller et al., 2003).

Fate mapping experiments have indicated approximately where skeletal patterning domains arise within early pharyngeal arches (Crump et al., 2006; Crump et al., 2004b; Eberhart et al., 2006). However, these fate maps lacked the precision to directly connect early gene expression patterns to later skeletal shapes. Here, we present expression patterns that allow us to precisely define the dorsal, intermediate, and ventral domains

within zebrafish pharyngeal arches. We propose that the ventral domain is comprised of the *hand2* expressing pharyngeal arch region, and the skeletal elements that are formed in this region. The ventral domain contains most of Meckel's and ceratohyal cartilages, and the dentary bone**.** The intermediate domain is the portion of pharyngeal arches that expresses all *Dlx* genes, besides *dlx2b* (which isn't expressed in anterior arches). Expression of the most restricted *Dlx* gene, *dlx4a,* reveals the intermediate domain's borders. The intermediate domain includes the jaw joint region, and the second arch joint region, as well as the opercle and branchiostegal bones. Arch mesenchymal expression of *dlx3b* and *dlx4b* is also restricted to the intermediate domain. The dorsal domain is the portion of the pharyngeal arch dorsal to *dlx4a* expression. Because *dlx2a* is expressed throughout the arch dorsal ventral axis, co-labeling of *dlx2a* and *dlx4a* reveals the dorsal domain. The dorsal domain contains most of the palatoquadrate cartilage, including the distinctive pterygoid process, the hyomandibular cartilage, and the maxillary bone. *dlx5a* and *dlx6a* expression does not correspond to a single domain.

In addition to defining D-I-V domains, this report examines the functional requirements for D-I-V patterning. We show that along with *dlx3b* and *dlx5a*, *dlx4b* is also redundantly required for intermediate domain skeleton. We report a transgenic revealing the expression pattern of *trps1*, a general marker of skeletal joint identity. We show that *nkx3.2* and *trps1* require *dlx3b/4b/5a* function for normal expression. We examine regulation between domains, noting that *hand2* inhibits ventral expression of *dlx3b, dlx4a, dlx4b,* and *dlx5a*. In *hand2* mutants, *nkx3.2* and *trps1* expand to fill ventral space beneath expanded intermediate domain skeleton. However, even in *hand2* mutants, expression of *trps1* and *nkx3.2* still requires *dlx3b/4b/5a* function. Despite differences in patterning ventral versus intermediate domains, we provide evidence that *hand2* and *dlx3b/4b/5a* act in concert to repress dorsal domain identity.

Materials and methods

Fish maintenance, husbandry, and strains

Fish were raised and maintained under standard conditions, and staged as described previously (Kimmel et al., 1995; Westerfield, 1995). Mutant lines were

maintained on the AB background, and morpholinos were injected into AB fish. *Df(Chr1)hand2*^{S6} (a null allele, hereafter: *hand2*^{S6}) and *Is(Chr1)hand2*^{C99} (A hypomorphic allele, hereafter: *hand2*^{C99}) homozygotes were identified using previously described fully penetrant phenotypes, including dramatic heart defects (Miller et al., 2003; Yelon et al., 2000). *Edn1* mutants were identified as previously described (Miller et al., 2000).

Trps1^{j1271aGt} (at most a hypomorphic allele) and *dlx5a*^{j1073Et} (a likely hypomorph, based on comparison with morpholinos) were generated using the *Tol2* transposon T2KSAG, which contains enhancerless *eGFP* (Kawakami et al., 2004), during a screen for vital markers with specific expression patterns. *Trps1*^{j1271aGt} and *dlx5a*^{j1073aEt} stocks have been submitted to ZIRC. Following identification, carriers were out-crossed to AB background fish for several generations. Tail-PCR (Parinov et al., 1999) was used to identify genomic flanking regions, revealing that the J1271a insertion is at chr19: 43671269, inside the first intron of *trps1*, and the J1073a insertion site is chr19: 40245837, inside the first exon of *dlx5a*. PCR primers in the transposon sequence and the flanking genomic DNA sequence were then designed and tested on over 100 embryos segregating the expression pattern to show that we had correctly identified the insertion generating the expression pattern (primer sequences available upon request).

Tissue labeling

Alcian blue and Alizarin red staining was as described (Walker and Kimmel, 2007). For vital bone staining, fish were treated overnight with .000033% Alizarin red in embryo medium, followed by de-staining in embryo medium. Fluorescent RNA in situ hybridization was carried out with a protocol modified from those described previously (Jowett and Yan, 1996; Welten et al., 2006). DNP labeled probes were revealed with tyr-Cy5, dig labeled probes were revealed using tyr-Cy3, fluorescein labeled probes were revealed with tyr-fluorescein (available from Perkin-Elmer). Our full RNA in situ protocol is available online (http://wiki.zfin.org/display/prot/Triple+Fluorescent+In+Situ). Probes used are *dlx2a* (Akimenko et al., 1994), *dlx3b* (Akimenko et al., 1994), *dlx5a* (Walker et al., 2006), *dlx6a* (Walker et al., 2006), *gsc* (Schulte-Merker et al., 1994), *dlx4a* (Ellies et al., 1997),

dlx4b (Ellies et al., 1997), *hand2* (Angelo et al., 2000), *nkx3.2* (Miller et al., 2003), *sox9a* (Yan et al., 2002), *eng2* (Ekker et al., 1992).

Antibody labeling was essentially as described (Nusslein-Volhard, 2002). For RNA in situ experiments and antibody staining experiments, embryos were raised in 0.0015% PTU (1-phenyl 2-thiourea) to inhibit melanogenesis (Westerfield, 1995). Confocal imaging was performed on a Zeiss LSM5 Pascal microscope, followed by image processing with Volocity software. Colors are digitally enhanced to increase visibility.

Morpholino oligo injection

Morpholinos are injected at 2-3nl into one to two cell staged embryos. Translation blocking morpholinos to *dlx1a* (Sperber et al., 2008), *dlx2a* (Sperber et al., 2008), *dlx3b* (Liu et al., 2003), and *dlx5a* (Walker et al., 2007), as well as a splice blocking morpholino to *dlx4b* (Kaji and Artinger, 2004) were purchased from Gene Tools using previously described sequences. *Dlx1a*-MO and *dlx2a*-MO were previously shown to be specific and effective through RNA rescue, and knockdown of transgenic *dlx1a-GFP* and *dlx2a-GFP* expression (Sperber et al., 2008). We confirm that *dlx3b*-MO strongly reduces Dlx3b immuno-labeling (data not shown, and(Liu et al., 2003). We also confirm that *dlx4b*-MO strongly disrupts *dlx4b* transcripts (Kaji and Artinger, 2004), without affecting any other *Dlx* gene (data not shown). Furthermore, in support of previous work (Liu et al., 2003), co-injection of *dlx3b*-MO with *dlx4b*-MO phenocopies otolith losses seen in a deletion that contains *dlx3b* and *dlx4b* (data not shown). In addition to the *dlx5a* translation blocking morpholino, we tested a splice blocking morpholino to *dlx5a* (*dlx5aE2I2*-MO: 5'- TATTCCAGGAAATTGTGCGAACCTG -3'). This morpholino had only nominal effects on splicing, and produced a different phenotypic suite than either the *dlx5a* translation blocking morpholino, or the *dlx5a* mutant. As a result, *dlx5aE2I2*-MO was not used in any further analysis.

Results

dlx3b, *dlx4b*, and *dlx5a* redundantly pattern intermediate domain skeletal identity

Co-injection of *dlx3b*-MO and *dlx5a*-MO causes intermediate-domain specific defects without affecting dorsal or ventral structures (supporting (Walker et al., 2006). Because *dlx4b* is in the same bi-gene cluster as *dlx3b* (Ellies et al., 1997), we hypothesized that *dlx4b* also functions in intermediate domain patterning. Injection of *dlx4b*-MO, and co-injection of *dlx3b*-MO with *dlx4b*-MO fails to cause striking phenotypes (Fig. 1C,G). However, co-injection of *dlx4b*-MO with *dlx5a*-MO causes low penetrance intermediate defects (Fig. 1G). Furthermore, fish co-injected with *dlx3b*-MO;*dlx4b*-MO;*dlx5a*-MO (henceforth called *dlx3b;4b;5a*-MO), show defects throughout the intermediate domain at high penetrance (Fig. 1E, G). This synergism indicates that *dlx3b*, *dlx4b*, and *dlx5a* function partially redundantly in facial patterning. *dlx5a*^{J1271aEt} homozygotes co-injected with *dlx3b*-MO and *dlx4b*-MO fish showed defects specifically within the intermediate domain (data not shown), similar to *dlx3b;4b;5a*-MO fish. In contrast, the most frequent defect in uninjected *dlx5a*^{J1271aEt} homozygotes is a low penetrant shortened symplectic phenotype, similar to *dlx5a*-MO treatment (Fig 1D and data not shown). Hence, with both a morpholino and a mutant, we confirm that *dlx5a* acts largely redundantly with *dlx3b* and *dlx4b* to pattern the intermediate domain.

dlx1a and *dlx2a* redundantly pattern intermediate and dorsal skeletal domains

In mouse, *Dlx1/2* have patterning requirements dorsal to *Dlx5/6* (Depew et al., 2002; Qiu et al., 1997). To test whether zebrafish *dlx1a*/*2a* has patterning requirements dorsal to *dlx3b/4b/5a*, we injected *dlx1a*-MO and *dlx2a*-MO together and separately. When injected alone, *dlx1a*-MO and *dlx2a*-MO cause little skeletal deformity (data not shown). In support of previous work (Sperber et al., 2008), *dlx1a*-MO;*dlx2a*-MO co-injection results in low penetrance intermediate domain defects (Fig. 1F). In addition, *dlx1a*-MO;*dlx2a*-MO treated fish often showed defects within the dorsal domain cartilages (palatoquadrate and hyomandibular cartilage) (Fig. 1F), indicating that the dorsal requirements of *dlx1a* and *dlx2a* are conserved.

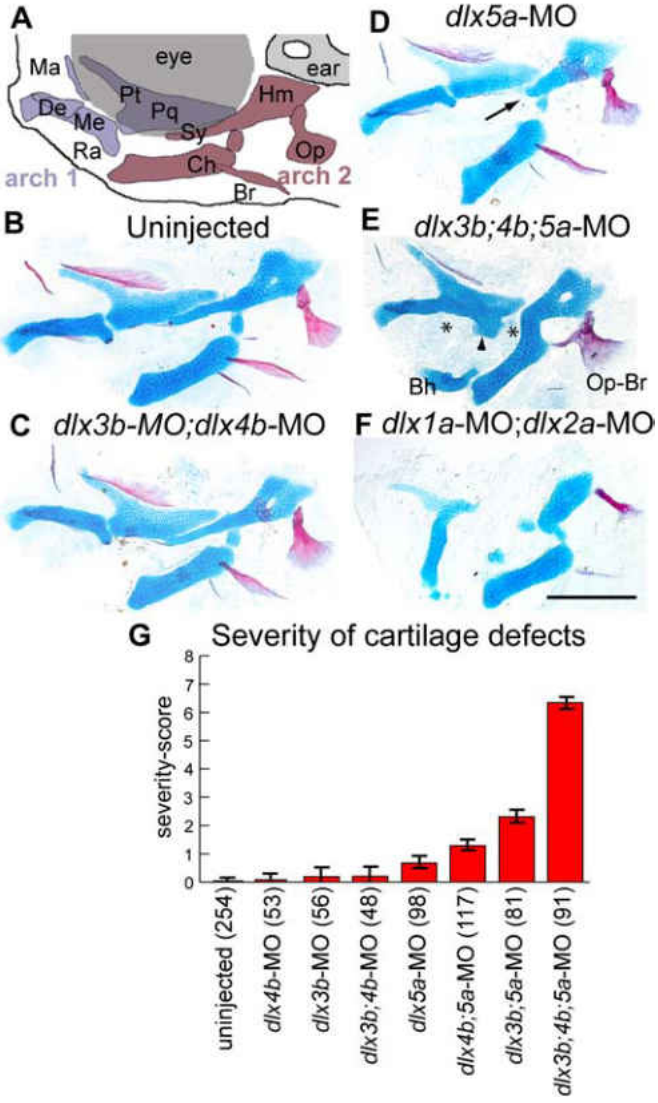

Figure 1: *Dlx* function is required in intermediate domain skeleton. (A) Schematic of facial skeleton. Anterior is to the left, dorsal is up. (B-F) Alcian blue (cartilage) and Alizarin red (bone) stained pharyngeal skeletons with *Dlx* morpholino treatments at 6 dpf. (B) Uninjected, (C), *dlx3b*-MO;*dlx4b*-MO, and (D) *dlx5a*-MO fish look very similar, though *dlx5a*-MO sometimes causes shortened symplectic cartilages (arrow). (E) Injection of *dlx3b;4b;5a*-MO frequently causes dramatic skeletal defects, including joint loss (asterisks), fusion of OP and BSR bones (Op-Br), and ectopic processes attached to the palatoquadrate (arrowhead), or ventrally in the face. (F) In contrast, *dlx1a*-MO;*dlx2a*-MO injection causes defects in both dorsal and intermediate cartilages. (G) Plot of severity-scores, showing that *dlx3b*-MO, *dlx4b*-MO, and *dlx5a*-MO interact to create more than additive changes in intermediate domain skeletal phenotypes. Error bars are 95% confidence intervals, determined by ANOVA. Fish were scored bilaterally for prominent cartilage defects: first arch joint fusions, second arch joint fusions, symplectic defects, palatoquadrate defects, and ectopic cartilages. Although each phenotype was seen at a range of expressivity, we assigned any defect a score of "1", irrespective of expressivity. The "severity-score" is the sum of these defects for both sides of the fish. Skeletal elements indicated in (A) are the first arch derived Meckel's cartilage (Me) including its retroarticular process (Ra), palatoquadrate (Pq) cartilage, and its pterygoid process (Pt) as well as maxillary (Ma) and dentary (De) bones. The second arch gives rise to the ceratohyal cartilage (Ch), the hyosymplectic cartilage, comprised of distinctive hyomandibular (Hm) and symplectic (Sy) regions, as well as opercle (Op) and branchiostegal (Br) bones. A remnant of the basihyal cartilage (Bh) remains attached to the Ch in (E), as a mounting artifact. Scale bar (F): 100 µm.

hand2 and *Dlx* delineate presumptive D-I-V domains

Several models have been proposed in which Dlx genes function combinatorially to impart dorsal-ventral skeletal identities (*e.g.* (Depew et al., 2005; Walker et al., 2006). To properly understand *Dlx* combinatorial patterning, we must understand how the *Dlx* gene's expression domains fit together, which we can directly assay using multi-color fluorescent RNA in situ hybridization. *Dlx2a* is expressed throughout the dorsal-ventral axis of pharyngeal arches, excluding mesodermal cores (Kimmel et al., 2001). At 36 hours post fertilization (hpf), *dlx4a* expression is intermediate along the dorsal-ventral axis of zebrafish pharyngeal arches, and expression is not seen in dorsal or ventral arch regions (Fig. 2F,K), as revealed by labeling *dlx4a* expression alongside *dlx2a*. *edn1* and *hand2* expression is ventral to *dlx4a* at 36 hpf (Fig. 2I,N). Thus we can delineate the 36 hpf ventral domain by *hand2* expression, intermediate domain by *dlx4a* expression, and dorsal domain by the expression of *dlx2a* dorsal to *dlx4a* (Fig. 2F). Similarly, at 36 hpf, *dlx3b* and *dlx4b* show intermediate specific expression, coincident with *dlx4a* boundaries within arch mesenchyme (Fig. 2C,H,M), though *dlx3b* also shows prominent epithelial expression (arrowheads in Fig. 2M). Other *Dlx* genes show broader expression than *dlx3b, dlx4b,* and *dlx4a* at 36 hpf (Fig. 2). The dorsal limit of *dlx5a* expression lies between the dorsal limits of *dlx4a* and *dlx2a* expression (Fig. 2G). In arch 1, *dlx5a* expression extends ventral to *dlx4a* expression (Fig. 2G), and is co-expressed with *hand2* (data not shown), indicating that *dlx5a* is expressed in the first arch ventral domain. However in the second arch, *dlx5a* expression shares a ventral boundary with *dlx4a* and is restricted from the ventral *hand2* expressing region (Fig. 2G and data not shown). Matching the in situ analysis, Dlx3b protein is nested both dorsally and ventrally within the *dlx5a*^{j1073aEt} expressing domain (Fig. 3). *Dlx5a* and *dlx6a* are largely co-expressed (Fig. 2B,G), though *dlx6a* has weaker expression intensity. Similar to *dlx2a*, the expression of *dlx1a* is seen broadly within pharyngeal arch mesenchyme, though with faint intensity (data not shown). *Dlx2b* expression is not detected in the first two arches (Stock et al., 2006) and data not shown). These results reveal a complex expression pattern by 36 hpf, with the expression of *hand2* ventral to *dlx3b/4a/4b,* which is nested within *dlx5a/6a,* which themselves are nested within *dlx1a/2a* boundaries (Fig. 2K-O).

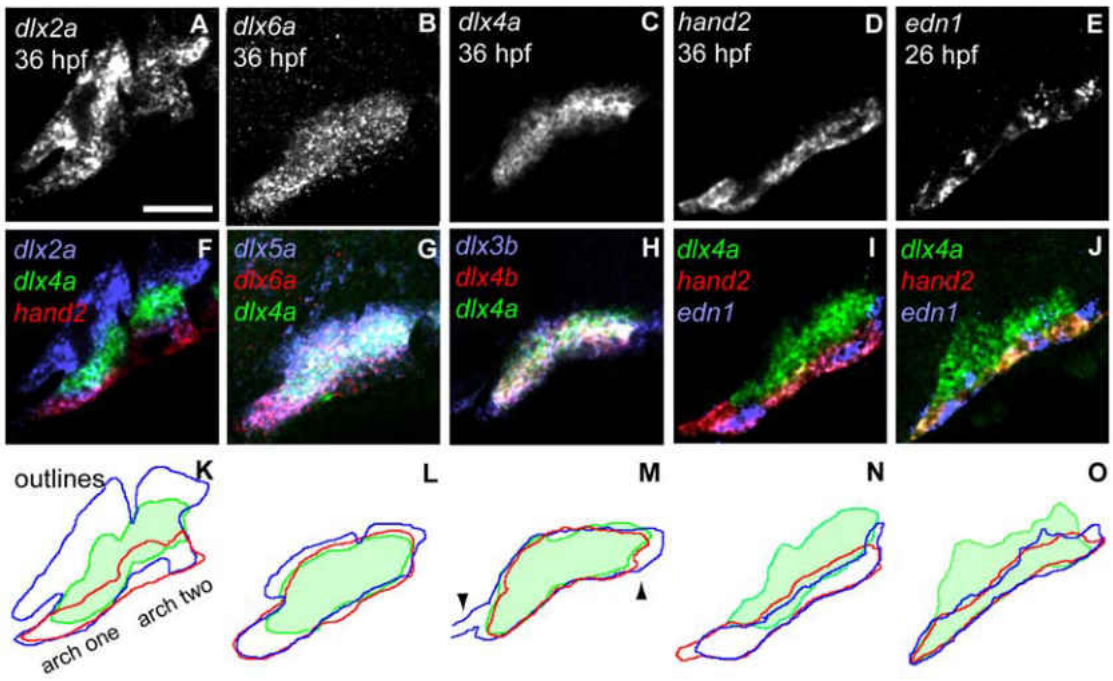

Figure 2: Early patterning domains are revealed by *Dlx*, *hand2*, and *edn1* expression. Images are single confocal sections, anterior to left, dorsal up. The images in (A-E) are single channels from the confocal images in (F-J). Outlines (K-O) of individual expression channels from (F-J) illustrate relative gene expression boundaries. (M) Arrowheads indicate *dlx3b* expression in the (left) stomodeum and (right) second endodermal pouch. Scale bar (A): 50 μm.

<u>*hand2* represses ventral expression of several *Dlx* genes</u>

Although the expression of *dlx4a* is intermediate-specific at 36 hpf (Fig. 2I), the earliest *dlx4a* expression is found in both ventral and intermediate arches (Fig. 2J). This observation of ventral *dlx4a* loss between 26 hpf and 36 hpf in WT fish, combined with the previous observation that *hand2* represses *dlx3b* (Miller et al., 2003), suggested that *hand2* ventrally represses *Dlx* expression. Indeed, the expression of *dlx3b*, *dlx4b*, and *dlx5a* expands ventrally in *hand2*^{s6} mutants at 36 hpf (Fig. 4). In WT fish, first arch expression of *dlx5a* extends more ventrally than *dlx3b* and *dlx4b*, whereas in *hand2*^{s6} mutant fish the three genes share a ventral expression border (Fig. 4C,D). Antibody staining for Dlx3b also expands ventrally in *hand2*^{s6} (data not shown). Furthermore, in *hand2*^{s6} fish, the expression of *dlx4a* expands, and fills the mesenchyme around *edn1*-expressing ventral mesodermal cores and ectoderm at 36 hpf (Fig. 4E,F). These results indicate that in WT, *hand2* inhibits the transcription of intermediate-domain-*Dlx* genes from the ventral domain.

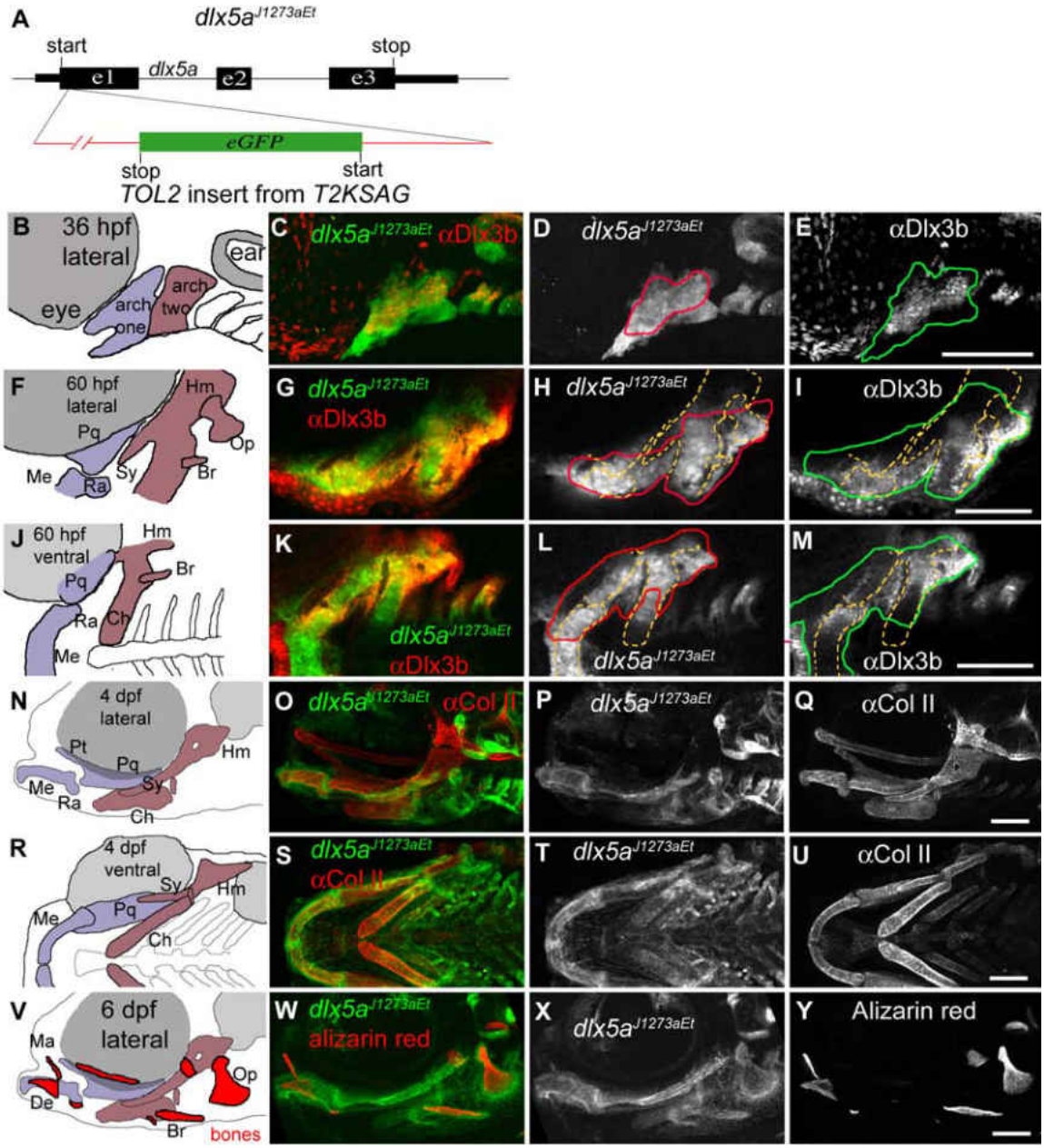

Figure 3: Anti-Dlx3b and *dlx5a*^{1073aEt} support *dlx3b* and *dlx5a* gene expression patterns. (A) A diagram of *dlx5a*^{1073aEt}. Transposon T2SKAG is inserted in the first exon of *dlx5a*, with *GFP* coding sequence in opposite orientation from *dlx5a*. Thus, although this insertion generates a loss-of-function allele of *dlx5a,* it is not likely to produce a *dlx5a:GFP* fusion protein. Instead, 5' RACE shows that *GFP* containing transcripts initiate from a cryptic promoter site within the transposon sequence suggesting that this weak promoter may allow the T2KSAG transposon to act as an enhancer trap, in this case revealing the activity of the enhancers driving *dlx5a* expression. (B-Y) Panels in the far left column are schematics of the views shown in confocal images. Skeletal abbreviations are as described in Fig. 1. Panels in the second-from-left column are merges of the single channel expression seen to the right. (C-E) Confocal projections at 36 hpf show that *dlx5a*^{J1073aEt} is expressed more broadly than Dlx3b immunolabeling. (G-I) Lateral

(anterior left, dorsal up) and (K-M) ventral (anterior left, lateral up) confocal sections reveal that at 60 hpf *dlx5a*^{J1073aEt} still shows expression broader than Dlx3b immunolabel. Inferred skeletal element locations are indicated with dotted yellow lines in single channel images. Gene expression outlines follow the color scheme shown in merged confocal images. (N-U) Projections of confocal stacks of ∝Col II/∝GFP label confirm *dlx5a*^{J1073a} expression within cartilage cells. (V-Y) Projections of confocal stacks showing GFP and Alizarin red label at 6 dpf confirm *dlx5a*^{J1073a} expression within bones. All fish shown are heterozygous for *dlx5a*^{J1073aEt}. Scale bars: 100µm.

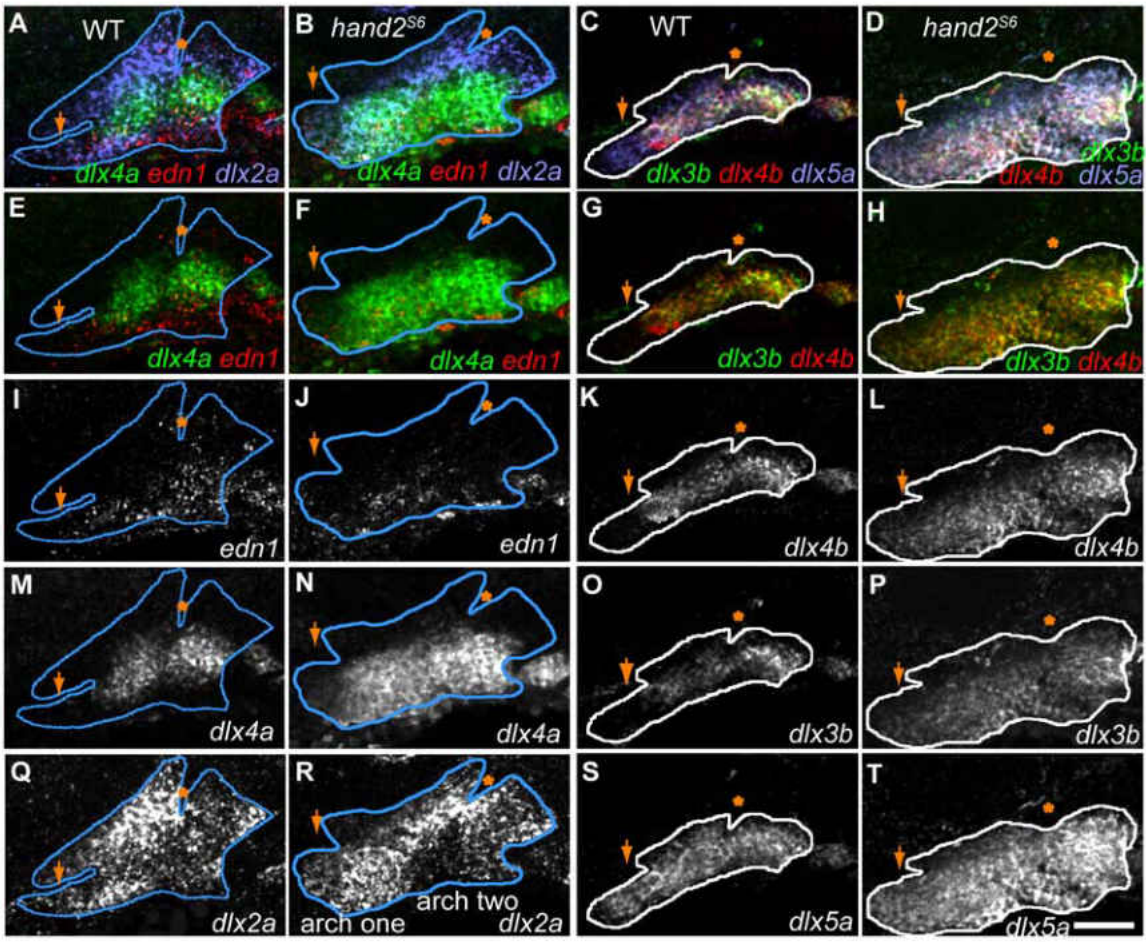

Figure 4: *Dlx* expression expands ventrally in *hand2* mutants. Images are projections from confocal stacks of 36 hpf RNA in situ, with anterior left, dorsal up.
For context, *dlx2a* (blue lines) or *dlx5a* expression (white lines) is outlined in the first two arches. In (A) WT fish, *dlx4b* is expressed dorsal to the *edn1* expressing mesoderm and ectoderm. However, in (B) *hand2*^{S6} fish, *dlx4a* is expressed both within the ventral *edn1* expressing region, and in the intermediate mesenchyme. Note that, though expanded, *dlx4a* expression remains ventral to the stomodeum (arrow) and first pouch (asterisk). Similarly, compared to (C) WT, *dlx3b* and *dlx4b* expression expands into ventral regions of *hand2*^{S6} (D), while remaining ventral to stomodeum and first pouch. (E-T) Separated confocal channels from panels A-D. Scale bar: 50 µm

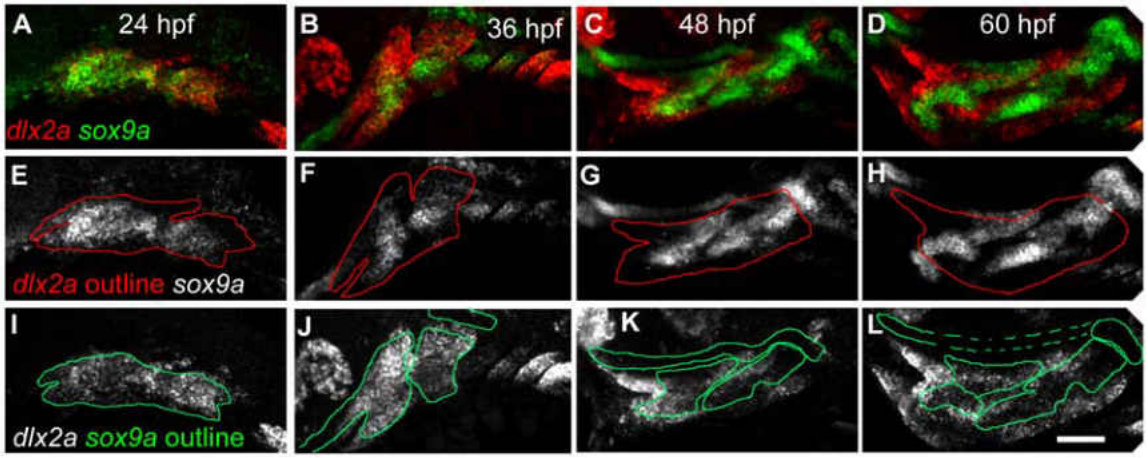

Figure 5: A time course of *sox9a* and *dlx2a* expression. (A-D) Projected confocal stacks showing *sox9a* and *dlx2a* expression at (A) 24 hpf, (B) 36 hpf, (C) 48 hpf, and (D) 60 hpf. Anterior to the left, dorsal up. (A) At 24 hpf, *dlx2a* and *sox9a* are co-expressed throughout most of crest derived pharyngeal arch regions. By 36 hpf (B) *sox9a* expression resembles rudimentary cartilaginous skeleton, including the presumptive neurocranium, dorsal to *dlx2a*. By 48 hpf (C) *dlx2a* expression is reduced in *sox9a* expressing cells, which increasingly resembles cartilaginous skeleton. By 60 hpf, (D) *dlx2a* and *sox9a* show little co-expression outside the intermediate domain. (E-L) The same images as A-D, but with (E-H) *sox9a* expression shown, and *dlx2a* outlined, or with (I-L) *dlx2a* expression shown, and *sox9a* outlined. Scale bar: 50 μm.

dlx3b/4b/5a has opposite regulatory effects to *hand2* on *gsc* and *nkx3.2* expression

The ventral inhibition of several *Dlx* genes by *hand2* suggests that *Dlx* and *hand2* may have some opposing roles in arch development. We examined the effect of *dlx3b/4b/5a* knockdown on two known *hand2* targets: *gsc* and *nkx3.2* (Miller et al., 2003), and the pre-skeletal marker *sox9a* (Fig. 5, building upon (Yan et al., 2005). In the WT first arch, we see co-expression of the jaw-joint-region marker *nkx3.2* with *dlx4a* and *sox9a*, but not *hand2* at 48 hpf (Figs. 6, 7). *Nkx3.2* expression is reduced in *dlx3b;4b;5a*-MO (Fig. 6J). Conversely, we see strong expansion of *nkx3.2* in *hand2*^{S6} mutants (Fig. 6K). The expanded *nkx3.2* expressing cells in *hand2*^{S6} also express *sox9a* (Fig. 6C). When we inject *dlx3b;4b;5a*-MO into *hand2*^{S6} (*hand2*^{S6}*;dlx3b;4b;5a*-MO), *nkx3.2* expression is dramatically reduced (Fig. 6L), suggesting that *hand2* represses *nkx3.2* expression via its repression of *dlx3b/4b/5a*.

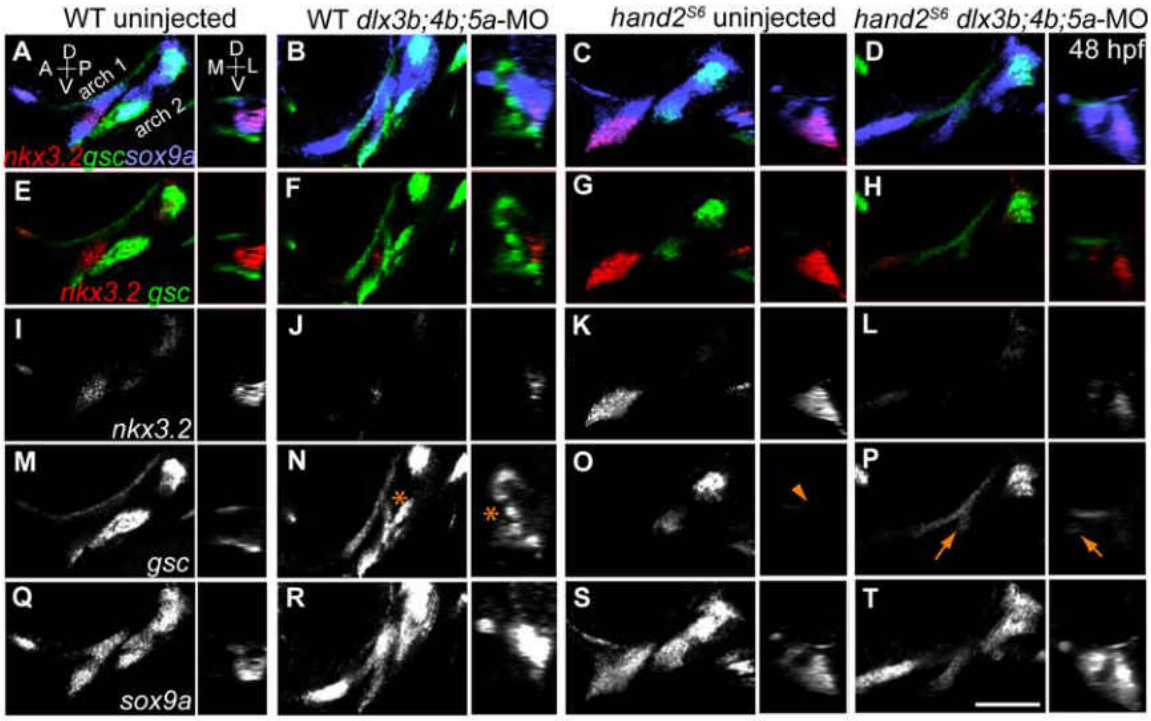

Figure 6: *hand2* and *dlx3b/4b/5a* have opposing roles in regulating *gsc* and *nkx3.2*. Each panel shows, (left) lateral views taken (anterior left, dorsal up) from single confocal sections, and (right) reconstructed orthogonal sections (medial left, dorsal up) through the first arch joint region of 48 hpf fish. Markers are indicated on the left panel of each row, and treatments indicated above each column. *Nkx3.2* expression is often reduced by (J) *dlx3b;4b;5a*-MO injection (80% penetrance), expanded in (K) uninjected *hand2*^{S6}, but reduced in (L) *hand2*^{S6}*;dlx3b;4b;5a*-MO. In (N) WT fish injected with *dlx3b;4b;5a*-MO the dorsal and ventral *gsc* domains are occasionally (7% penetrance) found fused together (asterisk), medial to (F) *nkx3.2* expression. In (O) uninjected *hand2*^{S6} fish, ventral first arch *gsc* is lost, but some dorsal expression remains (arrowhead). In (P) *hand2*^{S6}*;dlx3b;4b;5a*-MO, ventral *gsc* is defective in arch one, and sometimes reduced (45% penetrance) in arch two, while ectopic *gsc* is seen attached to dorsal arch one expression (55% penetrance, arrow), medial to *nkx3.2*. Scale bar: 100 μm.

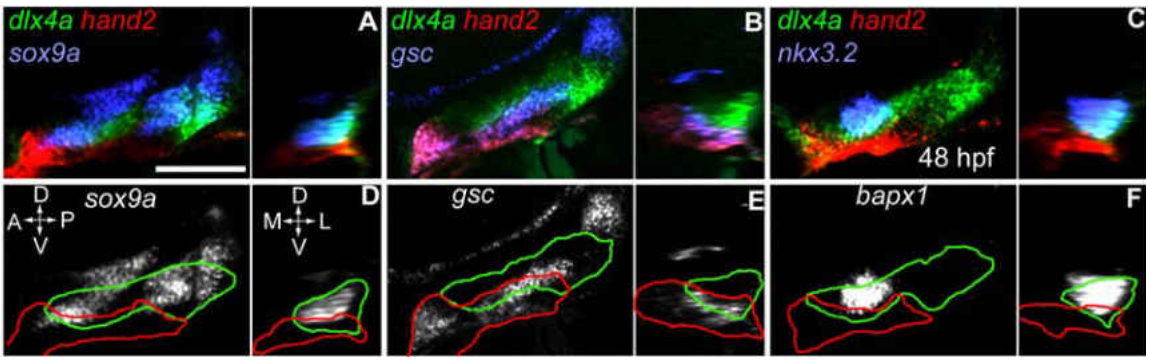

Figure 7: *nkx3.2* is expressed within the intermediate domain, while *gsc* is expressed within dorsal and ventral domains. For each panel, we show (right) comparable lateral confocal sections (anterior to the left, dorsal up), and (left) reconstructed orthogonal sections (medial to the left, dorsal up) taken through the presumptive jaw joint region. (A-C) Triple RNA in situ of *hand2* and *dlx4a* with (A) *sox9a*, (B) *gsc* and (C) *nkx3.2* at 48hpf. (D-F) *hand2* and *dlx4a* outlined over (D) *sox9a*, (E) *gsc*, and (F) *nkx3.2* channels taken from panels A-C. Scale bar: 100 μm.

gsc is expressed in ventral and dorsal bands within the first two pharyngeal arches, avoiding the first arch intermediate domain (Figs. 6,7). In agreement with previous reports (Miller et al., 2003), ventral first arch *gsc* expression is lost in *hand2*^{S6} (Fig. 6O). Conversely, in *dlx3b;4b;5a*-MO there are low penetrance fusions of the dorsal and ventral *gsc* expression bands (Fig. 6N). In *hand2*^{S6}*;dlx3b;4b;5a*-MO, there is an overall reduction in *gsc* expression (Fig. 6P). However in *hand2*^{S6}*;dlx3b;4b;5a*-MO there are sometimes small protrusions of *gsc* expression attached to the dorsal *gsc* domain (Fig. 6P). This ectopic *gsc* expression may represent expansions of the dorsal *gsc* domain. Hence, the WT function of *hand2* activates *gsc* and represses *nkx3.2* (in agreement with Miller et al., 2003), whereas *dlx3b/4b/5a* acts to repress *gsc* and activate *nkx3.2*.

<u>The combined loss of *hand2* and *dlx3b/4b/5a* results in expansion of dorsal identity</u>

The expansion of dorsal identity in *Dlx5*$^{-/-}$*;Dlx6*$^{-/-}$ mice (Depew et al., 2002) raises the question of whether dorsal identity also expands in zebrafish injected with *dlx3b;4b;5a*-MO. To assay dorsal identity we utilized the dorsal muscle marker *eng2* (Hatta et al., 1990), which specifically labels a portion of the first arch mesodermal core,

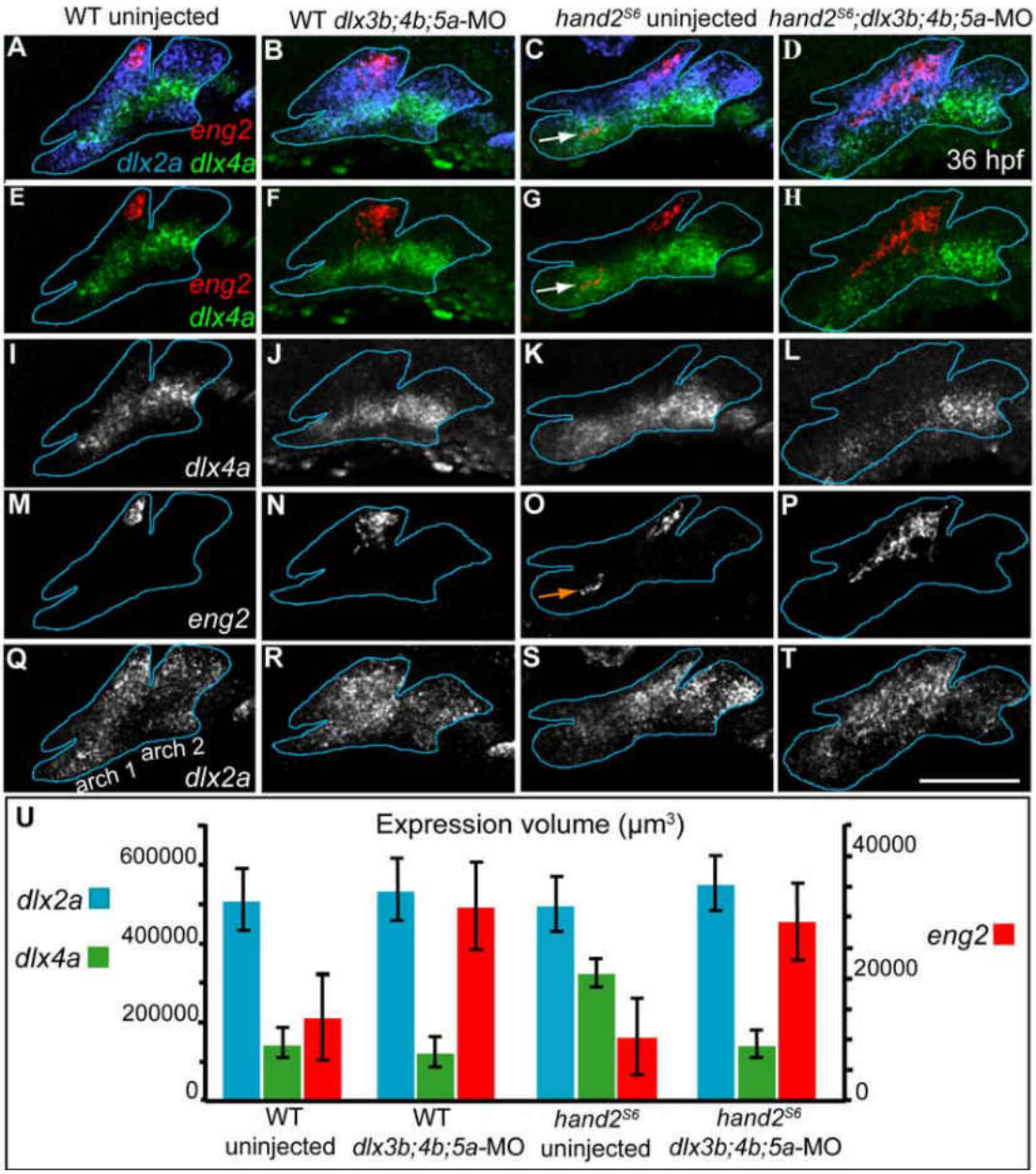

Figure 8: *hand2* and *dlx3b/4b/5a* repress dorsal identity. (A-T) Projections of confocal stacks of 36 hpf fish. Arch one and two are outlined in blue, using *dlx2a* expression as a guide. Markers are indicated on the left panel of each row, and treatments indicated above each column. Anterior is left, dorsal up. In *hand2*^{S6}, (O) ectopic *eng2* is indicated with an arrow. (U) Volumes (Y axis) of *dlx2a*, *dlx4a*, and *eng2* expression. Error bars are 95% confidence intervals, from ANOVA. Measurements were made on confocal stacks of randomly selected fish, using the 'find objects by intensity' function in Volocity software. Intensity thresholds were adjusted from fish to fish, to accurately identify expression. There are no significant differences between fish classes in average intensity levels. Each bar shows the combined volumes of arches one through three, because these arches were sometimes identified as one object by the software. Scale bar (T): 100 µm. *dlx2a* expression (Fig. 5U)

dorsal to *dlx4a* expression (Fig. 8A). Injection of *dlx3b;4b;5a*-MO into WT fish, causes an increase in *eng2* expression volume (Fig. 8N,U). However, these expanded *eng2* expression domains are still located dorsal to *dlx4a* expression (Fig. 8F). In *hand2*^{S6} mutants, *eng2* expression is found ventral to its location in WT (Fig. 8O, supporting (Miller et al., 2003). In *hand2*^{S6}, ectopic ventral nodules of *eng2* expression sometimes appear within mesoderm ensconced by *dlx4a* expression (Fig. 8G). Although *hand2*^{S6} mutants show changes in *eng2* expression shape, the average volume of *eng2* expression in *hand2*^{S6} mutants does not differ from WT (Fig. 8U). When *dlx3b;4b;5a*-MO is injected into *hand2*^{S6}*, eng2* expression expands in volume (Fig. 8U) and is ventrally elongated (Fig. 8H), indicating that *dlx3b/4b/5a* and *hand2* separately repress *eng2*. The overall expression of *dlx4a* is reduced in *hand2*^{S6}*;dlx3b;4b;5a*-MO, (Fig. 8U) indicating a further loss of intermediate identity in these fish. Despite the shifting patterning domains seen with *dlx3b/4b/5a* and *hand2* loss, we see no change in overall arch size as assayed by Collectively, these results indicate that *hand2* and *dlx3b/4b/5a* act in concert to inhibit dorsal identity in ventral/intermediate pharyngeal arches at 36 hpf.

Early arch expression domains map onto the developing skeleton

To clarify the connection between *hand2/Dlx* expression and skeletal domains, we co-labeled fish for *hand2* and *Dlx* expression alongside the pre-skeletal marker *sox9a*. Early in arch development, pharyngeal *sox9a* expressing cells express *dlx2a* (Fig 6, 7). However by 60 hpf, most of the *Dlx* expression that we observe is lateral to *sox9a* expression (not shown). *Dlx2a* expression is maintained in cartilages near the Meckel's-palatoquadrate joint, and the hyosymplectic-ceratohyal joint (Figs. 6,9A-C) and in mesenchyme lateral to these cartilages (not shown). All arch expression of *dlx2a* is ventral to the neurocranium (Fig. 6), consistent with previous findings (Verreijdt et al., 2006). *Dlx5a* is expressed within cartilages in the Meckel's-palatoquadrate and the hyosymplectic-ceratohyal joint regions at 60 hpf. *dlx5a* is also expressed in mesenchyme lateral to much of the skeleton, except for dorsal aspects of the palatoquadrate cartilage, hyomandibular cartilage, and most of the ceratohyal cartilage (Fig. 9E-L). *dlx5a*^{J1073aEt} expression is very similar to *dlx5a* in situ, but likely due to the longevity of GFP proteins,

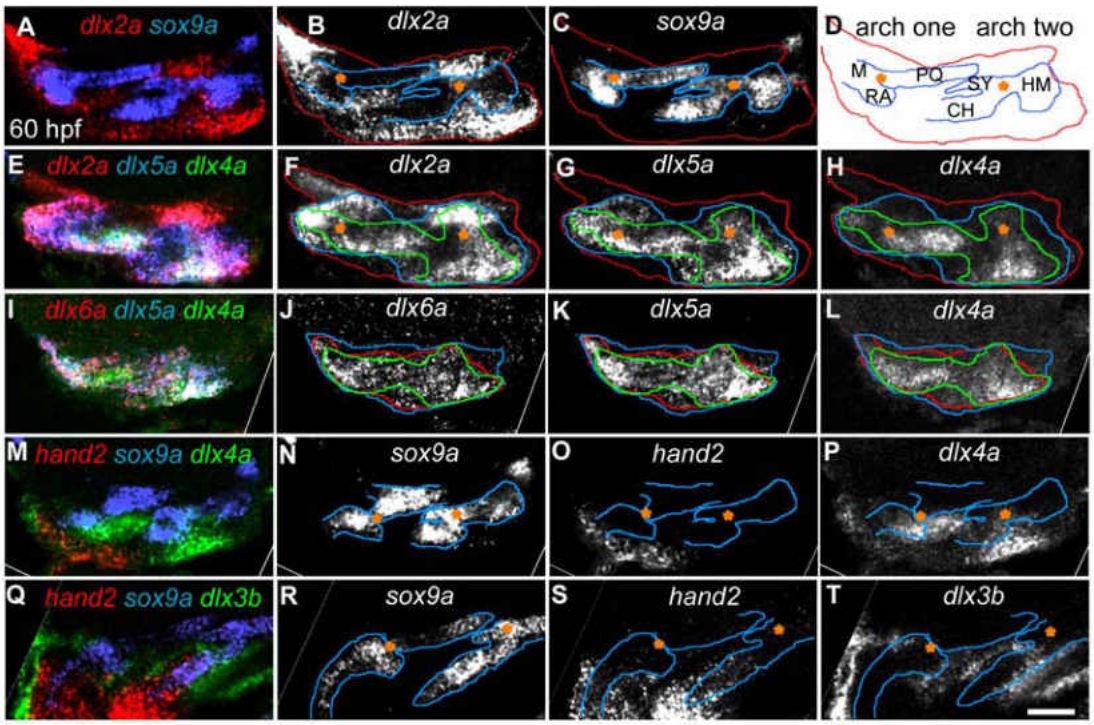

Figure 9: The patterning domains delineated by *Dlx* genes and *hand2* can be connected to specific pre-skeletal shapes at 60 hpf. (A-P) Lateral views (anterior to the left, dorsal up) of confocal sections illustrate differences in dorsal expression boundaries, while ventral views (Q-T) (anterior to the left, lateral up) illustrate ventral boundaries. (A-P) Merge of indicated markers is shown in the left column, while the other columns show single channels taken from the merge. Joints in the first two arches are indicated by asterisks. Confocal sections in I-L are lateral to cartilages, making the locations of underlying joints difficult to determine. Outlines in single channel panels follow the color schemes shown in the left column. Skeletal abbreviations are as in Fig. 1. Scale bar: 50 μm.

dlx5a^{J1073aEt} is detectable in cartilages longer than *dlx5a* RNA (Fig. 3). *Dlx6a* expression is very similar to *dlx5a*, though the dorsal *dlx6a* expression border may not extend as far dorsally as *dlx5a* (Fig. 9 I-L). Dlx3b and *dlx5a*^{J1073aEt} expression is found within precursor cells for both the opercle and branchiostegal bones (Fig. 3). At 60 hpf, *dlx4a* expression is found in the Meckel's-palatoquadrate joint, and in the hyosymplectic-ceratohyal joint, as well as in mesenchymal cells lateral to these cartilages (Fig. 9M-P). At 60 hpf, *dlx3b, dlx4b,* and *dlx4a* show similar expression, however as at 36 hpf, *dlx3b* is also strongly expressed in ectoderm (Fig. 9M-T and data not shown). In contrast, at 60 hpf, *hand2* is expressed within much of the Meckel's and ceratohyal cartilages, as well as the surrounding mesenchyme, ventral to *dlx3b* and *dlx4a* expression (Fig. 9M-T). Hence,

the relative dorsal-ventral expression borders of *hand2* and the various *Dlx* genes are maintained from 36 hpf to 60 hpf, though outside of joint regions there is a progressive loss of *Dlx* expression in chondral elements. The D-I-V boundaries revealed by *hand2* and *Dlx* at 60 hpf reveal which skeletal elements are formed from each expression domain.

Skeletal elements are homeotically transformed with lowered function of *hand2* and *dlx3b/4b/5a*

Our expression data suggest that ventral arch cells lose their ventral identities and acquire intermediate identities in *hand2* null mutants. When we lower *dlx3b/4b/5a* functions as well, we see a gene expression shift suggesting that dorsal identity expands. By these interpretations, we might also expect to see dorsalized homeotic phenotypes in arch-derived skeletons of such mutant and morpholino-injected fish. We constructed a phenotypic series of skeletal preparations to learn if the predicted homeosis is present (Fig. 10). Although there is extensive phenotypic variation (Fig. 11), we found that the first arch skeletal phenotypes show the predicted changes most clearly. In WT fish, there is a clear distinction between Meckel's and palatoquadrate shapes (Figs. 1A, 10A). In *dlx3b;4b;5a*-MO injected fish, the jaw joint region is fused, but Meckel's cartilage is still immediately recognizable (Fig. 1D, 11C). Conversely, with just a partial loss of *hand2*, Meckel's cartilage is shortened, and the dentary bone is misshapen, but the joint-cleft between Meckel's and palatoquadrate cartilage is still clearly present (Fig. 10B; homozygous mutants for the *hand2* hypomorphic allele, *c99*). However, with stronger loss of *hand2* function, the distinction between Meckel's and palatoquadrate is blurred (Fig. 10D; homozygotes for the *hand2* deficiency *s6*, and Fig. 10C; transheterozygotes of *S6* and *C99*). Instead, we interpret the midline cartilages in $hand2^{S6}$ as being transformed into ectopic palatoquadrate cartilage. Consistent with this interpretation, structures shaped like ectopic pterygoid cartilages variably seen in the $hand2^{S6}$ midline (arrows in Figs. 10C,D, 11E,F). The ectopic expression of *dlx3b*, *dlx4b*, and *dlx5a* seen in $hand2^{S6}$ raises the possibility that the ectopic cartilages seen in $hand2^{S6}$ require *dlx3b/4b/5a*

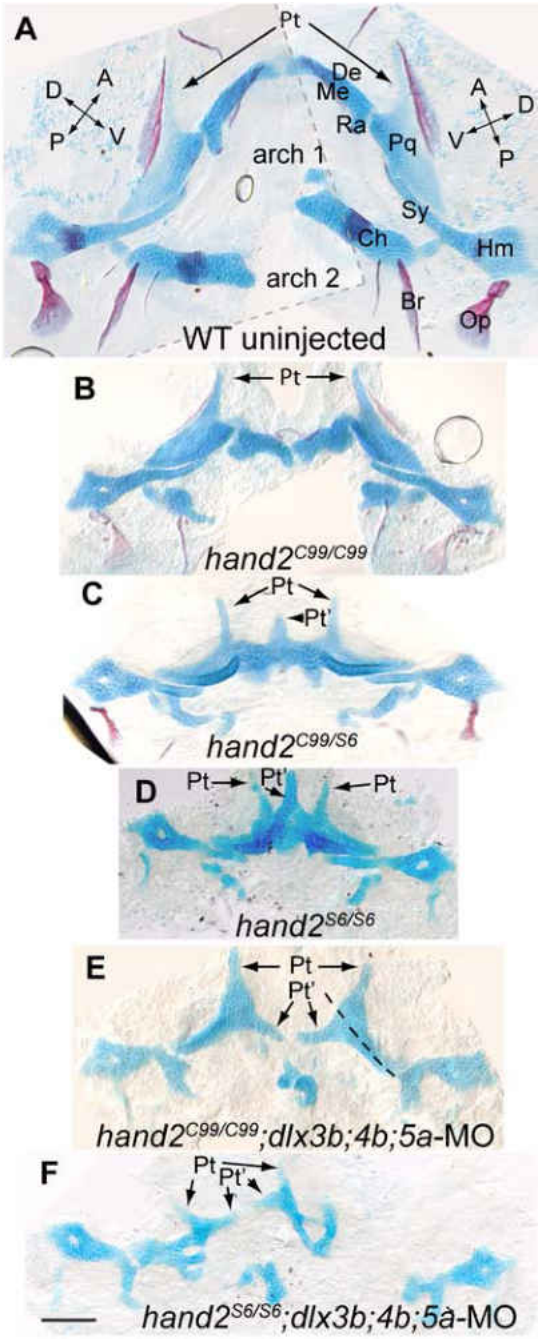

Figure 10: *hand2* mutants, and *hand2* mutants injected with *dlx3b;4b;5a*-MO show homeotic skeletal phenotypes. (A-F) Alcian blue and Alizarin red staining at 6 dpf. Images are flat mounted bilateral pharyngeal arches, oriented with midline to the center, and anterior up. The WT skeleton (A) was too large for a single image at this magnification, so two images were overlaid for this panel (border indicated with a grey dotted line). (B) *hand2*^{C99} homozygotes have reduced ventral, but normal intermediate and dorsal domain skeleton. (C) In trans-heterozygous fish carrying *hand2*^{C99} and *hand2*^{S6}, defects are typically more severe than in *hand2*^{C99} homozygotes, but less severe than in (D) *hand2*^{S6} homozygotes. In *hand2*^{S6} homozygotes, broad cartilages often span the midline, similar in shape to duplicated palatoquadrates, complete with pterygoid processes (arrows). When *hand2*^{C99} homozygotes are injected with *dlx3b;4b;5a*-MO (E), joints are lost in both arches, and the remainder of Meckel's cartilage is tapered out into a shape similar to a pterygoid process. A dashed line indicates the first arch dorsal-ventral plane of symmetry. The cartilage expansions of *hand2*^{S6} are lost when *dlx3b;4b;5a*-MO is injected (F). The palatoquadrate of *hand2*^{S6}*;dlx3b;4b;5a*-MO is often severely defective, though the distance between the first and second arch derived skeleton seen on the left side of (F) is exaggerated by mounting artifacts. Scale bar: 100 µm.

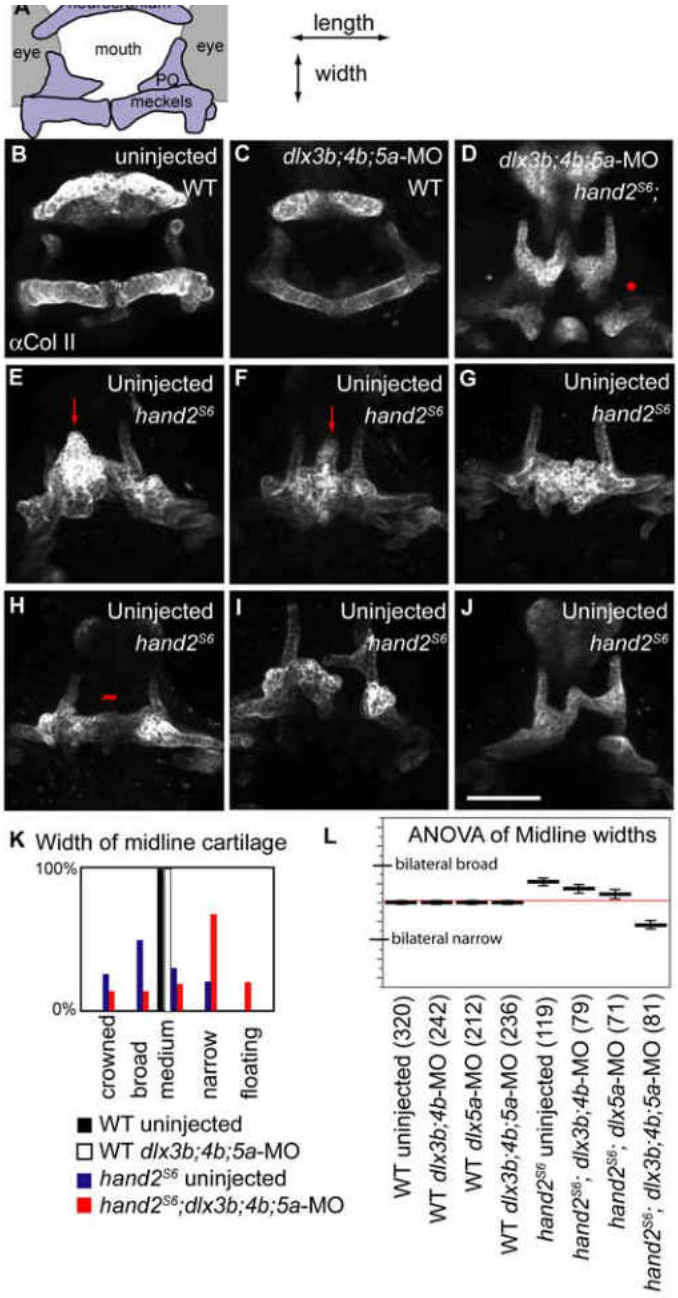

Figure 11: The shapes of first arch derived skeleton are highly variable in *hand2*^{S6}, but show significant changes after *dlxb3;4b;5a*-MO injection. (A) Schematic of anterior view, medial to the center, dorsal up. (B-J) Anterior views of fish immunolabeled for Collagen Iia1. (E) is the same fish as is shown in Figure 8C, for comparison of lateral to anterior view. Images are projections of confocal stacks. (B) Uninjected, and (C) *dlx3b;4b;5a*-MO injected WT fish have similar ventral shapes. (D) *hand2*^{S6} homozygotes injected with *dlx3b;4b;5a*-MO typically have narrowed midline cartilages, ("narrow"), which may be separated from posterior PQ (asterisk: "floating"). (E-J) A phenotypic series of midline cartilage shapes in uninjected *hand2*^{S6}. (E, F) The ventral midline sometimes contains a cartilaginous peak (arrow: "crowned"). (G) In other fish, the palatoquadrate expands ("broad"), but without ectopic pterygoids. (H) The ventral cartilages are sometimes similar to WT in width (tilde: "medium"), though they are shortened in length. (I) Cartilages are not always bilaterally symmetrical. (I, J) Rarely, narrow cartilages are also seen in uninjected *hand2*^{S6}, (K) however, a histogram of fish in each shape class shows that uninjected *hand2*^{S6} homozygotes typically look dramatically different from *hand2*^{S6} homozygotes injected with *dlx3b;4b;5a*-MO. (L) The shape classes were converted into a numeric score of midline size, and the means of these scores are plotted as thick black lines. Global mean is indicated with a thin red line. Error bars are 95% confidence intervals, determined by ANOVA. Number of fish scored is given in parentheses. Scale bar (J): 100 μM.

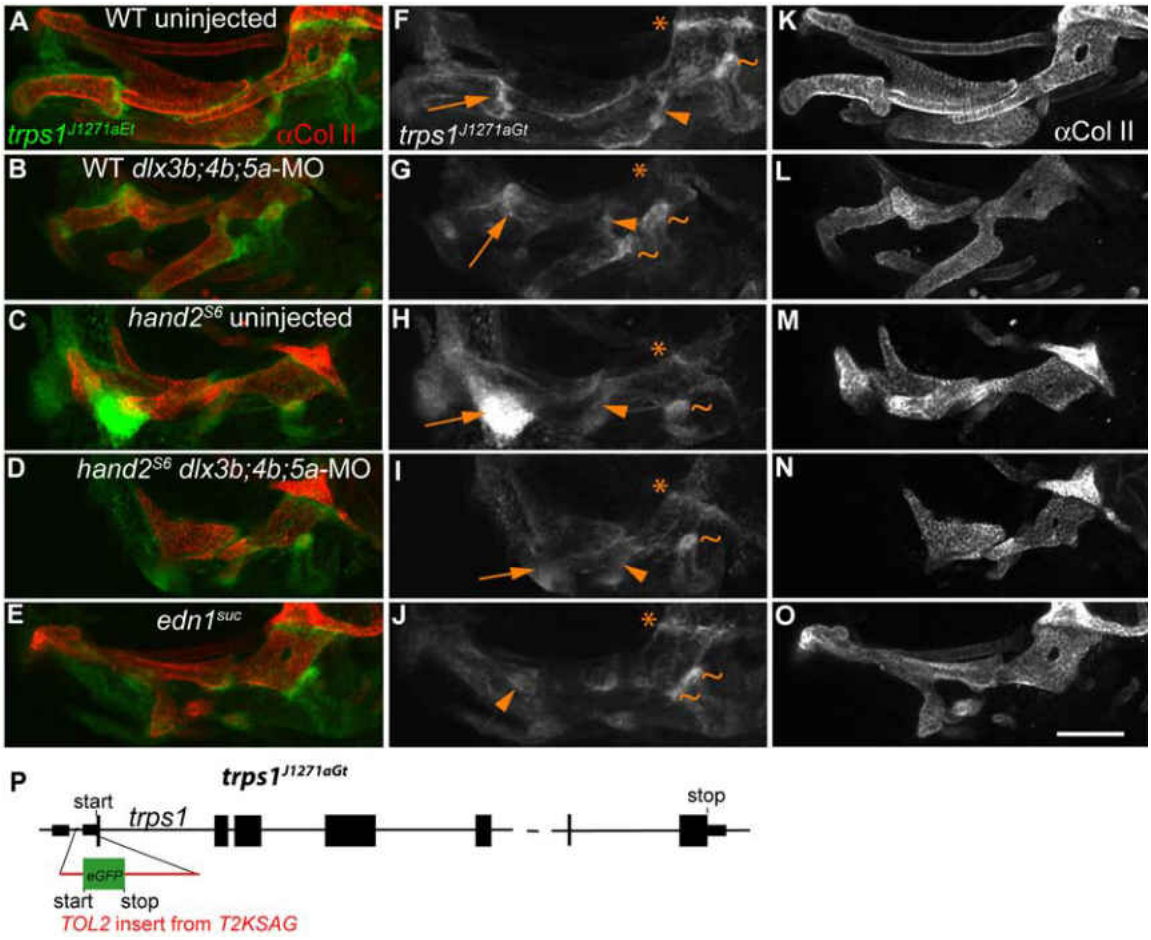

Figure 12: Jaw joint expression of *trps1*^{J1271aGt} is regulated by Edn1 signaling, and the Edn1 targets *hand2* and *dlx3b/4b/5a*. Confocal projections of 4 dpf anti-Collagen II and *trps1*^{J1271aGt} labeling is shown, merged in the left panel, and split in the center and right panels. Treatments are indicated in the left column. Anterior is left, dorsal up. (A) In WT, *trps1*^{J1271aGt} expression is faint in skeleton, and very bright in joints. (B) *dlx3b;4b;5a*-MO injection reduces *trps1*^{j1271aGt} in the first, (arrow) and second (arrowhead) arch joints, while the fused OP-BSR (tildes) bone expresses ectopic *trps1*^{j1271aGt}. (C) In *hand2*^{S6}, the jaw joint expression of *trps1*^{J1271aGt} expands dramatically, beneath broad ectopic cartilages. (D) In *hand2*^{S6}*;dlx3b;4b;5a*-MO, the expanded cartilages and *trps1*^{J1271aGt} expression domains in the first arch are reduced compared to uninjected *hand2*^{S6}. (E) In *edn1* mutants, the first and second arch joint expression of *trps1*^{J1271aGt} is lost, and conversely the opercle-hyomandibular joint expands. Throughout these treatments, the hyomandibular-neurocranium joint (asterisk) is normal. (P) Diagram of the J1271a insertion site in *trps1 (*Genbank GU556967). Intronic sequence is not to scale. We identified the 5' end (Genbank GU474515) of the *trps1* gene by 5' race from a predicted, incomplete *trps1* sequence, ENSDART0000098144. *Trps1* 5' race revealed a single 5' noncoding exon, with the J1271a integration site in the first intron. The splice acceptor orientation in T2KSAG predicts that it should be spliced into the processed message, with translation beginning at the initiating methionine in GFP, likely making J1271a a gene trap. Scale bar (O): 100 μm.

function. Consistent with this hypothesis, the ectopic midline cartilages seen in *hand2*^{S6} homozygotes are reduced when *dlx3b;4b;5a*-MO is injected (Figs. 10E, 11D, 12D). the cartilages protruding from the reduced palatoquadrate are shaped like ectopic pterygoid processes (arrows in Fig. 10E). Injection of *dlx5a*-MO, or co-injection of *dlx3b*-MO with *dlx4b*-MO into *hand2*^{S6} homozygotes produced subtler shifts in skeletal shape than injection of *dlx3b;4b;5a*-MO (Fig. 11L). When the hypomorphic *hand2*^{C99} homozygotes are injected with *dlx3b;4b;5a*-MO, these pterygoid shapes are also seen, and there is a remarkable symmetry along the dorsal-ventral axis, consistent with the predicted homeosis (arrows in Fig. 10F)

Joints are key structures in the intermediate domain, and thus are predicted to expand in *hand2* mutants. We used a transgenic line, *trps1*^{j1271aGt} (see Fig. 12P for details of the construct), in combination with cartilage labeling, to examine the joint and skeletal phenotypes more closely. *Trps1*^{J1271aGt} is strongly expressed in joint regions of WT fish (Fig. 12A; matching our in situ results, not shown), consistent with findings in mouse (Kunath et al., 2002). Although reduced in intensity, we surprisingly see distinctive expression of *trps1*^{J1271aGt} in the joint-region of *dlx3b;4b;5a*-MO injected fish, even though a joint-cleft is lost (Fig. 12B). Instead, the *trps1*^{J127aAGt} expressing cells lie just next to fused cartilages (Fig. 12B). In the corresponding region of *hand2*^{S6} fish, *trps1*^{j1271aGt} labeling was dramatically expanded (Fig. 12C), revealing expansion of joint-cell fate that is completely unrecognized by skeletal staining alone. In marked contrast, *trps1*^{j1271aGt} expression is highly reduced in the first arch of *hand2*^{S6}*;dlx3b;4b;5a*-MO compared to uninjected mutants, similar to *edn1* loss. (Fig. 12D,E). Hence, we infer that joint cell identity is established by Edn1 signaling, is repressed by *hand2*, and requires *dlx3b/4b/5a* function.

Discussion of *hand2/Dlx* results

The homeotic shape changes and molecular marker shifts we observe (Fig. 13B) indicate that *hand2* and *Dlx* genes impart distinct identities to D-I-V domains in the first two arches (Fig. 13C). In previous modeling, all *Dlx* genes were thought to be co-expressed with *hand2* in ventral aspects of arches (Depew and Simpson, 2006; Walker et al., 2006). Indeed we show that there is initial co-expression of ventral *dlx4a* and *hand2*. However

dlx3b, dlx4b, and *dlx4a* expression soon becomes restricted both dorsally and ventrally in the first two arches, indicating that by 36 hpf zebrafish *Dlx* genes are more fully nested than was previously thought (Fig. 13). Intermediate-restricted *Dlx* nesting is also present in lamprey which, along with our finding, suggests that dorsal/ventral *Dlx* restriction is basal within vertebrates (Cerny et al., 2010). Furthermore, a recent also demonstrates that genes are restricted from ventral arch regions in mouse (Barron et al., 2011), which in combination with my work and the work on lamprey (Cerny et al., 2010) indicates that restriction of Dlx expression to the intermediate domain is a conserved feature across vertebrates.

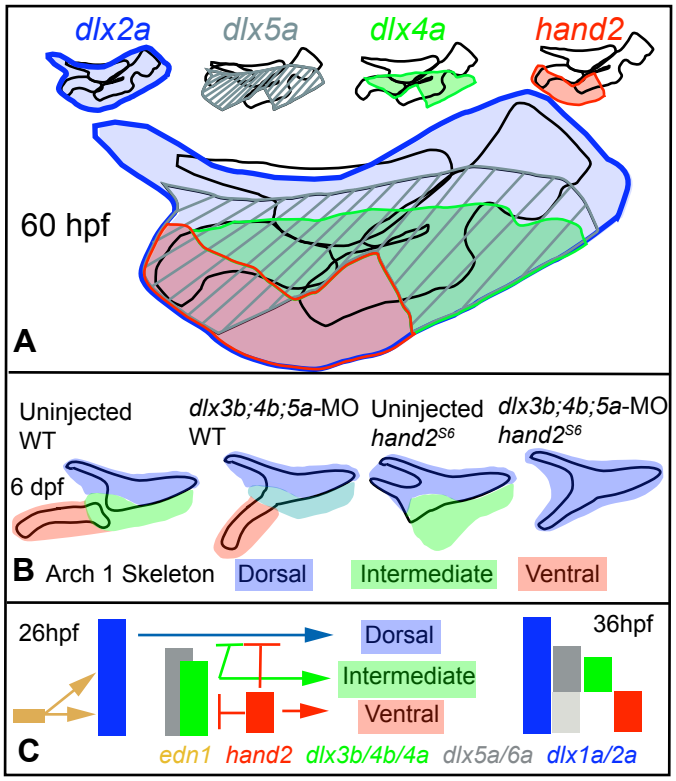

Figure 13: A model of D-I-V pattern formation. (A) Schematic of gene expression domains relative to cartilaginous skeleton, based on our 60 hpf RNA in situ data. The relationships of bones to domains are described in the text. (B) Proposed homeotic shifts in dorsal, intermediate, and ventral domains. In *dlx3b;4b;5a*-MO, intermediate identity is reduced, resulting in joint loss, while dorsal expands, causing a hybrid intermediate-dorsal identity (light blue). In *hand2* mutants, ventral identity is lost, while intermediate and dorsal identity expands. In *hand2* mutants injected with *dlx3b;4b;5a*-MO, both ventral and intermediate identity are lost, while dorsal identity expands. (C) A regulatory network for domain formation suggested by the patterning shifts observed in *edn1*, *hand2,* and *dlx3b/4b/5a* knockdown. By 36 hpf, repression from *hand2* results in ventral loss of *dlx3b/4b/4a* in both arches, as well as second arch *dlx5a/6a* down-regulation (light grey).

In both the recent lamprey and mouse studies, homologues of *dlx3* are restricted from the ventral region of both arch 1 and 2, while *dlx5a/dlx6a* only lack ventral arch two expression, but are found in ventral arch 1- so the detailed shape of individual *Dlx* genes

also appears to be conserved. We provide new evidence that *dlx3b*, *dlx4b*, and *dlx5a* have overlapping functions in intermediate domain patterning, coincident with their overlapping expression within the intermediate domain. By 36 hpf, *hand2* is expressed ventral to *dlx4a,* correlating with its specific requirements in ventral domain patterning (Miller et al., 2003). The stacked expression of *dlx4a* and *hand2* persists until after major cartilage domains have been formed. We recognize that due to the dynamic nature of gene expression, only precise fate maps can definitively connect expression patterns between different time-points. Nonetheless, the differential expression and requirements of *dlx1a/2a*, *hand2*, and *dlx3b/4b/5a* provides a mechanism to generate discrete D-I-V domains within pharyngeal arches and skeleton (Fig. 13).

Similar to the findings in mouse (Qiu et al., 1997), zebrafish *dlx1a* and *dlx2a* function redundantly to pattern dorsal identity. However more ventrally restricted Dlx genes *dlx3b/4b/5a* lack dorsal requirements, supporting a correlation between Dlx expression and function. We have also noted additional *Dlx* nesting: *dlx3b/4b* nest within the *dlx5a* expression domain. It will be important for future work to test the functional relevance of this deeper Dlx nesting, which may reveal patterning sub-domains.

Skeletal shape changes in Edn1 signaling pathway mutants are correlated with changes in *hand2* and *Dlx* expression. *mef2ca* and *furina* mutants, which only partially reduce Edn1 signaling, result in the loss of *dlx4b* and *dlx5a* expression, but no persistent losses in *hand2* expression (Miller et al., 2007; Walker et al., 2006). The skeletal defects in *mef2ca* and *furina* mutants include joint loss, ectopic cartilages, and second arch bone fusion, but no ventral defects (Miller et al., 2007; Walker et al., 2006), similar to *dlx3b;4b;5a*-MO. In contrast, *edn1* mutants and *plcß3* mutants, which strongly reduce Edn1 signaling, cause strong loss of *hand2*, *dlx3b*, and *dlx5a* expression (Miller et al., 2000; Walker et al., 2006; Walker et al., 2007). The skeletal defects seen in *edn1* and *plcß3* mutants include severe defects in both intermediate and ventral skeleton(Miller et al., 2000; Walker et al., 2006; Walker et al., 2007), similar to *hand2*^{S6}*;dlx3b;4b;5*a-MO. Furthermore, prominent expansions of the dorsal marker *eng2* are seen in both *edn1* mutants ((Miller et al., 2003) and *hand2*^{S6}*;dlx3b;4b;5a-MO*. Hence, the overall arch patterning domains identified in this study of *hand2/Dlx* expression and function closely mirror the domains identified previously from studies of Edn1 signaling.

We examined skeletal phenotypes in fish treated with morpholinos to various combinations of *dlx1a*, *dlx2a*, *dlx3b, dlx4b*, and *dlx5a*, revealing redundant patterning roles for these genes. However, the conclusions we draw are limited because we lack known null alleles in any *Dlx* gene. Furthermore, all *dlx4a* and *dlx6a* morpholinos tested to date have failed to convincingly disrupt splicing, or produce any skeletal phenotype (data not shown). It will be very important for future studies to examine null alleles of *Dlx* genes. For example, zebrafish *dlx5a*$^{-}$*;dlx6a*$^{-}$ nulls could conclusively test whether loss of these two genes in fish results in the homeotic transformations observed in *Dlx5*$^{-}$*;Dlx6*$^{-}$ mutant mice. While we have demonstrated that *dlx3b/4a/4b* expression doesn't extend as far dorsally as *dlx5a/6a*,we have not observed a functional consequence of this expression difference. The expression difference between *dlx3b/4a/4b* and *dlx5a/6a* may be present because the major D-I-V domains are further subdivided into smaller patterning domains by *Dlx* expression. With genetic nulls we could conclusively assay the functional relevance of expression differences between *dlx3b/4a/4b* and *dlx5a/6a*.

In WT zebrafish, *trps1* expression faithfully labels joint regions. However, in our mutants we found several examples of *trps1*-expressing joint cells that do not connect skeletal elements. For instance, although *dlx3b;4b;5a*-MO injection causes a fusion between Meckel's and palatoquadrate cartilages, some *trps1* expression is found in cells surrounding the location where the joint would have been. Similarly some expression of *nkx3.2* remains, indicating that even when normally jointed cartilages are fused together, remnants of joint pattern can remain. In *dlx3b;4b;5a*-MO, *trps1* expression spans the fused opercle-branchiostegal bone, including a region of the bone that does not connect to skeleton. As a more extreme example, in *hand2*^{S6}, Meckel's cartilage is lost, and instead there is an enormous mass of ectopic *trps1* expressing cells. In *hand2*^{S6}, the most anterior *trps1* expressing cells sometimes extend well beyond any apparent bone or cartilage, indicating that joint cells can arise separately from skeleton. The disassociation of joint cells from jointed skeletons in our mutants leads us to ask how WT fish obtain a perfect correlation of jointed skeleton with jointing cells. It will be intriguing to discover the developmental relationship between joint cells, and jointed skeletal elements.

Losses in ventral or intermediate domain identity result in compensatory expansion of identity from other domains (Fig. 13). When *hand2* is lost, *dlx3b, dlx4a,*

dlx4b, and *dlx5a* expression expands ventrally at 36 hpf. New research indicates that *hand2* also ventrally inhibits *Dlx* expression in mouse (Barron et al., 2011). Crest-specific knockout of mammalian *Hand2* causes increase of *Dlx5* and *Dlx6* expression, but not *Dlx3* (Barron et al., 2011). This finding suggests that either the regulation of *Dlx3* has shifted between fish and mammals, or that the ectodermal *Hand2* expression regulates *Dlx3*. Coincident with the expansion of these *Dlx* genes, we observe expansion of intermediate domain cartilages, *trps1* expression, and *nkx3.2* expression in $hand2^{s6}$. Injecting *dlx3b;4b;5a*-MO into $hand2^{s6}$ mutants results in a loss of joint identity, indicating that *hand2* represses joint identity via its repression *dlx3b/4b/5a*. When both *hand2* and *dlx3b/4b/5a* functions are reduced, the arch volume (indicated by 36 hpf *dlx2a* expression) remains fairly constant, and dorsal identity expands. The expansion of dorsal identity in $hand2^{s6}$*;dlx3b;4b;5a*-MO is similar to expansions of dorsal identity observed in Edn1 pathway mutants. For example, dorsalizing homeosis are seen in both zebrafish and mouse *Edn1* mutants (Kimmel et al., 2003; Ozeki et al., 2004), and *EdnrA* mutants/morpholinos (Nair et al., 2007; Ruest et al., 2004), as well as mouse $Dlx5^{-}$;$Dlx6^{-}$ mutants (Beverdam et al., 2002; Depew et al., 2002). Functional knockdowns in our study focused on markers broadly and specifically required for ventral and intermediate domain identity. Recent work has shown that the dorsally expressed gene *jag1b* helps to specify dorsal identity, in part, by repressing *Dlx* gene expression (Zuniga et al., 2010). Several more candidate genes for dorsal specification genes have been recently proposed (Jeong et al., 2008; Zuniga et al., 2010), which may provide powerful insights into the interplay between dorsal, intermediate, and ventral pharyngeal arch specification.

In addition to *Dlx* genes, many other genes are likely very important to intermediate domain formation. For instance, the *Dlx* target *bapx1* is crucial to the formation of a portion of the first arch intermediate domain (Miller et al., 2003). In chapter III of this thesis, I demonstrate that two more genes, *fras1* and *itga8,* are vital to reliable intermediate domain morphogenesis.

CHAPTER III

EPITHELIAL-MESENCHYMAL INTERACTION BETWEEN *fras1* AND *itga8* STABILIZES ZEBRAFISH PHARYNGEAL ARCH INTERMEDIATE DOMAIN DEVELOPMENT

The work described in this chapter is being prepared for publication. Yi-Lin Yan and Ruth A. Bremiller performed in situ hybridization on tissue sections in John H. Postlethwait's lab. Macie B. Walker did the initial mapping, to identify *fras1* mutants. She also performed initial descriptions of *b1048* mutant skeletal phenotypes. Thomas J. Carney, who worked in the lab of Matthias Hammerschmidt at the time, sequenced *fras1* cDNA from the *b1048* and *b1130* alleles, revealing that these mutants were caused by lesions in *fras1*. Matthias Hammerschmidt contributed the Fras1 antibody. Charles B. Kimmel has assisted with editing this chapter, and is the principle investigator on this project. All other work and writing for this paper is my own.

Chapter summary

Lesions in the epithelially-expressed human gene *FRAS1* cause Fraser syndrome, a complex disease with many variable symptoms, including ear defects, kidney defects, and lung defects. In mouse, mutation of the mesenchymally expressed gene *Itga8* produces kidney and lung defects similar to those seen in mouse *Fras1* mutants. A potential physical connection between Fras1 and Itga8 proteins has been indicated by adhesion assays in cell culture. However, no prior study has tested Fras1-Itga8 interaction in vivo, nor investigated the facial defects of *Fras1* mutants. Here we show that zebrafish *fras1* and *itga8* mutants exhibit similar defects in facial endoderm (an epithelial tissue), and facial skeleton (derived from mesenchyme). We propose that the skeletal elements and epithelia found defective in zebrafish *fras1* and *itga8* mutants are homologous to the ear anatomy found defective in human Fraser patients. Zebrafish *fras1;itga8* double mutant fish look highly similar to both single mutants, indicating *fras1-itga8* interaction in vivo. We report zebrafish *itga8* expression in mesenchymal facial tissues adjacent to

fras1 expressing epithelia. However, neither *itga8* nor *fras1* are expressed in facial skeleton by the time that morphological defects are first seen. The spatiotemporal relationship of epithelial and skeletal defect formation in *fras1* and *itga8* mutants indicate that epithelial defects may underlie at least some of the skeletal defects. Skeletal defects of *fras1* and *itga8* mutants present a high degree of fluctuating asymmetry, which we interpret as an indicator of developmental instability. We propose a model wherein epithelial-mesenchymal adhesion between Fras1 and Itga8 produces an endodermal structure that stabilizes skeletal formation.

Introduction to *fras1* and *itga8*

The genetic basis of epithelial-mesenchymal interactions in facial development has been a topic of considerable interest for many years. Epithelia are comprised of cohesive planar sheets of cells, while mesenchyme is comprised of immature loosely associated cells. The epithelial expressed gene *FRAS1* (Gautier et al., 2008; McGregor et al., 2003; Vrontou et al., 2003) and the mesenchymally expressed gene integrin α8 (*ITGA8*) (Schnapp et al., 1995a) are relatively recent entries to the expanding pantheon of genes that mediate epithelial-mesenchymal interactions. *FRAS1* is required for normal epithelial morphogenesis in humans (McGregor et al., 2003; Slavotinek et al., 2006), mouse (McGregor et al., 2003; Vrontou et al., 2003) and zebrafish (Carney et al., 2010). Mutations in human *FRAS1* causes Fraser syndrome (McGregor et al., 2003; Slavotinek et al., 2006), a complex disorder with a multitude of variably expressed symptoms (Fraser, 1962; Gattuso et al., 1987; Slavotinek and Tifft, 2002; Thomas et al., 1986; van Haelst et al., 2007). Symptoms of Fraser syndrome frequently include pronounced craniofacial skeletal defects, middle ear defects, and ear canal reduction, amongst many other defects (Gattuso et al., 1987); however the developmental basis of craniofacial and ear defects found in Fraser syndrome patients have not been investigated in any system. In mammals the middle ear skeleton is derived from mesenchyme in the first two pharyngeal arches, whereas the ear canal is derived from the first pharyngeal pouch, and ectodermal cleft [see (Chapman, 2011) for recent review]. In zebrafish, the first two pharyngeal arches produce jaw, and jaw supporting skeleton (Kimmel et al., 1998). Pharyngeal arches are contain neural crest derived mesenchyme, surrounded by

surrounded by epithelia. Arch mesenchyme later differentiates into facial skeleton and connective tissues. Early in pharyngeal arch development, neural crest derived mesenchyme is surrounded medially by endoderm and laterally by ectoderm (Kimmel et al., 2001). Pharyngeal pouches form via lateral endoderm protrusion, connecting medial endoderm to ectoderm, thereby segmenting the arches along the anterior-posterior (A-P) axis [reviewed in (Graham et al., 2005)].

In mouse (McGregor et al., 2003; Vrontou et al., 2003) and zebrafish (Gautier et al., 2008) *Fras1* mRNA is expressed by epithelial cells, including endoderm and ectoderm surrounding pharyngeal arches. Fras1 protein contains motifs implicated in signaling and adhesion (McGregor et al., 2003; Vrontou et al., 2003), as well as a transmembrane domain. Furin protease activity releases the large extracellular portion of Fras1 into basal lamina underlying epithelia (Carney et al., 2010). Mature Fras1 protein is secreted into the sub-lamina densa (Dalezios et al., 2007) of epithelial basal lamina (Carney et al., 2010; Chiotaki et al., 2007; Kiyozumi et al., 2006), which is the portion of the basal lamina directly apposed to embryonic mesenchyme. Fras1 forms a colossal ternary complex with many proteins, including the Fras Related ECM (Frem) proteins Frem1 and Frem2 (Carney et al., 2010; Chiotaki et al., 2007; Kiyozumi et al., 2006; Petrou et al., 2007), that reciprocally stabilize one another at the basal lamina (Kiyozumi et al., 2006; Petrou et al., 2007). Lesions in *FRAS1* (McGregor et al., 2003; Slavotinek et al., 2006) and *FREM2* (Jadeja et al., 2005; Shafeghati et al., 2008) underly some cases of Frasers syndrome, whereas *FREM1* lesions cause the related disorders MOTA (Slavotinek et al., 2011) and BNAR (Alazami et al., 2009); nonetheless, the genetic cause of many cases of Fraser syndrome remain unexplained (van Haelst et al., 2008). Diagnosis of Fraser-spectrum syndromes require examination of multiple symptoms (Thomas et al., 1986). Germane to our work, major diagnostic symptoms of Fraser syndrome include renal agenesis and lung defects, while minor diagnostic criteria include dysplastic ears and aural stenosis (reduction of the ear canal) among other traits (van Haelst et al., 2007). Similarly, mice lacking *Fras1* exhibit severe pleiotropic phenotypes, including epithelial adhesion defects (Short et al., 2007), kidney agenesis (Pitera et al., 2008; Vrontou et al., 2003), and lung defects (Petrou et al., 2005).

Similar to *Fras1* mutants, *Itga8* mouse mutants also exhibit severe epithelial adhesion defects (Benjamin et al., 2009), kidney agenesis (Muller et al., 1997), and lung defects (Benjamin et al., 2009); suggesting a connection between these two genes (McGregor et al., 2003; Pitera et al., 2008). Furthermore, adhesion assays in cell culture reveal that Itga8 binds the RGD containing portion of Frem1, indicating a potential direct interaction between Itga8 and the Fras/Frem complex (Kiyozumi et al., 2005). Itga8 is a transmembrane protein involved in cell adhesion (Schnapp et al., 1995b) and signaling (Linton et al., 2007; Muller et al., 1997). In rats, Itga8 protein is found in the mesenchyme of many developing organs, and smooth muscles in adult tissues (Schnapp et al., 1995a), with consistent patterns found in human (Schnapp et al., 1995a), mouse (Muller et al., 1997), and chick (Bossy et al., 1991). In avian and mammalian studies, the highest levels of Itga8 protein are found in mesenchymal or connective tissues adjacent to the epithelial basal lamina (Bossy et al., 1991; Schnapp et al., 1995a). In mammalian intestine (Benoit et al., 2009), and developing lungs (Benjamin et al., 2009), mesenchymal cells lacking *Itga8* fail to adhere to their associated epithelia; As a result, associated epithelia fail to undergo normal morphogenesis (Benjamin et al., 2009; Muller et al., 1997).

In this study, we investigate epithelial-mesenchymal interactions between *fras1* and *itga8* during zebrafish facial development. We show that that *fras1* and *itga8* are each necessary for normal morphogenesis of facial skeleton and endoderm. Skeletal and epithelial facial defects seen in *fras1*, and *itga8* single mutants as well as *fras1;itga8* double mutants appear extremely similar to one another, consistent with a model wherein these two genes function together in a protein complex during facial development. WT endoderm is able to rescue both epithelial and skeletal phenotypes in *fras1* mutants, but WT endoderm is unable to rescue *itga8* mutant phenotypes; indicating that *fras1* and *itga8* function arises from separate tissues. We report that *itga8* mRNA is expressed in arch mesenchyme, adjacent to epithelial *fras1* expression from at least 36 to 72 hours post fertilization (hpf). Using time-lapse and time-course analysis, we demonstrate that in *fras1* and *itga8* mutants, epithelial defects arise between 36 and 72 hpf, concurrent with symplectic extension defects, but prior to second arch skeletal fusion. We provide a

spatio-temporal model for how epithelial-mesenchymal interactions between *fras1* and *itga8* produce normal morphology in facial epithelia and skeleton.

Materials and methods

Fish maintenance, husbandry, morpholinos, and strains

Fish were raised and staged as described previously (Kimmel et al., 1995; Westerfield, 1995). Mutant lines were maintained on the AB background, except as designated. *fras1* mutants were identified using previously described fully penetrant tail phenotypes, or previously described genotyping protocols (Carney et al., 2010). *b1161* mutants were discovered by screening N-ethyl-N-nitrosourea mutagenized Alcian blue/alizarin red stained gynogenetically doubled haploids, molecular cloning of the *itga8*^{b1161} lesion is detailed below. *itga8*^{b1161} mutants were identified using PCR primers *itga8*IDF (CCCAGTTACATAACAAAGGTCCGAG) and *itga8*IDR (TAAGCCCAGTCAAGTTTTTGCC) to produce a 510 bp band in WT, a 431 bp band in mutant, and both sizes in heterozygous fish. Transgenic construction of *cart:GFP* (DeLaurier, personal communication), *sox10:mRFP* (Kirby et al., 2006), and *her5:GFP* (Tallafuss and Bally-Cuif, 2003) are all described elsewhere. For morpholinos, 2-3 nl of solution is injected into one to two cell staged embryos. Morpholinos used: *itga8*ATG-MO: CCCTGTGTGTCCGAGTGTAATCCAT *itga8* mismatch-MO: CCgTcTGTcTCCGAcTcTAATCCAT (mismatched bases lowercase) and *itga8*E25I25-MO: GCACAGGACAGAGAGTTTACCTCCA.

Tissue labeling

Whole mount antibody labeling and RNA in situ hybridization was performed as described (Chapter II). RNA in situ hybridization followed by NBT/BCIP staining is as (Rodriguez-Mari et al., 2005). NBT/BCIP RNA in situ hybridization, embryos were raised in 0.0015% PTU to inhibit melanogenesis (Westerfield, 2007), however PTU was not added for any other experiment. Fluorescent RNA in situ hybridization on tissue sections combines and modifies the whole mount fluorescent in situ protocols with tissue section RNA in situ protocol. Alcian/Alizarin staining on fixed samples performed as

described (Walker and Kimmel, 2007) and vital staining with Alizarin red is as described (Chapter II). Most imaging was performed on a Zeiss Pascal LSM 5 laser-scanning confocal microscope, followed by processing with Velocity and ImageJ software. Some images are taken on a Leica SD6000 spinning disc confocal microscope with Borealis Illumination Technology, followed by processing with Metamorph software.

Time lapse microscopy

Fish were mounted essentially as described for time-lapse microscopy (Westerfield, 2007), but in 0.05% agarose to reduce developmental delay. Z-stacks were collected every 30 minutes. After imaging, fish were raised and re-examined for skeletal phenotypes to confirm health and the presence/absence of defects observed during time lapse. Stacks were corrected for Z-drift in LSM software, followed by further processing in Velocity and ImageJ software. Confocal transverse section plane is tracked manually within Volocity software.

Endoderm transplantation

Endoderm transplantation experiments were performed essentially as described (Crump et al., 2004a; Crump et al., 2004b; Walker et al., 2007). In brief, donors were injected at early one cell stage with *TARAM** RNA and 1% rhodamine-dextran. At 3-4 hpf, 20-30 donor cells are transferred to host embryos near the yolk margin. At 34-38 hpf, hosts were scored under fluorescence dissecting microscopes and selected for strong labeling of medial endoderm underlying the first two arches and early pouch 1. Hosts were then raised to 7 days post fertilization (dpf), and imaged. For transplantation experiments, donor embryos and the caudal end of host tails (unlabeled with donor) are PCR genotyped.

GenBank accession numbers

WT *itga8* cDNA: pending, as of thesis submission.

itga8^{b1161} cDNA: pending, as of thesis submission.

Results

fras1 stabilizes normal cartilage development

In zebrafish forward genetic craniofacial and tail epithelial screens, we discovered several *fras1* mutants (Carney et al., 2010) displaying prominent skeletal defects and tail epithelial defects (Fig. 1, 2). In this study, we focus primarily on the developmental basis of second arch skeletal defects in the *fras1*^{b1048} allele. Three cartilage defects are frequently found in *fras1*^{b1048} mutants (Fig. 1A-J): 1. first arch fusion connecting Meckel's and palatoquadrate cartilage ("Me-Pq fusion"; Fig. 1E), 2. second arch fusion connecting symplectic and ceratohyal cartilages ("Sy-Ch fusion"; Fig. 1H), and 3. shortened symplectic cartilage ("Sy short"; Fig. 1I). These three cartilage defects are each found with partial penetrance in *fras1*^{b1048} mutants (Table 1). Each cartilage defect can occur separately (Fig. 1H,I), or combined (Fig. 1J), and the presence of one defects is a very poor indicator of the presence of any other (Fig. 1K). Although the presence of most cartilage defects are significantly correlated with one another (ChiSquare $P<0.05$; Fig. 1K), the correlations are quite weak (average $R^2=0.09$; Fig. 1K). Furthermore, when the sum of left and right defects were compared, correlations become insignificant (ChiSquare $P>0.05$). In contrast to highly symmetric WT fish, *fras1*^{b1048} mutants are highly asymmetric, (Table 1). *fras1*^{b1048} mutants show very little side bias in cartilage defects (2% right side bias per defect). When phenotypes fluctuate between two sides of an embryo, this is often taken as an indicator of developmental instability [e.g. (Dongen, 2006)], thus the high level of fluctuating asymmetry found in *fras1*^{b1048} mutants (Table 1) indicates that WT *fras1* stabilizes skeletal development. All three *fras1* alleles causing Fras1 protein truncation (*fras1*^{b1048}, *fras1*^{te262}, *fras1*^{b1130}, Fig. 1L) (Carney et al., 2010) show the same cartilage defects, with similar variability (Fig. 1M, Table 2), indicating that phenotypic variation is not allele or background specific (Table 2). The hypomorphic allele *fras1*^{tm95b} shows weak defects at best, indicating that a strong loss of *fras1* is needed for skeletal phenotypes. Cartilage defects in *fras1*^{b1048} mutants are quite specific: joint cartilages (interhyal and retroarticular) are usually unaffected by fusion in the mutants (Fig. 1A-J, Table 2), and dermal bone defects are not prominent (Fig. 3A,C).

Hence, we infer that zebrafish *fras1* generates reliable skeletal morphology by stabilizing the development of specific skeletal elements.

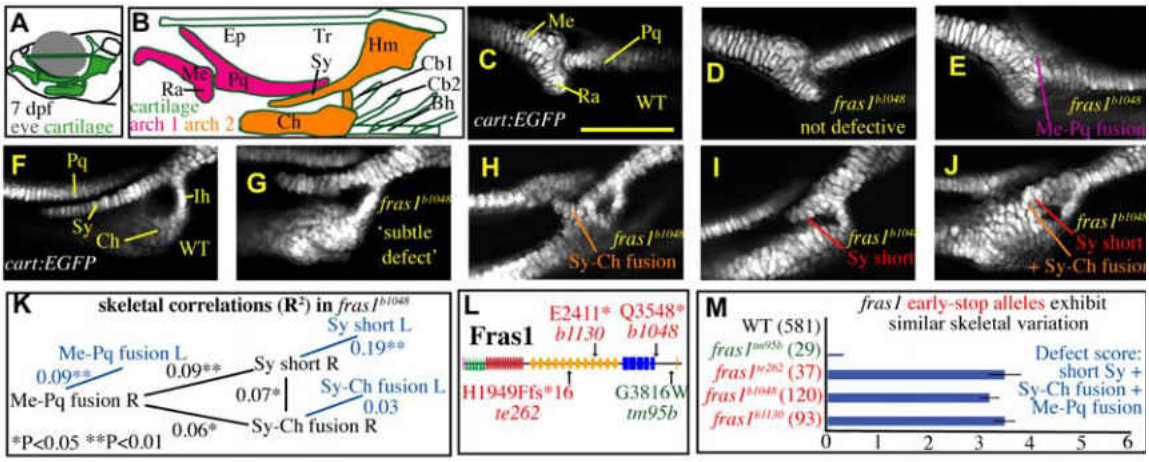

Figure 1: Skeletal defects are variably present in *fras1*^{b1048} mutants. (A) Overview of zebrafish head at 7 dpf, showing cartilage locations. (B) Schematic of cartilages and abbreviations used in this paper. (C-J) *cart:GFP* expression revealing cartilage morphology. Images are single Z sections, tilted for optimal viewing angle in AIM software. Anterior to left, dorsal up. (C) WT first arch skeleton. (D,E) In some *fras1*^{b1048} mutants, the first arch appears (D) very similar to WT, while in others (E) the first arch skeleton appears fused (magenta label) (F) WT second arch cartilages. (G-J) *fras1*^{b1048} mutant second arch cartilages from fish expressing (G) only subtle Sy stacking defects, (H) 'Sy-Ch fusion' (orange label), (I) only 'Sy short' (red label), (J) both 'Sy-Ch fusion' and 'Sy short' phenotypes. (K) Diagram of correlations between skeletal defects, scored using *cart:EGFP* expression, calculated using "contingency analysis" in JMP software. Only weak associations are found between any two comparisons. (L) Diagram of Fras1 protein, and *fras1* alleles, is modified from (Carney 2010). (M) Quantification of cartilage defects in different *fras1* alleles, scored on fish stained with alcian blue/alizarin red. "Defect score": the average sum of Sy-Ch fusion, Sy short, Me-Pq fusion including both sides of a fish. Cartilage abbreviations used in paper: Arch 1 derived (pink): Me: Meckel's cartilage, Pq. Palatoquadrate, Ra. Retroarticular process of Meckel's cartilage. Arch 2 derived (orange): Ch. Ceratohyal, Ih. Interhyal, Hm. Hyomandibular region of hyosymplectic cartilage, Sy. Symplectic extension of hyosymplectic cartilage. Neurocranial cartilages (empty green, Dorsal): Ep. Ethmoid plate, Tr. Trabecula. Posterior cartilages: Cb1 First ceratobranchial cartilage, Cb2 second ceratobranchial cartilage, Bh basihyal. Scale bar: 100 µm.

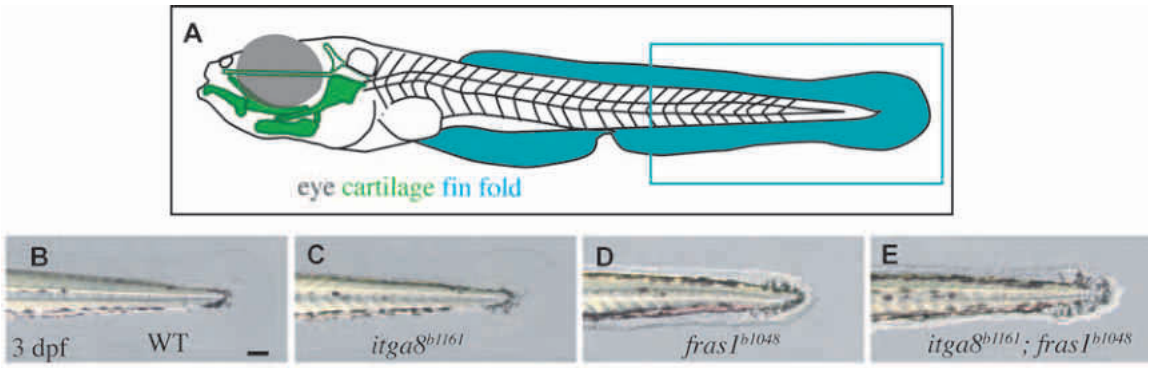

Figure 2: Fin fold defects are not prominent in *itga8*^{b1161} mutants. (A) Schematic depicting the region shown in B-E (teal box). Anterior to left, dorsal up. (B-E) Light microscopy showing that (B) WT fish have a well formed fin fold at 72 hpf, as do (C) *itga8*^{b1161} mutants. In contrast, (D) *fras1*^{b1048} mutants show prominent fin fold defects, as previously described. (E) *fras1*^{b1048};*itga8*^{b1161} mutants show fin fold defects similar to the *fras1*^{b1048} single mutant. Scale bar: 100µm.

	fish #	Defect score	Asymm. score	Me-Pq fusion	Sy-Ch fusion	Sy short
WT	223	**0.0**	**0.0**	2%	0%	0%
***itga8*^{b1161}**	78	**2.1**	**0.4**	36%	18%	51%
***fras1*^{b1048}**	63	**3.7**	**0.3**	60%	50%	72%
***itga8*^{b1161}; *fras1*^{b1048}**	33	**4.4**	**0.5**	77%	55%	88%

Table 1: Penetrance of skeletal defects at 7 dpf. Fish were scored live, using *cart:EGFP* expression to mark cartilages. "Defect score" calculated as in Figure 1. "Asymm. score" also has a scale of zero to one: the absolute value of left minus right defect, summed for the three major cartilage defects, divided by number of fish times three. That is, "A" = ($|\text{Sy short}_{l\text{-}r}| + |\text{Sy-Ch fusion}_{l\text{-}r}| + |\text{Me-Pq fusion}_{l\text{-}r}|$) / 3N. Individual defects are shown as the frequency of occurrence per side.

	fish #	genetic background	Defect score	Me-Pq fusion	Ra reduced	Sy-Ch fusion	Sy short	Ih reduced
WT	581	mixed	0.0	0%	0%	0%	0%	0%
fras1 ^{tm95b}	29	TU	0.3	10%	5%	0%	9%	0%
fras1 ^{te262}	37	TU	3.5	57%	14%	59%	59%	4%
fras1 ^{b1048}	93	ABXWIK	3.2	52%	0%	54%	55%	10%
fras1 ^{b1130}	120	EK	3.5	33%	2%	83%	56%	3%

Table 2: Three *fras1* alleles cause similar skeletal defects. Shown are penetrance of skeletal defects per side of 7 dpf fixed fish stained with Alcian blue and alizarin red. Defect score is the same data shown graphically in Fig. 1. Genetic background of each allele is indicated. WT data comes from combined scoring of WT siblings of the mutant fish shown in this table. Thus, WT data contains scoring from each genetic background.

itga8 mutants have skeletal defects similar to *fras1* mutants

During our screen for craniofacial mutants, we also uncovered a second mutant, *b1161*, showing skeletal defects very similar to *fras1* mutants (Fig. 3A-C), though lacking fin fold defects (Fig. 2). All three *fras1* mutant skeletal phenotypes are seen in *b1161* mutants (Fig. 3B), with similar levels of fluctuating asymmetry (Table 1). *b1161* mutants occasionally survive to adulthood, and the progeny of homozygous incrosses show phenotypic variation similar to heterozygous incrosses (Table 3), eliminating maternal effect as a source of *b1161* phenotypic variation. Bulked segregant analysis using RAD-tagged SNPs (Floragenex) (Baird et al., 2008) places *b1161* on a 10 mb region of linkage group 16 (Fig. 3E). Finer mapping on individual fish locates *b1161* to a smaller interval containing *itga8* (Fig. 3E). Sequencing of both *itga8* cDNA and *itga8* genomic DNA reveals that *b1161* mutants contain a complex lesion in exon 25 of *itga8* (Fig. 3F). The mutation in *itga8* tightly linked to *b1161* results in cDNA frameshifted midway through the integrin alpha domain (Fig. 3G), indicating a strong loss of *itga8* gene function. In support of our interpretation that *b1161* phenotypes are caused by loss of *itga8* function, all *b1161* cartilage phenotypes are also seen in WT fish injected with morpholinos to *itga8,* though *itga8* morpholino phenotypes are less specific than *itga8*^{b1161} (Table 3). Hence, we conclude that skeletal phenotypes in *b1161* are caused by *itga8* mutation. The similarity of cartilage defects in *fras1* and *itga8* mutants suggest that these two genes may function in the same genetic pathway during facial development.

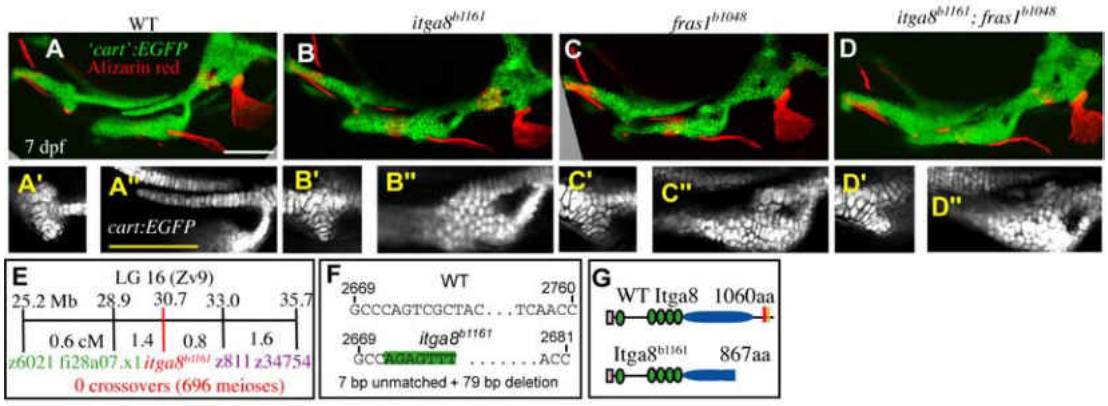

Figure 3: Skeletal defects in *itga8* and *fras1;itga8* mutants appear similar to *fras1* mutants. (A-D) Confocal projections showing bone (Alizarin red stain) and cartilage (*cart:EGFP* expression), with GFP channel shown magnified confocal sections (A'-D', A''-D'') to highlight cartilage morphology at joint regions. Similar cartilage defects are seen in (B) *itga8*^{b1161}, (C) *fras1*^{b1048}, and (D) *itga8*^{b1161}*;fras1*^{b1048} mutants, including (A'-D') M-Pq fusion, (A''-D'') Sy-Ch fusion with short Sy. (E) Linkage analysis reveals no crossovers between *b1161* phenotypes and the *itga8*^{b1161} lesion. Markers in purple map to the north of *som*, and markers in green map to the south of *b1161*. (F) Diagram illustrating the complex *itga8*^{b1161} lesion in exon 25, which contains 7 bp of sequence unmatched to WT, followed by a 79 bp deletion. (G) Diagram of Itga8 protein in WT and *itga8*^{b1161} mutants. Pink box is a signaling motif, green circles are integrin beta domains, blue oval is integrin alpha domain, red box is the transmembrane domain, and orange box is an intracellular integrin domain. Scale bars: 100 µm. Scale bar in A is applicable to A-D. Scale bar in B is applicable to A'-D' and A''-D''.

	fish #	average defects	Me-Pq fusion	Sy-Ch fusion	Sy short	Ra reduced	Ih reduced	Hm defect	Pq red.	Sy "float"	Ch rotated	Edema
WT uninjected	431	0.0	0%	0%	1%	0%	0%	0%	0%	0%	0%	1%
itga8 mismsatch-MO 3 mg/ml	74	0.1	0%	0%	3%	1%	0%	2%	1%	1%	0%	3%
*itga8*TB-MO 1 mg/ml	240	0.7	3%	1%	31%	2%	1%	7%	0%	0%	1%	2%
*itga8*E25I25-MO 1 mg/ml	145	0.1	4%	0%	1%	1%	0%	3%	1%	0%	14%	1%
*itga8*E25I25-MO 1 mg/ml plus *itga8*TB-MO 1 mg/ml	134	2.4	43%	8%	69%	18%	14%	33%	6%	3%	38%	17%
*itga8*TB-MO 3 mg/ml	131	1.8	27%	7%	55%	13%	7%	24%	5%	5%	17%	12%
itga8^{b1161} homozygous incross	68	2.5	26%	57%	42%	2%	0%	0%	0%	0%	0%	0%

Table 3: *itga8* morpholino causes all phenotypes seen in *itga8*^{b1161} mutant, though with less specificity. Shown are penetrance of skeletal defects per side of 7 dpf fixed fish stained with Alcian blue and alizarin red. WT data comes from the combined scoring of WT fish in each experiment shown in this table. Morpholino data comes from a minimum of three separate days of injection, performed in parallel, with a minimum of three replicates. The three independent injections each produced consistent results for all morpholinos, and the combined data from all experiments is shown in this table. Injection of *itga8* translation blocking morpholino (*itga8*TB-MO) produces dose-dependant skeletal phenotypes. Injection of *itga8* mismatch-MO, a variant of to *itga8*ATG-MO with

5 bp scrambled, produces no cartilage phenotypes. Injection of splice blocking morpholino targeting the *itga8* exon25-intron25 junction (*itga8*E25I25-MO), disrupts ~50% of WT mRNA splicing (data not shown), but produced no specific phenotypes alone. However, co-injection of *itga8E25I25*-MO with a low-dose of *itga8ATG*-MO produces more-than-additive skeletal defects. Defect score (red numbers) is calculated using only the phenotypes seen frequently in *itga8* and *fras1* mutants (green numbers), as described in Fig. 1. In morpholino injected fish, half of the cartilage fusions look identical to *itga8*^{b1161} fusions, but half of the morpholino induced cartilage fusions affect a broader region than those seen in *itga8*^{b1161} mutants (eg- increased penetrance of Ih and Ra reduction: blue numbers). In addition, *itga8* morpholinos sometimes cause defects in structures unaffected by *itga8*^{b1161} mutants (purple numbers): hyomandibular shape defects (Hm defect), reduction of posterior palatoquadrate cartilage (Pq red), a gap between the hyomandibular cartilage plate and the symplectic region (Hs gap), misoriented ceratohyal cartilage (Ch rotated), and edema. The differences between morpholino injected fish and mutants cannot be accounted for by maternal transcripts; homozygous *itga8*^{b1161} larvae born from homozygous *itga8*^{b1161} mutant parents show only the phenotypes of *itga8*^{b1161} mutants with heterozygous parents, (Fig. 1, Table 1).

Skeletal morphology in *itga8*^{b1161}*;fras1*^{b1048} is similar to both single mutants

fras1^{b1048}*;itga8*^{b1161} double mutants show skeletal phenotypes similar to the single mutants (Fig. 3D). While the *fras1*^{b1048}*;itga8*^{b1161} phenotypic penetrance is slightly greater than single mutant penetrance (Table 1); this slight increase in double mutant skeletal phenotypes is less than additive, and may be due to small double mutant sample size. Fluctuating asymmetry is present in *fras1*^{b1048}*;itga8*^{b1161} double mutants, at levels similar to either single mutant (Table 1). Because all aspects of skeletal defects in the double mutant *itga8*^{b1161}*;fras1*^{b1048} are comparable to either single mutant, we propose a model wherein Fras1 and Itga8 proteins interact in a protein complex during zebrafish facial development. Such a model is consistent with the previous observation that mammalian Itga8 adheres to a member of the Fras/Frem complex (Kiyozumi et al., 2005).

itga8 expression in pharyngeal arch mesenchyme is flanked by epithelial *fras1* expression

The genetic interaction between *fras1* and *itga8* suggests that these genes should be expressed in either the same tissue, or else in interacting tissues. On tissue sections from 60 hpf fish, *itga8* expression is seen in arch mesenchyme, but not epithelia surrounding arches (Fig. 4A-D). Four *itga8* probes covering separate regions of the *itga8* transcript reveal the same expression patterns (data not shown). At 60 hpf, *itga8* is co-

expressed with the mesenchymal marker (Akimenko et al., 1994; Kimmel et al., 2001) *dlx2a* (Fig. 4A) but not *col2a1* (Fig. 4B,C) a cartilage marker (Yan et al., 1995) or *fras1* (Fig. 4A-C). Consistent with previous reports (Carney et al., 2010; Gautier et al., 2008), zebrafish *fras1* expression is prominent in ectoderm and endoderm surrounding pharyngeal arches at 60 hpf (Fig. 4A-C,F). Whereas *itga8* mRNA expression appears normal in *fras1*^{b1048} mutants (Fig. 4D,E), *fras1* mRNA labeling appears somewhat stronger in *itga8*^{b1161} mutants (Fig. 4F,G). The slight increase in *fras1* expression seen in *itga8*^{b1161} mutants could indicate that *itga8* represses *fras1*. However, we were unable to detect a pronounced difference in anti-zebrafish-Fras1 (Carney et al., 2010) labeling between WT and *itga8*^{b1161} mutants (Fig. 4H,I). Thus, if present, repression of *fras1* mRNA by *itga8* does not produce prominent effects on protein levels. Two antibodies to human ITGA8 were tested on zebrafish (SCBT H-180, Sigma-Aldrich HPA003432), neither of which showed specific expression patterns. In WT zebrafish Fras1 protein is basal to epithelia surrounding pharyngeal arches (Fig. 4H), consistent with previous reports of zebrafish Fras1 localization to basal laminae (Carney et al., 2010). Basal localization of Fras1 protein is maintained in *itga8*^{b1161} mutants (Fig. 4I), at similar levels to WT. In contrast, anti-Fras1 label is strongly reduced in *fras1*^{b1048} and *itga8*^{b1161}*;fras1*^{b1048} mutants (Fig. 4J,K), consistent with loss of Fras1 protein in these mutants. These expression analyses indicate that *itga8* and *fras1* are expressed in mesenchyme and epithelia respectively, independent of one another.

itga8 and *fras1* mutants consistently display defects in facial epithelia at 72 hpf

Mammalian *Fras1* and *Itga8* both have well studied roles in epithelial morphogenesis [e.g. (Muller et al., 1997; Vrontou et al., 2003)] prompting us to examine facial epithelia in *fras1* and *itga8* mutants. At 72 hpf *fras1*^{b1048} mutants, *itga8*^{b1161} mutants, and *fras1*^{b1048}*;itga8*^{b1161} mutants show pronounced endoderm defects (Figs. 4, 5). In 72 hpf WT the first endodermal pouch encountered along the A-P axis (called "late-p1" for reasons discussed below) separates palatoquadrate and symplectic cartilages from the ceratohyal cartilage, connecting medial endoderm to ectoderm (Fig. 5A,B,D,H). However, *fras1*^{te262} (not shown), *fras1*^{b1048}, *itga8*^{b1161} and *fras1*^{b1048}*;itga8*^{b1161} fish each

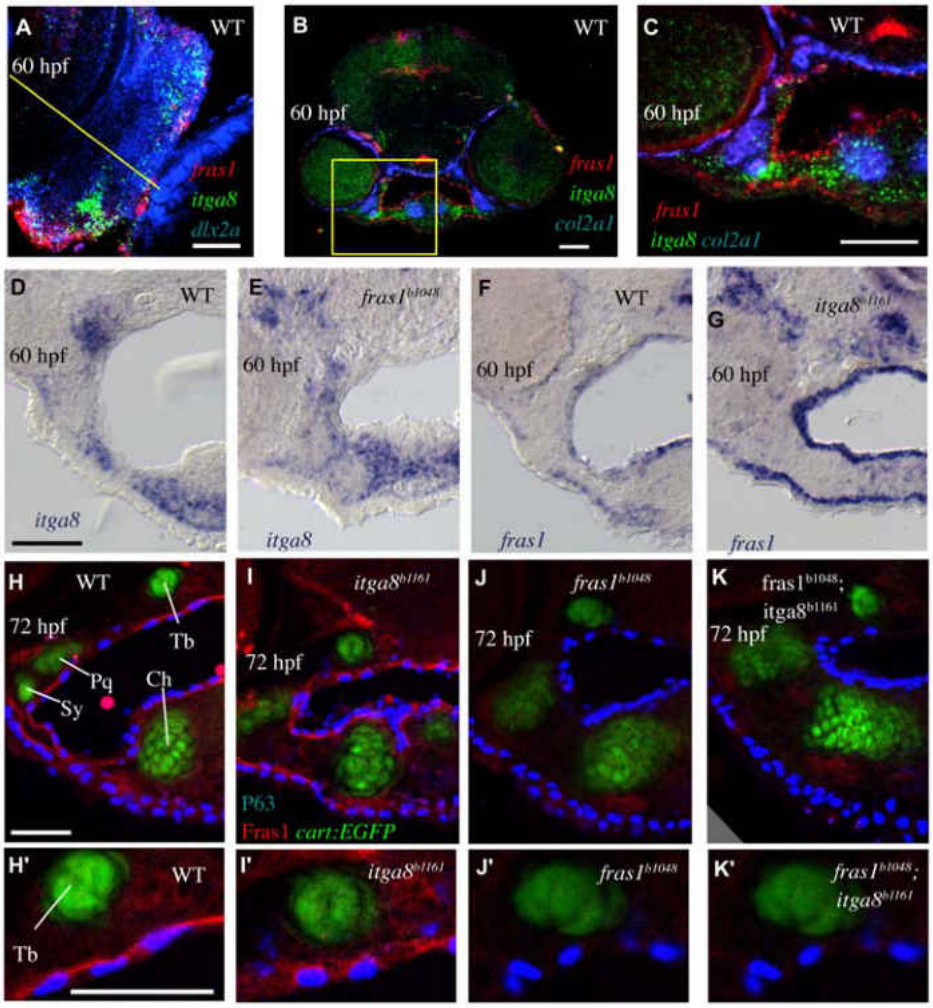

Figure 4: *fras1* and *itga8* are independently expressed in separate, but adjacent, facial tissues. (A) Sagittal confocal section of fluorescent whole mount RNA in situ shows that *itga8* is expressed in mesenchyme along with *dlx2a*, but *itga8* is not expressed with the epithelial marker *fras1*. Anterior to left, dorsal up. Yellow line indicates level of tissue sections used for images in (B-K). (B) Low magnification transverse section, dorsal up, with the area magnified in C-K boxed in yellow. (C-K) Transverse sections of tissues, lateral to left, dorsal up. (B, C) Fluorescent RNA in situ on transverse section at (B) low and (C) higher magnification, confirms *fras1* expression in both endoderm and ectoderm, with *itga8* expressed in adjacent mesenchyme. (B,C) *itga8* is not co-expressed with the cartilage marker *col2a1*. (D-G) RNA in situ hybridization on transverse section, developed with NBT/BCIP label. (D,E) Expression of *itga8* mRNA appears similar in WT and *fras1*^{b1048} mutants. (F,G) *fras1* mRNA labeling is somewhat stronger in *itga8*^{b1161} mutants than in comparable WT sections. (H-K) anti-Fras1 and anti-P63 labeling on sections from *cart:EGFP* expressing fish. In (H) WT and (I) *itga8*^{b1161} mutants, Fras1 is seen basal to the epithelial marker P63. Fras1 labeling is strongly reduced in (J) *fras1*^{b1048} mutants, and (K) *itga8*^{b1161};*fras1*^{b1048} mutants. (H'-K') High resolution detail of panels H-K. All scale bars: 50 μm. Scale bars in D, H, H' are applicable to their respective rows.

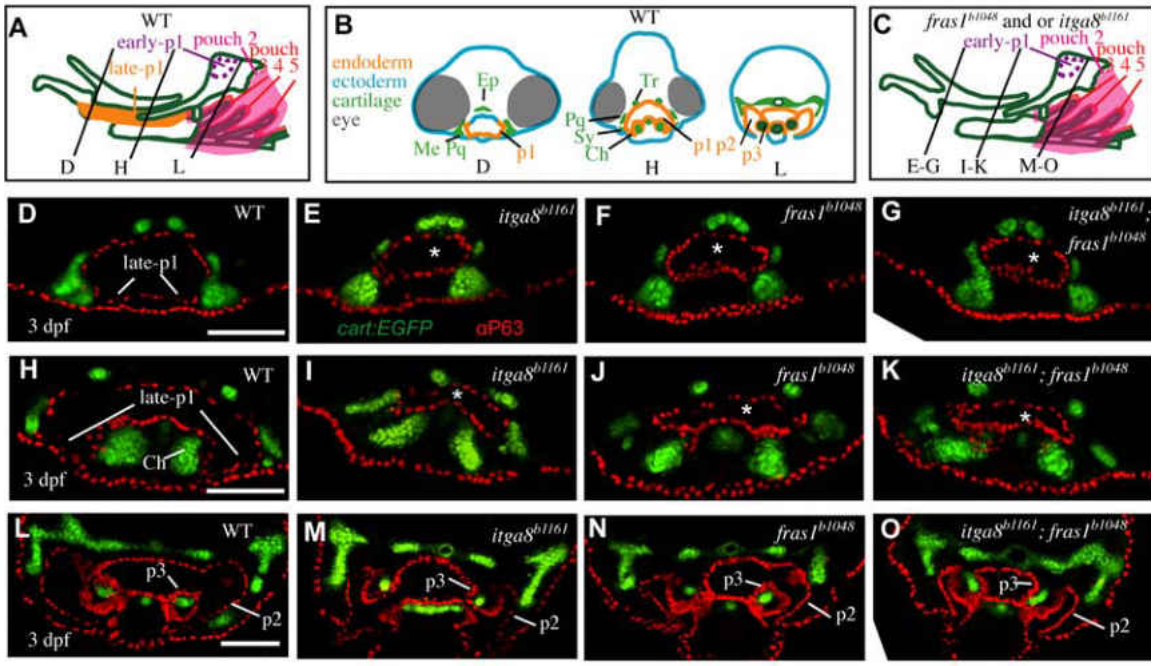

Figure 5: *fras1*^{b1048}, *itga8*^{b1161}, and *fras1*^{b1048};*itga8*^{b1161} mutants show pouch 1 defects at 72 hpf. (A-C) Illustrations of endoderm and cartilage, on (A,B) WT, and (C) mutant fish; viewed in (A,C) sagittal or (B) transverse section. (D-O) Tissue sections labeled with anti-P63 (epithelia) and *cart:GFP*, taken from the section level of of (D-G) meckels-palatoquadrate joint, (H-K) symplectic cartilage, and (L-O) opercular flap. (I-T) *itga8*^{b1161}, *fras1*^{b1048}, and *itga8*^{b1161};*fras1*^{b1048}mutants each exhibit similar loss (asterisk) of late-p1, but not pouches two or three. Scale bars (D,H,L): 100 µm. Each scale bar is applicable to its row.

specifically lack the first endodermal pouch at 72 hpf (Fig. 5A-G). The similarity of *fras1*^{b1048};*itga8*^{b1161} double mutant endoderm phenotypes to both single mutants is further evidence consistent with the hypothesis that both genes function in a shared protein complex. In 72 hpf WT fish, the first endodermal pouch extends from the retroarticular process to the interhyal cartilage, and this endodermal region remains medial in *fras1* (not shown) and *itga8*^{b1161} (Movie 1) mutants. In contrast to this pronounced pouch 1 defect, posterior pouches appear normal in *fras1*, *itga8* mutants: the opercular flap (pouch two) and gill arches (pouches 3-7) are present in *itga8*^{b1161} and *fras1*^{b1048} mutants at 72 hpf (Fig. 5L-O). All *fras1*^{b1048} (N=8), *fras1*^{te262} (N=8), and *itga*^{8b1161} (N=15) mutants examined show similar defects in pouch 1 at 72 hpf. These results indicate that both *fras1* and *itga8* are required for pouch 1 morphogenesis.

fras1 and *itga8* are specifically required for late-p1 formation

Although *fras1/itga8* mutants show pronounced defects in pouch 1 at 72 hpf, pouch structure looks normal in these mutants at 36 hpf (Fig. 6), indicating that the *fras1/itga8* dependant endoderm morphogenesis occurs between 36 and 72 hpf. The expression pattern of *fras1* mRNA in epithelia and *itga8* mRNA in mesenchyme is found throughout this 36 to 72 hpf period (Figs. 7,8A-F). At 36 hpf, *itga8* is seen throughout neural crest derived arch cells, however *itga8* expression is lost in differentiated cartilage cells (Fig. 7). In WT fish at 36 hpf , a tube of endoderm is medial to the first two arches (Fig. 8A,D,G), with an early forming portion of pouch one separating the dorsal regions of arch one from arch two (Fig. 6). This early forming portion of pouch 1 appears to contribute primarily to a dorsal structure medial to the hyomandibular cartilage (Fig. 7). Between 36 hpf and 72 hpf, large portions of WT medial endoderm continues to move latero-ventrally, separating ventral arch 1 from dorsal arch 2 (Fig. 8A-I). Ectoderm remains flat over arches between 36 and 72 hpf, indicating that the connection of late-p1 to ectoderm occurs via endoderm protrusion, rather than an ectodermal ingression (Fig. 7, 8A-I). Live imaging confirms that WT fish form late-p1 through lateral migration of medial endoderm (Movie 2). In contrast, *fras1*^{b1048} mutants fail to show lateral movement of medial endoderm (Fig. 8J-L). Lateral endoderm movement in WT fish can be quantified by decreases in the distance between endoderm and ectoderm through this time (Figs. 8,9, blue lines). In contrast, endoderm-ectoderm distance remains constant in *fras1*^{b1048} and *itga8*^{b1161} mutants (Fig. 8M). We note that, similar to skeletal phenotypes, there is variation in the degree of mutant endoderm defects (Fig. 8M). However, unlike skeletal phenotypes, endoderm in all mutant fish examined appears substantially different from WT fish by 72 hpf (Fig. 8M). Even at 84 hpf, endoderm-ectoderm distances remain large in *fras1*^{b1048} mutants, indicating that the failure of endoderm movement is not simply due to developmental delay (Fig. 8M). These analyses support our hypothesis that the facial epithelial defects seen in *fras1* and *itga8* mutants at 72 hpf are caused by specific failure of late-p1 formation.

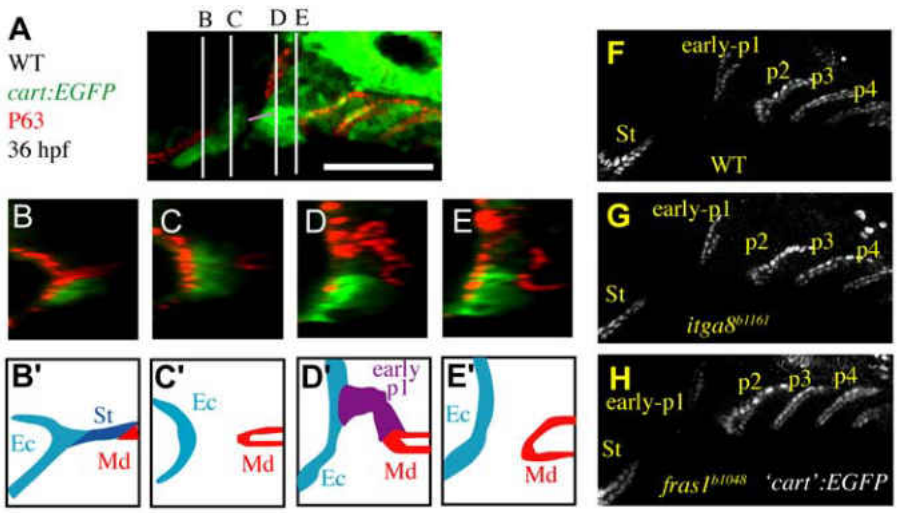

Figure 6: At 36 hpf, *fras1* and *itga8* endoderm morphology looks similar to WT. (A) Confocal section of WT with pre-cartilage cells labeled with *cart:EGFP* and P63, anterior to left, dorsal up. Lavendar line indicates the length measured for 36 hpf "Sy length". White lines indicate section levels for B-E. (B-E) Four confocal transverse sections reconstructed from the confocal stack in A. Lateral to the left, dorsal up. (B'-E') Illustration of tissue . Sections shown are from levels in A. (B) Level of stomadeum, (C) Middle of arch 1, (D) Level of pouch 1, (E) Middle of arch 2. At 36 hpf, a tube of endoderm lies medial to the length of arches; early early-p1 separates dorsal A1 from A2, while posterior pouches fully separate posterior arches (F-H) Confocal sections shown anterior to left, dorsal up. Panel F shows the same as fish as panel A, but without lines or GFP expression, to clarify epithelial morphology. (F) WT pouch structure is similar to (G) *itga8*^{b1161} and (H) *fras1*^{b1048} pouch structure at 36 hpf. Abbreviations: Ec surface ectoderm, Md medial endoderm, p1 pouch 1, p2 pouch 2, p3 pouch 3, p4 pouch 4, St stomadeum. Scale bar: 100 µm.

Figure 7: Developmental series of *fras1* and *itga8* mRNA expression on tissue sections. (A-H) Transverse sections, dorsal up. Sections are tilted, placing the left side of each section posterior to the right side. Sections are selected to illustrate both early pouch 1 (left side) and the approximate region of late pouch 1 shown in other figures (right side). (A-D) *fras1* expression is seen in epithelia surrounding pharyngeal arches at (A) 36 hpf, (B) 48 hpf, (C) 60 hpf, (D) 72 hpf. The early forming portion of pouch 1 appears to remain dorsal (early-p1), while the late forming portion of pouch 1 protrudes ventrally (late-p1). (E-H) *itga8* expression is seen in arch mesenchyme, but not cartilage or epithelia. At each stage examined, arrows drawn perpendicular to epithelia adjacent to prominent *itga8* expression suggest the direction of endoderm movement over the next 12 hours. Scale bar: 100 µm.

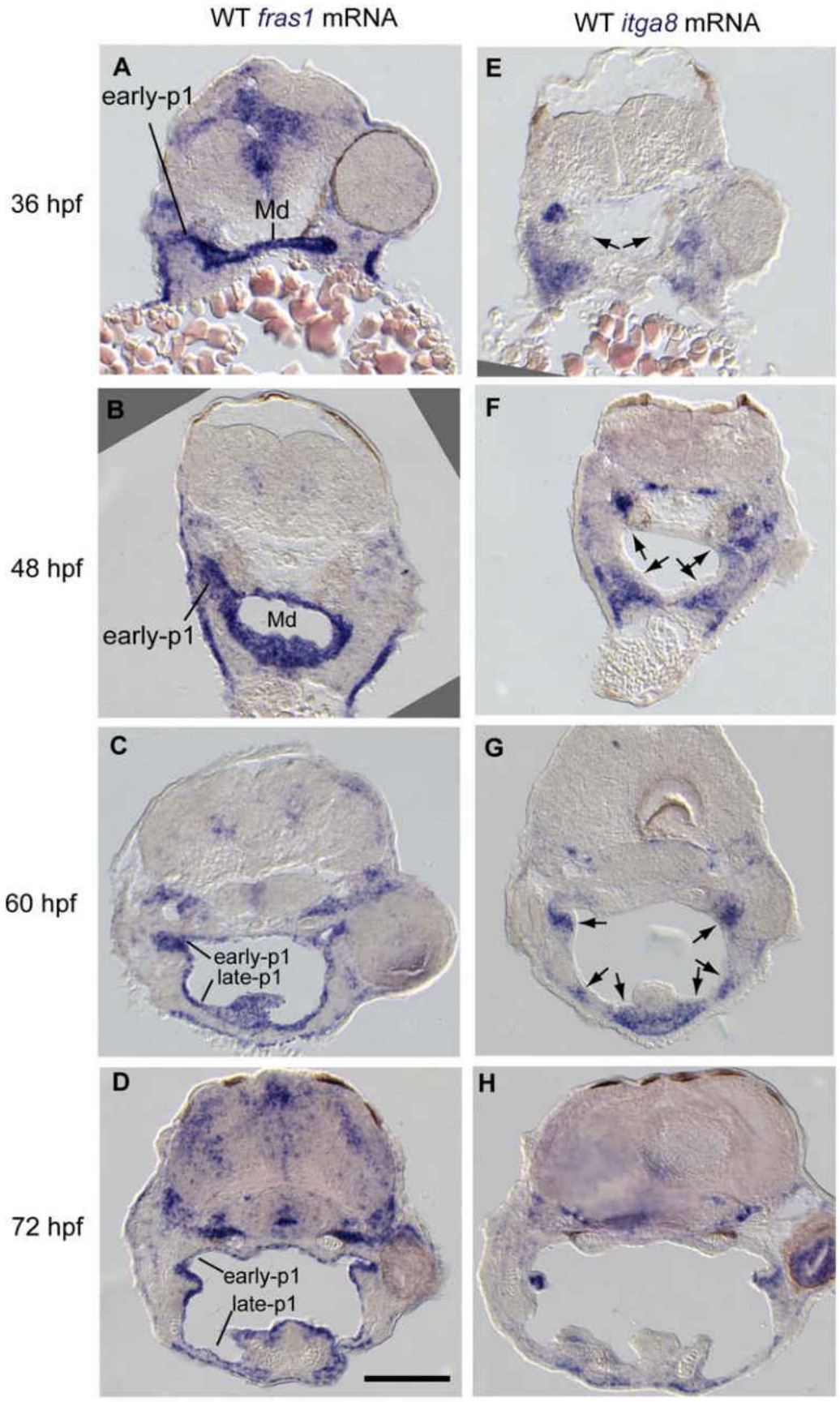
WT fras1 mRNA
WT itga8 mRNA
36 hpf
48 hpf
60 hpf
72 hpf
A
early-p1
Md
E
B
Md
early-p1
F
C
early-p1
late-p1
G
D
early-p1
late-p1
H

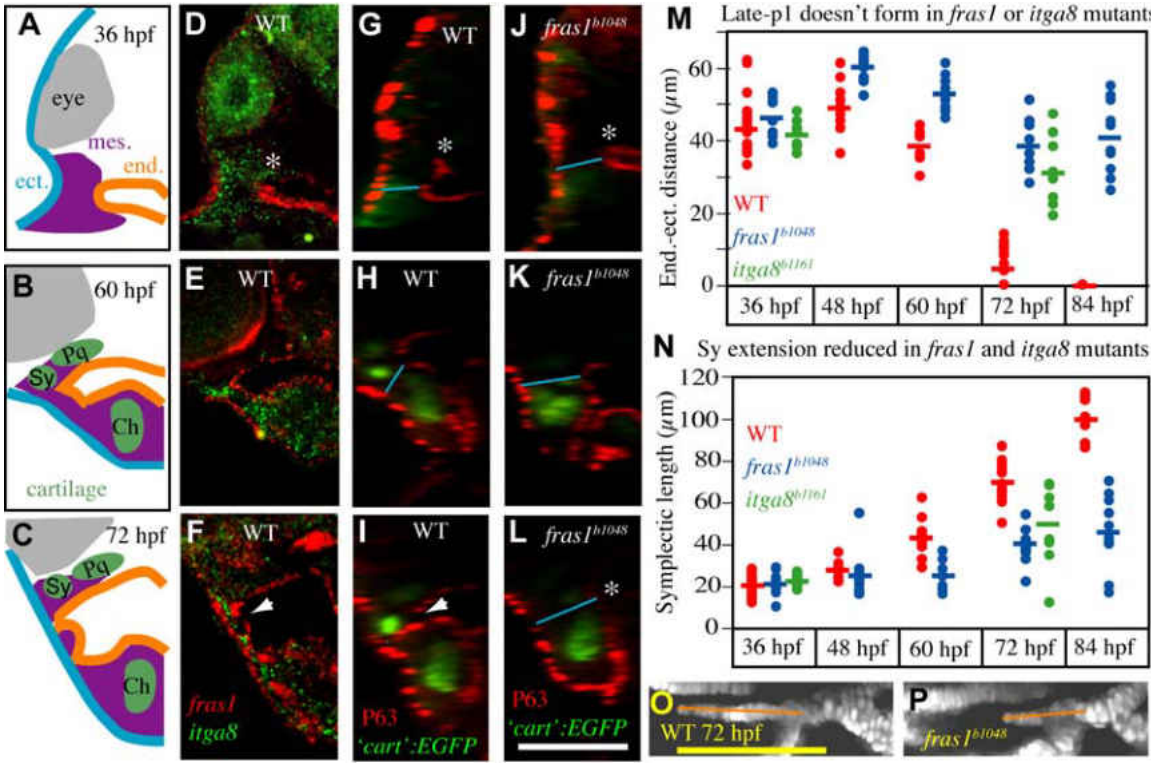

Figure 8: In *fras1*^{b1048} and *itga8*^{b1161} mutants, late-P1 defects and symplectic length defects develop during the same time period. (A-C) Schematics of transverse sections shown in D-L at (A) 36 hpf, (B) 60 hpf, and (C) 72 hpf. Schematic show ectoderm (teal), arch mesenchyme (purple), endoderm (orange), cartilage (green), and eye (grey). (D-F) RNA in situ hybridization on tissue sections, illustrating *fras1* expression in epithelia surrounding arches and *itga8* expression in arch mesenchyme, from 36 to 72 hpf. (G-L) Confocal transverse section reconstructed from Z-stacks, illustrating that WT endoderm (G-I) protrudes laterally between 36 and 72 hpf (arrowheads), whereas endoderm in (J-L) *fras1*^{b1048} mutants viewed at the equivalent section remains medial (asterisk). (M,N) Measurements of (M) endoderm-ectoderm distances and (N) Sy lengths, taken from the same fish. Graphs show individual measurements as dots, and horizontal bars illustrate the mean of each group. (M) The minimum distance between endoderm and ectoderm was measured as illustrated in G-L (teal lines) on randomly selected fish. (N) Symplectic length measured from the center of interhyal to the anterior tip of the symplectic. (M) Whereas WT fish decrease their endoderm-ectoderm distance from 36 to 84 hpf, *fras1*^{b1048} and *itga8*^{b1161} mutants maintain a relatively constant endoderm-ectoderm distance through this time course. (O,P) Confocal section of 72 hpf symplectic cartilage, labeled with *cart:EGFP*, oriented anterior to left, dorsal up. Orange lines illustrate Sy length measurements. In (O) WT fish, Sy is typically longer than in (P) *fras1*^{b1048} mutants. Scale bars: 100 μm. Bar in L applies to A-L, Bar in O applies to O,P.

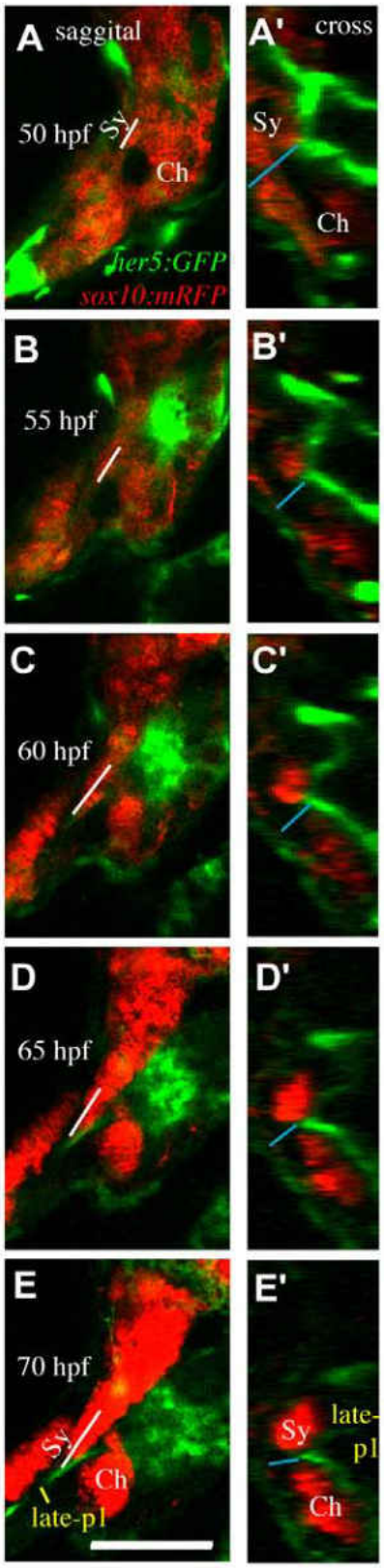

Figure 9: Time lapse microscopy shows WT symplectic extension concurrent with endoderm migration. (A-E') *sox10:mRFP* labels cartilages, *her5:GFP* labels endoderm and some neural cells. Still images from time-lapse microscopy showing symplectic growth (white line), and endoderm-ectoderm distance (blue line) from 50 to 70 hpf. (A-E) Confocal section, anterior to left, dorsal up. Images centered using StackReg in ImageJ. By 70 hpf, Sy extends out of the plane of section. (A'-E') Transverse sections, lateral to left, dorsal up, constructed from the same confocal stacks. Between 50 and 70 hpf, the endoderm moves laterally through a region between symplectic and ceratohyal cartilages. Time lapse imaged fish are slightly developmentally delayed, resulting in a mild reduction of endoderm migration and cartilage growth by 70 hpf. Scale bar: 100 µm.

Symplectic extension occurs concurrent with late-p1 formation

fras1 and *itga8* mutants exhibit both skeletal and epithelial defects in the same region of the pharyngeal arch, leading us to investigate the spatio-temporal relationship of cartilage and endoderm defects. In WT fish, Sy extension occurs concurrent with late-p1 formation (Fig. 8M-P), an observation confirmed through time-lapse microscopy of WT fish co-expressing skeletal and endodermal markers (Fig. 9A-E, Movie 2). In WT fish, symplectic cells migrate out of the path that endoderm will follow during late-p1 formation (Movie 2), further indicating a connection between these two processes. In *fras1*^{b1048} and *itga8*^{b1161} mutants, symplectic length does not extend as rapidly as WT symplectic length between 48 to 72 hpf (Figs. 8, 9); the same time period that endoderm defects become apparent in *fras1*^{b1048} and *itga8*^{b1161} mutants (Fig. 8M,N). When WT, *fras1*^{b1048}, and *itga8*^{b1161} mutants were scored at 3.5 dpf (~76 hpf),

and then the same fish are re-scored at 4.5 dpf, and 7.5 dpf, there is little change in the penetrance of shortened symplectic cartilages (Table 4). Hence, it appears that symplectic length defects form in the same time and place as late-p1 defects, and are stable thereafter.

		fish #	Defect score	Me-Pq fusion	Sy-Ch fusion	Sy short
WT	3.5 dpf	142	0.1	3%	0%	0%
	4.5 dpf	142	0.0	0%	0%	0%
	7.5 dpf	142	0.0	0%	0%	1%
fras1^{b1048}	3.5 dpf	32	3.5	78%	9%	86%
	4.5 dpf	32	4.1	83%	39%	84%
	7.5 dpf	32	4.5	83%	56%	84%
itga8^{b1161}	3.5 dpf	18	1.9	53%	0%	42%
	4.5 dpf	18	1.6	33%	6%	42%
	7.5 dpf	18	2.2	44%	22%	42%

Table 4: Second arch cartilage fusion usually occurs after 3 dpf in *fras1* and *itga8* mutants. Fish were scored live at 3.5 dpf, and then the same fish were re-scored at 4.5 dpf and 7.5 dpf. Defect score and individual defect percent calculated as in Figure 1.

Endoderm defects in *fras1* and *itga8* mutants precede second arch skeletal fusion

Although the short symplectic phenotype occurs concurrent with late-p1 formation, second arch cartilage fusion often occurs well after late-p1 formation (Table 4). At 3.5 dpf, after late-p1 formation occurs in WT, second arch cartilage fusions are rarely present in *fras1* and *itga8* mutants (Fig. 10A,B, Table 2). When the same fish are re-scored at 4.5 dpf, the penetrance of second arch cartilage fusions has increased in both *fras1* and *itga8* mutants (Table 4). A further increase in second arch cartilage fusion is seen when the *fras1* and *itga8* mutant fish are then re-scored at 7.5 dpf (Fig. 10A-D, Table 4). In contrast to symplectic length defects, in which mutant symplectic cartilages resemble younger, unextended, WT symplectic cartilages, we could find no WT stage

with the type of second arch cartilage fusions seen in *fras1* and *itga8* mutants (Movie 3). Instead, time-lapse microscopy of cartilage development in *fras1*^{b1048} mutants shows collision of symplectic to ceratohyal cartilages, after these two elements have separated (Movie 4), a process never seen in WT development (Movie 3). Hence, we infer that *fras1*^{b1048} mutant symplectic length defects typically occur during a different developmental window than symplectic length and late-p1 defects.

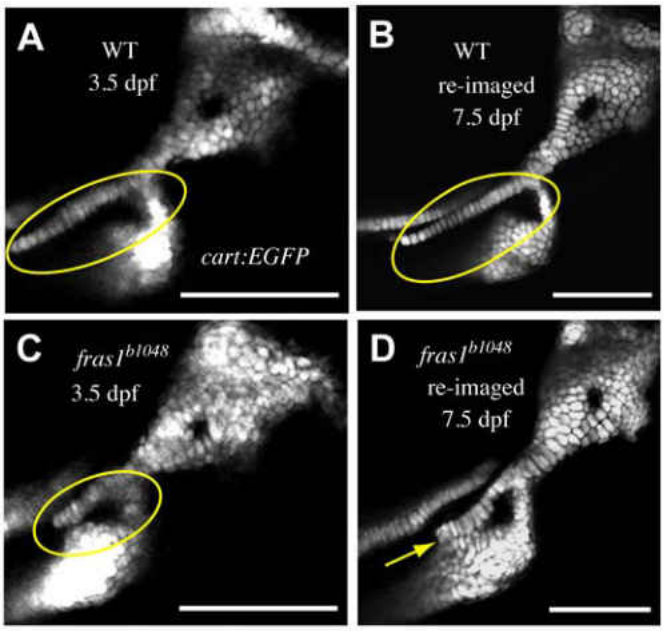

Figure 10: Second arch cartilages can fuse after 3 dpf. (A-D) Confocal sections of (A) WT or (C) *fras1*^{b1048} mutants at 3.5 dpf, and (B,D) the same fish re-imaged at 7.5 dpf. (A-D) Images are shown anterior to left, dorsal up. Note that at (C) 3.5 dpf *fras1*^{b1048} has a space between symplectic and ceratohyal cartilage (yellow oval), but at (D) 7.5 dpf, these elements are fused together (arrow). Scale bars: 100 µm.

WT endoderm rescues *fras1* mutants

Because *fras1* is expressed in both facial ectoderm and endoderm (Gautier et al., 2008), and *fras1* mutants exhibit a specific endoderm morphogenesis defect, we hypothesize that endodermal *fras1* function is critical to facial morphogenesis. To test this hypothesis, we performed reciprocal transplants of WT and *fras1* mutant endoderm (Fig. 11). WT endoderm that is transplanted into a WT host undergoes normal morphogenesis, as does the facial skeleton in these mosaics (19/19 transplants, Fig. 8A). *fras1* mutant hosts containing *fras1* mutant endoderm display characteristic loss of late-P1 (6/6 transplants, Fig. 11C), and the skeletal variation expected for non-mosaic *fras1* mutants (Tables 1,2,4). When WT endoderm is transplanted into *fras1* mutant hosts, both endoderm shape and cartilage shape appear similar to that seen in WT to WT transplants (7/7 transplants, Fig. 11B), indicating that endodermal expression of WT *fras1* is

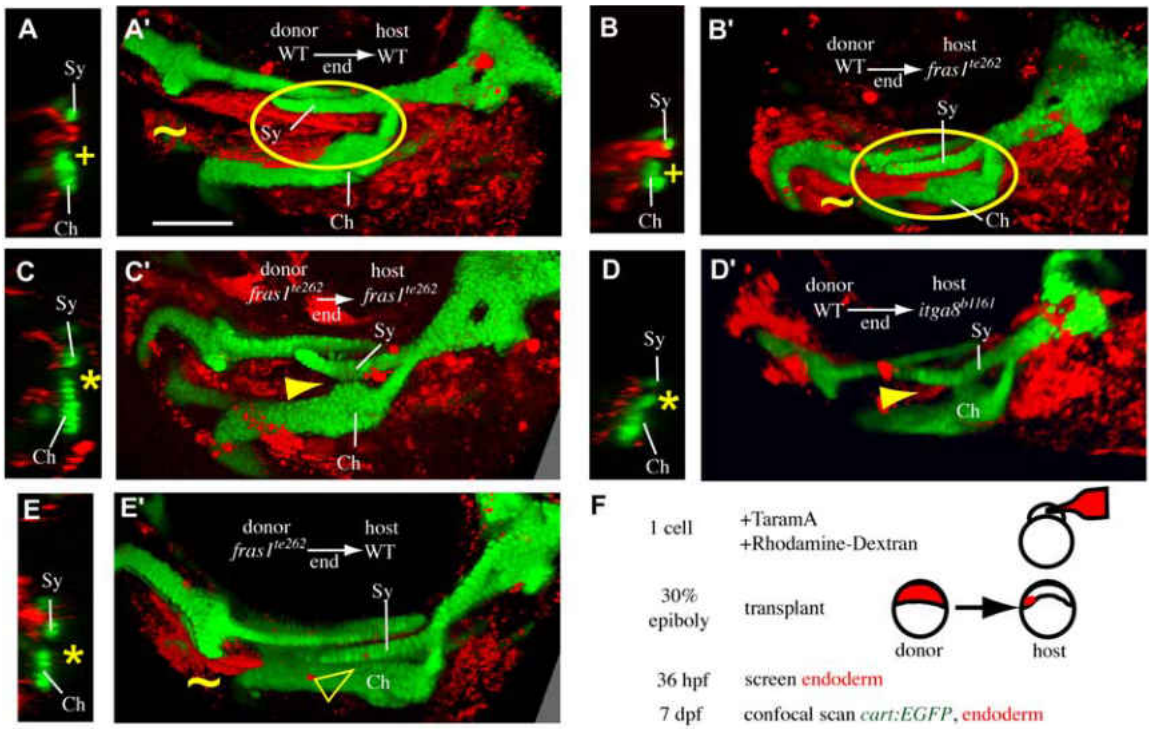

Figure 11: Transplantation reveals that WT, endoderm can rescue *fras1*, but not *itga8* mutants. (A-E) Confocal transverse sections taken at a section level midway through Sy length at 7 dpf. Medial to the left, dorsal up. In (A) WT→WT and (B) WT→*fras1*^{b1161} mosaic fish, late-P1 protrudes between Sy and Ch (plus sign). However in (C) and *fras1*^{te262}→*fras1*^{te262} and (D) WT→*itga8*^{b1161} mosaics, endoderm remains medial to Sy and Ch (asterisk). (E) Half of the *fras1*^{te262}→WT mosaics examined exhibited defective endoderm medial to Sy and Ch. (A'-E') Rendered confocal stacks show endoderm and skeletal morphology along the A-P axis. Anterior to the left, dorsal up. Image rendering makes both tissues opaque, allowing visualization of endoderm covering separated Sy and Ch cartilages (circles) found n (A') WT→WT transplants and (B') WT→*fras1*^{te262} transplants. Fused cartilages covering endoderm (arrowheads) in (C') *fras1*^{b1048}→*fras1*^{b1048} transplants, and (D') WT→*itga8*^{b1161} transplants. In (E') *fras1*^{te262}→WT transplants, despite the lack of endoderm separating the Sy Ch region, cartilages were not fused (open arrowhead), perhaps due to the presence of lateral endoderm in the first pharyngeal arch (tilde). (F) Overview of transplantation protocol. Scale bar: 100 μm.

sufficient for *fras1* function in facial morphogenesis. In contrast, WT endoderm fails to rescue either the endoderm or skeletal defects of *itga8* mutant hosts (4/4 hosts Fig. 11D). Failure of WT endoderm to rescue *itga8*^{b1161} mutants is consistent with our finding that *itga8* is expressed in mesenchyme, not endoderm. When *fras1* mutant endoderm is transplanted into WT hosts, endoderm defects are sometimes seen in the second

pharyngeal arch (6/12 hosts, Fig. 11E), but even when present, neither the endodermal nor skeletal defects were as pronounced as in non-mosaic *fras1* mutants (see discussion). Our transplantation experiments support the hypotheses that *itga8* and *fras1* function in separate tissues during facial development, and that endodermal *fras1* expression is sufficient for normal facial morphology.

fras1 genetically interacts with *Dlx* genes in intermediate domain formation

The phenotypes seen in *fras1* mutants are all found within the characteristic intermediate domain, defined previously using *Dlx* expression (see chapter II), suggesting a potential connection between *fras1* and *Dlx* genes. However, the nature of cartilage fusion in *fras1* mutants differs somewhat from *Dlx*-MO injected fish. In *dlx3b;4b;5a*-MO (see chapter II) injected WT fish, first arch cartilage fusion almost always includes loss of the retroarticular cartilage, while second arch cartilage fusion goes through the interhyal cartilage (Fig. 12; see also Chapter II). These joint elements (retroarticular and interhyal cartilages) are typically (Fig. 12B) maintained in *fras1* mutants. Injection of *dlx3b*-MO, *dlx4b*-MO, and *dlx5a*-MO individually into WT fish typically causes no effect on skeletal shape (Fig. 12; also Chapter II). However, injection of *dlx3b*-MO into *fras1* mutants increases the prevalence of joint element loss, and increases the overall fusion rate (Fig. 12B). The effect of *dlx4b*-MO on *fras1*^{b1048} mutants is not statistically significant, however fras1 is injected with both *dlx3b*-MO and *dlx4b*-MO more cartilage defects are seen than fras1 mutants injected with only *dlx3b*-MO. When *dlx5a*-MO was injected into *fras1* mutants, we also observe dramatic increases of joint element loss and overall cartilage fusions, compared to uninjected *fras1* mutants (Fig. 12A,B). Thus, using two constructs: *fras1*^{b1048} mutants injected with *dlx3b*-MO;*dlx4b*-MO and *fras1*^{b1048} mutants injected with *dlx5a*-MO, we confirm a strong genetic interaction between *fras1* and *Dlx* genes. In both cases, injection of individual *Dlx*-MO converts the *fras1* mutant fusion type into a morphology much more similar to *dlx3b;3b;5a*-MO phenotypes. This genetic interaction suggests a potential molecular connection between *fras1* and *Dlx* in intermediate domain patterning.

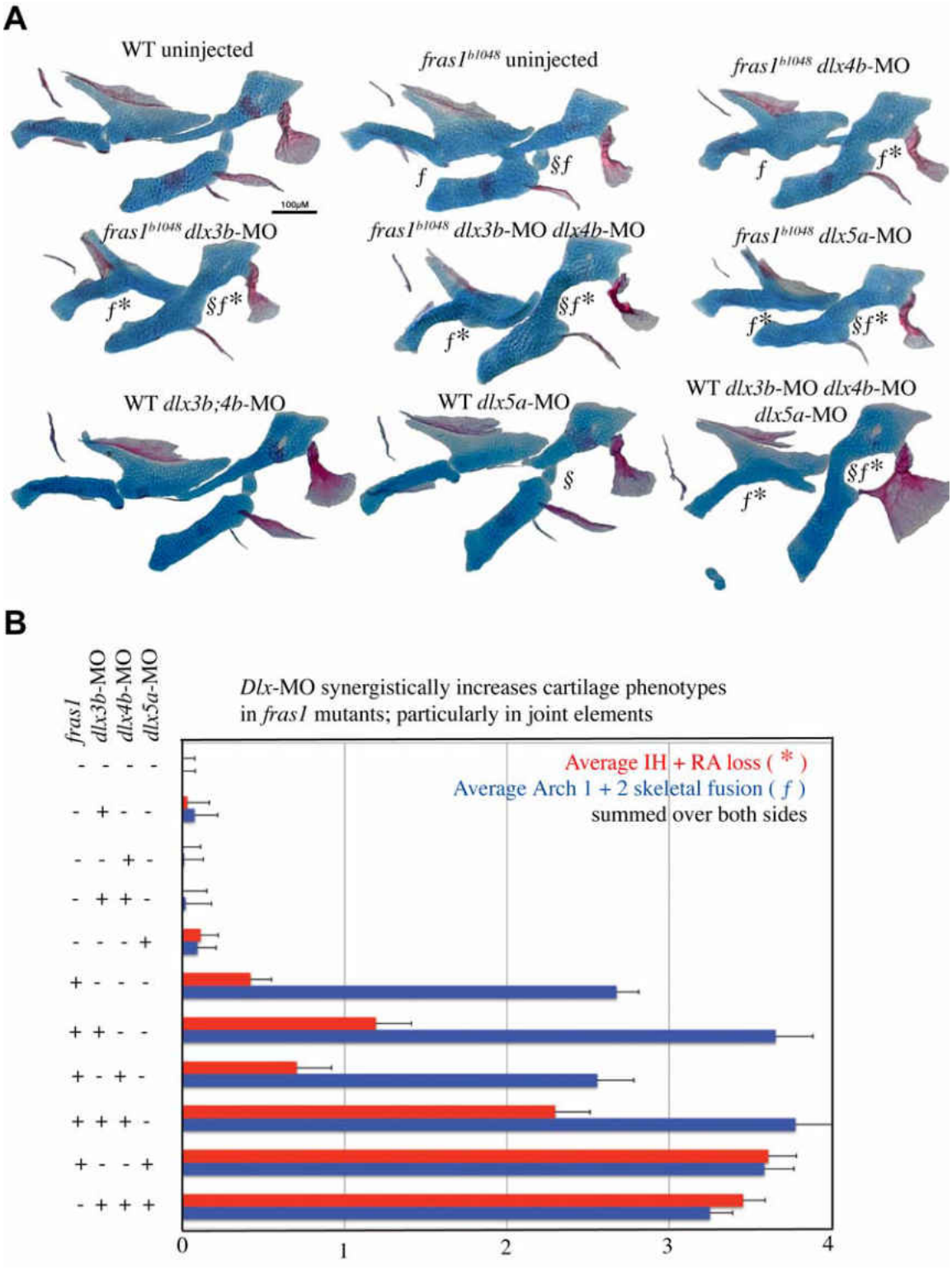
A
WT uninjected
fras1b1048 uninjected
fras1b1048 dlx4b-MO
100µM
fras1b1048 dlx3b-MO
fras1b1048 dlx3b-MO dlx4b-MO
fras1b1048 dlx5a-MO
WT dlx3b;4b-MO
WT dlx5a-MO
WT dlx3b-MO dlx4b-MO dlx5a-MO
B
Dlx-MO synergistically increases cartilage phenotypes in fras1 mutants; particularly in joint elements
fras1
dlx3b-MO
dlx4b-MO
dlx5a-MO
Average IH + RA loss (*)
Average Arch 1 + 2 skeletal fusion (f)
summed over both sides
0
1
2
3
4

Figure 12: Genetic interaction between *fras1* and *Dlx* genes. (A) Alcian blue/alizarin red stained skeletons, shown anterior to left, dorsal up. Connective tissues and background cropped out in Adobe Photoshop. The same WT+*dlx3b;4b*-MO and WT+dlx5a-MO fish also shown in Chapter II. § denotes short symplectic, *f* denotes fusion, * denotes joint element loss. Sometimes ectopic protrusions (*p*) and nodules (*n*) are also seen in WT fish injected with *dlx3b;4b;5a*-MO. (B) Averaged scoring of joint fusion (Me-Pq fusion and Sy-Ch fusion summed over both sides) and joint element loss (Ra reduction and Ih loss, summed over both sides) in WT, or *fras1* mutant fish injected with indicated combinations of *dlx3b*, *dlx4b*, or *dlx5a* morpholino. Error bars are 95% confidence intervals (1.96 times the S.E.M.). Quantification of joint element loss and joint fusion extracted in *dlx3b;4b;5a*-MO scoring extracted from a dataset presented in Chapter II.

Discussion of *fras1* and *itga8*

The similarity of discrete facial defects observed in fish with mutations in the epithelially expressed gene *fras1*, the mesenchymally expressed gene *itga8*, and in *fras1;itga8* double mutants indicate that *fras1* and *itga8* participate in epithelial-mesenchymal interactions during zebrafish facial development. Fittingly, endoderm expressing WT *fras1* can rescue both endodermal and skeletal defects of otherwise *fras1* mutant fish, indicating that endodermal *fras1* plays a vital role in facial morphogenesis. Whereas WT fish mosaically carrying *fras1* mutant endoderm don't show defects as strong as non-mosaic *fras1* mutants, it is notable that mosaic fish lacking *fras1* only in the endoderm show any defects at all, further indicating a critical role for endodermal *fras1*. A failure of *fras1* mutant endoderm in a WT host to produce endoderm defects could be due to an important role of ectodermal *fras1* during endodermal morphogenesis. Alternatively it could be due to incomplete endoderm transplantation so that some WT endoderm remains present. Because endoderm is disrupted in *fras1* mutants, but ectoderm shape is normal, we focus on the function of endoderm in or modeling of *fras1* function (Fig. 13). In contrast, endoderm WT for *itga8* is unable to rescue any *itga8* mutant facial phenotype, consistent with our hypothesis that *itga8* functions in arch mesenchyme (Fig. 13A).

Although late-p1 appears to differ in development from the early forming portion of pouch 1 previously annotated (Kimmel et al., 2001) as the entirety of pouch 1, three lines of evidence indicate that late-p1 is a portion of the first pharyngeal pouch. Late-p1

is the most anterior pouchlike structure in the 72 hpf pharynx, indicating that it is the first pouch. Late-p1 separates large portions of the first arch from the second arch; as one

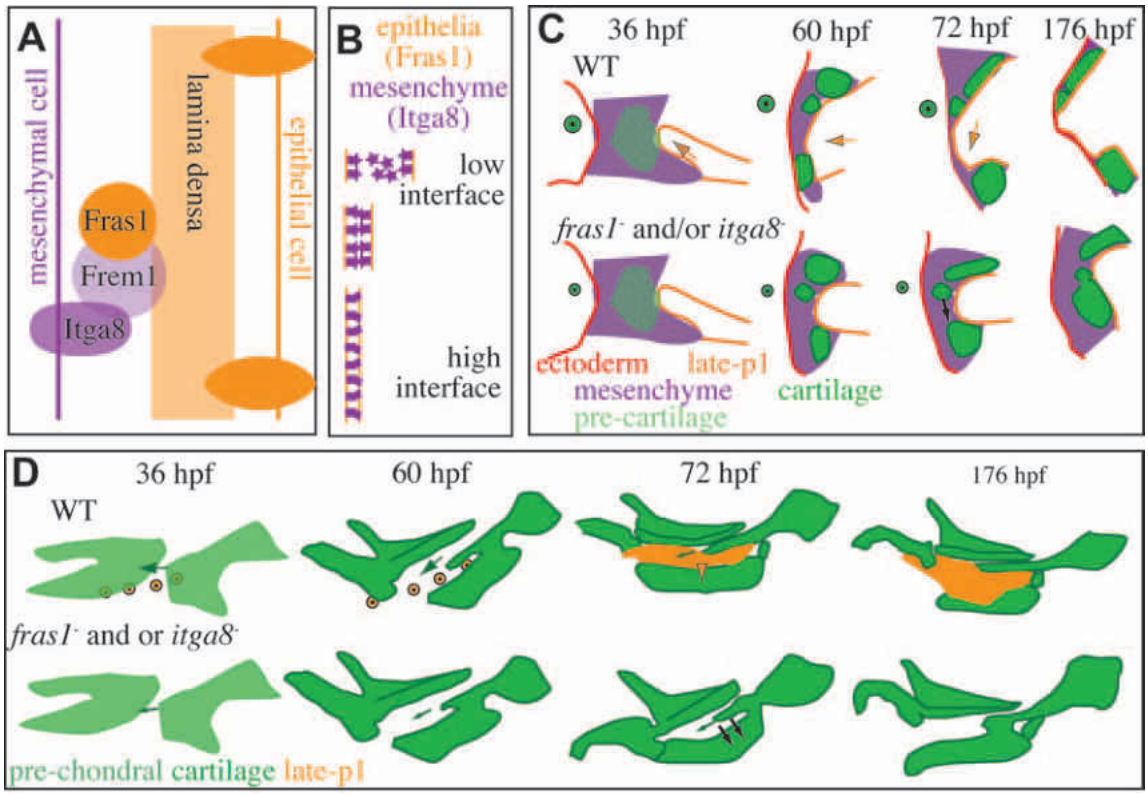

Figure 13: Epithelial-mesenchymal adhesion model for Fras1 and Itga8 function. (A) Proposed model of physical interaction between Fras1 and Itga8, occurring via Frem1a/Frem1b, to connect epithelia to mesenchyme. See (Pavlakis et al., 2011) for a recent review of the physical connection between Fras1 and epithelial cells. (B) Conceptual schematic showing how increases in the Fras1-Itga8 interface could drive endoderm migration. The movement of late-p1 is primarily across a plane (transverse, C) orthoganol to the primary plane (sagittal: D) of cartilage morphogenesis. Nonetheless, late-p1 and cartilage formation are intertwined in three dimensions. The lateral movement of endoderm is through space occupied by symplectic forming cells, and into a region that separates symplectic from ceratohyal. Vector arrows indicate the movements of late-p1 (orange), Sy growth (green), or Sy fusion (black) between time points; vector size is proportional to amount of movement. The circumpunct (circle-with-a-dot) symbol indicates movement out of the plane of the page towards the viewer.

would expect from the first pouch. In salamander, a structure annotated as “pouch 1” appears highly similar to zebrafish late-p1 (Lehman, 1987). Furthermore, we note that, similar to early pouches, late-p1 forms via lateral protrusion of medial endoderm. For these reasons, we infer that late-p1 is indeed a late forming portion of pouch 1.

Connections between *fras1*, *itga8*, and epithelial-mesenchymal interactions may occur via adhesion or via or non-adhesive signaling. Mammalian Fras1 has been strongly implicated in epithelial adhesion to connective tissues [reviewed in (Pavlakis et al., 2011; Short et al., 2007)], and Itga8 has been shown to adhere mammalian mesenchymal tissues to epithelia (Benjamin et al., 2009). There may be a close physical connection between epithelial Fras1 and mesenchymal Itga8: cells expressing mammalian Itga8 adhere to the RGD domain of Frem1 (Kiyozumi et al., 2005), a mesenchymally expressed. protein (Gautier et al., 2008; Smyth et al., 2004) (Fig. 13A). These observations lead us to propose that during zebrafish facial development Fras1 and Itga8 help bind arch epithelia to arch mesenchyme (Fig. 13A). The mesenchymally expressed proteins Frem1a and Frem1b may form physical linkers between Fras1 and Itga8 proteins (Fig. 13A). Whereas zebrafish *frem1a* mutants lack any facial phenotype (not shown) this may be due to redundancy with *frem1b*, a gene for which no mutation is currently available. Alternatively, Fras1 and Itga8 may each increase epithelial-mesenchymal adhesion without interacting in the same complex.

Adhesive interaction between Fras1 and Itga8 can explain the observed genetic interaction, late-p1 defects and skeletal phenotypes. Adhesion of Fras1 expressing endoderm to Itga8 expressing mesenchyme could help drive the morphogenesis of late-p1, which consistently fails in both *fras1* and *itga8* mutants (Fig. 13B,C). The movements of endoderm during late-p1 formation can be modeled by a simple tendency of *fras1* and *itga8* expressing cells to increase contact with one another (Fig. 13B). For instance, during late-p1 formation, arrows drawn orthogonal to epithelia pointing toward the highest *itga8* expression, also point toward the direction of endoderm movement (Fig. 7, 13C). Adhesion between *fras1* and *itga8* expressing cells may permit other factors to drive late-p1 morphogenesis.

Both *fras1* and *itga8* mutants exhibit skeletal defects; however, neither *fras1* nor *itga8* mRNA is expressed in cartilage when those defects become apparent. It is possible that Itga8 protein perdures in cartilage cells, allowing a direct endoderm-cartilage connection. However, the effect of *fras1* and *itga8* on skeletal shape may be an indirect effect of the role these genes play in late-p1 morphogenesis. WT late-p1 physically separates symplectic cartilage from the ceratohyal cartilage (Fig. 13C,D). Loss of late-p1

in *fras1* and *itga8* mutants removes this barrier, enabling the possibility of fusion (Fig. 13C,D). WT late-p1 morphogenesis brings endoderm into a position previously occupied by symplectic forming cells, possibly exerting forces that help drive symplectic extension (Fig. 13C,D Movie 2). In *fras1* and *itga8* mutants, a failure of late-p1 morphogenesis could result in reduced forces driving symplectic extension, resulting in shorter symplectic length (Fig. 13C,D). In the WT first arch, endoderm does not separate the skeletal elements that are fused in *fras1* and *itga8* mutants. Nonetheless, it is possible that lateral movement of endoderm helps pull palatoquadrate and Meckel's cartilages apart from one another, thereby preventing skeletal fusion. Thus, the presence or absence of late-p1 as a mechanical stabilizer to cartilage formation can explain all three cartilage phenotypes.

Although these three mechanisms for skeletal defects all rely on mechanical interactions, it is entirely possible that signaling involving *fras1* and *itga8* impacts prechondral cells. Skeletal phenotypes seen in *fras1* and *itga8* mutants all cluster within the discrete *Dlx*-defined intermediate domain (Chapter II) along the dorso-ventral axis of the arches, suggesting a potential connection between early signaling from Fras1 and Itga8 and the early *Dlx*-mediated patterning. Whether mechanical or chemical, an extensive literature exists linking endoderm to skeletal morphology [Reviewed (Knight and Schilling, 2006)]. For instance, loss of early-p1 in zebrafish *itga5* mutants results in loss of the dorsal region of hyomandibular cartilage (Crump et al., 2004b), further demonstrating a role of integrins in the formation of both pouch one and second arch skeletal. Furthermore, posterior pouch loss in *fgf3* mutants results in variable fusion of posterior skeletal elements (Albertson and Yelick, 2005); analogous to the variable anterior arch cartilage fusions seen in *fras1* and *itga8* mutants after anterior pouch loss.

Although the effects of genetic background and environment can never be completely excluded (Dongen, 2006), the consistently high degree of fluctuating asymmetry we observe in *fras1* and *itga8* mutant skeletal phenotypes indicate that developmental instability may influence the presence of skeletal traits within individual fish (Polak, 2003b). Several recent reviews [e.g. (Dongen, 2006)] have challenged the notion that left-right asymmetry is a valid measure of developmental instability; this single measure reduces the dataset to one degree of freedom effectively equal to "one".

Hence, asymmetry should be measured along multiple axes when possible (Graham et al., 2010). In individual *fras1* and *itga8* mutants we find asymmetry within three orthogonal axes. Skeletal defects are found asymmetrically on 1. left versus right sides, 2. arch one versus arch two, and 3. within the same skeletal element observed over time (late Sy-Ch fusion). Thus, we propose that *fras1* and *itga8* function stabilizes zebrafish skeletal development, but is not absolutely required for skeletal formation. Such a stabilizing process can be envisioned by imagining epithelia as a mold that helps guide skeletal cartilage formation (Fig. 13C,D). In the absence of late-p1, skeletal defects will not necessarily occur. However without the developmental stabilization provided by late-p1, inherent developmental instability is more likely to result in overt skeletal defects. This model differs from most previously examined models of developmental instability [reviewed in (Dongen, 2006; Graham et al., 2010; Polak, 2003a)], by invoking a physical developmental stabilizer (late-p1) rather than a chemical one. However, such a model is not without precedent, a recent study of fluctuating asymmetry in sagittal craniosynostosis suggested that dura mater attachment sites may physically stabilize cranial suture formation (Deleon and Richtsmeier, 2009). Our measurement of asymmetry used a rough metric, bilateral binary scoring of three gross morphological characters. Further analysis using morphometric techniques may provide insights into the developmental instability revealed by *fras1* and *itga8* mutations. Nonetheless, it seems that our simple scoring has low measurement error, compared to the extensive variation observed. When phenotypes were scored on fixed skeletal preparations (Fig. 1K) we find similar penetrance to fish scored live using *cart:GFP* expression (Table 1). We also find similar results when fish are scored on a steriomicroscope and then re-scored on a confocal (not shown).

There are several potential connections between our model of *fras1* and *itga8* function in zebrafish faces and human Fraser syndrome. The stochastic nature of skeletal variation we observe in zebrafish faces suggests that in addition to genetic factors previously proposed (Slavotinek and Tifft, 2002), at least some of the variation seen in Fraser syndrome patients could also be stochastic, resulting from a loss of developmental stability. This hypothesis is further supported by the observation that siblings can suffer from dramatically different degrees of Fraser syndrome symptoms (Prasun et al., 2007).

The facial structures we find defective in zebrafish, pouch one and portions of anterior pharyngeal skeleton, are homologous to the Eustachian tube and middle ear skeleton in humans. Both ear canal and middle ear defects have been reported in patients with Fraser syndrome (Gattuso et al., 1987), although description of the nature of middle ear defects has been limited at best. If this homology is correctly guiding us, then epithelial-mesenchymal interaction defects between FRAS1 and ITGA8, leading to disrupted pouching in particular, may underlie some of the ear defects found in Fraser patients. The highly similar facial phenotypes of zebrafish *fras1* and *itga8* mutants suggest *ITGA8* as a candidate gene for human Fraser-spectrum syndromes with unknown causes. Although we have intentionally limited our research to facial development, a genetic interaction between zebrafish *fras1* and *itga8* supports a previously proposed connection (McGregor et al., 2003; Pitera et al., 2008) of these two genes during mammalian kidney formation. Similar to pharyngeal pouches, lung formation is normally an outpocketing of rostral endoderm. Mutation of *Fras1* (Petrou et al., 2005) or *Itga8* (Benjamin et al., 2009) in mouse also induces similar discrete lung defects: specific fusion of medial and caudal lobes, after failure of epithelial elaboration. Hence, *Fras1* and *Itga8* appear to be epithelial-mesenchymal partners in multiple organ contexts of disparate vertebrates. If this generality holds true, then epithelial-mesenchymal interaction between *FRAS1* and *ITGA8* leading to epithelial pouching may be a repeated motif in many of the pleiotropic symptoms of human Fraser syndrome.

CHAPTER IV

GENERAL DISCUSSION

Sometimes the first step in creating a biological shape is defining which cells are needed to make that structure. Many genes carrying a characteristic "homeodomain" protein motif have become famous for their ability to define structural identity; loss of homeodomain proteins can cause loss of the identity they define, while gain of gene expression can induce that structure ectopically. In the second chapter of this thesis, I examined a family of homeodomain genes, the *Dlx* genes, that define an intermediate-domain along the dorsal-ventral axis of jaw-forming-structures (pharyngeal arches). Homeodomain-containing genes are far from the only important players in generating arch identity. For instance, *hand2* lacks a homeodomain, but instead binds DNA through a "basic helix-loop-helix" domain. Previous work has shown that *hand2* is vital to generating ventral domain identity (Miller et al., 2003). In this work, I show that *hand2* does so, in part, by inhibiting intermediate-domain identity. In combination, *hand2* and *Dlx* appear to inhibit dorsal-domain identity.

After domain-identities have been defined, some pharyngeal arch mesenchymal cells differentiate into skeleton and undergo complex movements to create a functional jaw skeleton. In the third chapter, I investigated two genes (*fras1* and *itga8*), which seem to be involved in processes that occur while craniofacial cartilages initially are shaped. Surprisingly, neither *fras1* nor *itga8* is expressed in cells of jaw skeleton during this time. Instead, *fras1* mRNA is expressed in epithelia (cells connected in a sheet), and *itga8* mRNA is expressed in arch mesenchyme (loosely associated mesenchymal cells), both of which are tissues that surround skeletal cells. I developed a model wherein adhesion of Fras1 protein to Itga8 protein draws two sheets of epithelia closer together, generating a tight mold that stabilizes skeletal development in the intermediate domain. In this model, the effects of *fras1* and *itga8* on skeleton is indirect, acting via endodermal movements.

There is a potential connection between this early patterning and later stabilization of the zebrafish pharyngeal arch intermediate domain. Loss of both *Dlx*

genes and *fras1* results in more-than-additive skeletal defects, indicating that these genes somehow genetically interact. Elucidating the molecular connection between *Dlx* genes and *fras1* will require further research, and may also provide new insights into both the patterning and stabilization of craniofacial shapes.

APPENDIX

LIST OF SUPPLEMENTAL MOVIES

Movie 1: Late-p1 is lost in *itga8*^{b1161} at 72 hpf, without affecting posterior pouch structures. Movie is select sections through the first three pharyngeal arches of (A) WT and (B) *itga8*^{b1161} mutant heads, aligned using "StackReg" in imageJ (Thevenaz et al., 1998). *cart:EGFP* expression reveals cartilges and anti-P63 labeling reveals epithelia. Section levels along the A-P axis are indicated by the black bar in (C). Abbreviations are as given in Figs 1, S1. Scale bar: 100 μm.

Movie 2: Time lapse imaging shows concurrent late-p1 and symplectic morphogenesis. (A,B) *her5:GFP* expression reveals late-p1 morphogenesis, while *sox10:mRFP* expression shows skeletal morphogenesis, including Sy extension and Ih formation. Images taken every 30 minutes from 51 to 85 hpf. (A) confocal transverse section showing lateral movement of medial endoderm between Sy and Ch. Lateral to left, dorsal up. (B) Confocal sagittal section from the same movie showing Sy extension, anterior to left, dorsal up. Because Sy extends throughout movie, the section taken for panel A moves through time, as indicated by the blue line in (B') inset. Scale bar: 100 μm.

Movie 3: Time lapse imaging of WT skeletal development. Images taken every 30 minutes from 34.5 to 79 hpf. Images are rendered projections of confocal stacks. Anterior to left, dorsal up. Image rendering demonstrates that symplectic cartilage moves over ceratohyal, but does not fuse.

Movie 4: Time lapse imaging of *fras1*^{b1048} mutant skeletal development, showing an unusually early-forming cartilage fusion of symplectic to ceratohyal. Images taken every 30 minutes from 55 to 71 hpf. Images are rendered projections of confocal stacks. Anterior to left, dorsal up.

REFERENCES CITED

Akimenko, M. A., Ekker, M., Wegner, J., Lin, W. and Westerfield, M. (1994). Combinatorial expression of three zebrafish genes related to distal-less: part of a homeobox gene code for the head. *J Neurosci* **14**, 3475-86.

Alazami, A. M., Shaheen, R., Alzahrani, F., Snape, K., Saggar, A., Brinkmann, B., Bavi, P., Al-Gazali, L. I. and Alkuraya, F. S. (2009). FREM1 mutations cause bifid nose, renal agenesis, and anorectal malformations syndrome. *Am J Hum Genet* **85**, 414-8.

Albertson, R. C. and Yelick, P. C. (2005). Roles for fgf8 signaling in left-right patterning of the visceral organs and craniofacial skeleton. *Dev Biol* **283**, 310-21.

Angelo, S., Lohr, J., Lee, K. H., Ticho, B. S., Breitbart, R. E., Hill, S., Yost, H. J. and Srivastava, D. (2000). Conservation of sequence and expression of Xenopus and zebrafish dHAND during cardiac, branchial arch and lateral mesoderm development. *Mech Dev* **95**, 231-7.

Baird, N. A., Etter, P. D., Atwood, T. S., Currey, M. C., Shiver, A. L., Lewis, Z. A., Selker, E. U., Cresko, W. A. and Johnson, E. A. (2008). Rapid SNP discovery and genetic mapping using sequenced RAD markers. *PLoS One* **3**, e3376.

Barron, F., Woods, C., Kuhn, K., Bishop, J., Howard, M. J. and Clouthier, D. E. (2011). Downregulation of Dlx5 and Dlx6 expression by Hand2 is essential for initiation of tongue morphogenesis. *Development* **138**, 2249-59.

Benjamin, J. T., Gaston, D. C., Halloran, B. A., Schnapp, L. M., Zent, R. and Prince, L. S. (2009). The role of integrin alpha8beta1 in fetal lung morphogenesis and injury. *Dev Biol* **335**, 407-17.

Benoit, Y. D., Lussier, C., Ducharme, P. A., Sivret, S., Schnapp, L. M., Basora, N. and Beaulieu, J. F. (2009). Integrin alpha8beta1 regulates adhesion, migration and proliferation of human intestinal crypt cells via a predominant RhoA/ROCK-dependent mechanism. *Biol Cell* **101**, 695-708.

Beverdam, A., Merlo, G. R., Paleari, L., Mantero, S., Genova, F., Barbieri, O., Janvier, P. and Levi, G. (2002). Jaw transformation with gain of symmetry after Dlx5/Dlx6 inactivation: mirror of the past? *Genesis* **34**, 221-7.

Bossy, B., Bossy-Wetzel, E. and Reichardt, L. F. (1991). Characterization of the integrin alpha 8 subunit: a new integrin beta 1-associated subunit, which is prominently expressed on axons and on cells in contact with basal laminae in chick embryos. *EMBO J* **10**, 2375-85.

Carney, T. J., Feitosa, N. M., Sonntag, C., Slanchev, K., Kluger, J., Kiyozumi, D., Gebauer, J. M., Coffin Talbot, J., Kimmel, C. B., Sekiguchi, K. et al. (2010). Genetic analysis of fin development in zebrafish identifies furin and hemicentin1 as potential novel fraser syndrome disease genes. *PLoS Genet* **6**, e1000907.

Cerny, R., Cattell, M., Sauka-Spengler, T., Bronner-Fraser, M., Yu, F. and Medeiros, D. M. (2010). Evidence for the prepattern/cooption model of vertebrate jaw evolution. *Proc Natl Acad Sci U S A* **107**, 17262-7.

Chapman, S. C. (2011). Can you hear me now? Understanding vertebrate middle ear development. *Front Biosci* **16**, 1675-92.

Chiotaki, R., Petrou, P., Giakoumaki, E., Pavlakis, E., Sitaru, C. and Chalepakis, G. (2007). Spatiotemporal distribution of Fras1/Frem proteins during mouse embryonic development. *Gene Expr Patterns* **7**, 381-8.

Crump, J. G., Maves, L., Lawson, N. D., Weinstein, B. M. and Kimmel, C. B. (2004a). An essential role for Fgfs in endodermal pouch formation influences later craniofacial skeletal patterning. *Development* **131**, 5703-16.

Crump, J. G., Swartz, M. E., Eberhart, J. K. and Kimmel, C. B. (2006). Moz-dependent Hox expression controls segment-specific fate maps of skeletal precursors in the face. *Development* **133**, 2661-9.

Crump, J. G., Swartz, M. E. and Kimmel, C. B. (2004b). An integrin-dependent role of pouch endoderm in hyoid cartilage development. *PLoS Biol* **2**, E244.

Dalezios, Y., Papasozomenos, B., Petrou, P. and Chalepakis, G. (2007). Ultrastructural localization of Fras1 in the sublamina densa of embryonic epithelial basement membranes. *Arch Dermatol Res* **299**, 337-43.

Deleon, V. B. and Richtsmeier, J. T. (2009). Fluctuating asymmetry and developmental instability in sagittal craniosynostosis. *Cleft Palate Craniofac J* **46**, 187-96.

Depew, M. J., Lufkin, T. and Rubenstein, J. L. (2002). Specification of jaw subdivisions by Dlx genes. *Science* **298**, 381-5.

Depew, M. J. and Simpson, C. A. (2006). 21st century neontology and the comparative development of the vertebrate skull. *Dev Dyn* **235**, 1256-91.

Depew, M. J., Simpson, C. A., Morasso, M. and Rubenstein, J. L. (2005). Reassessing the Dlx code: the genetic regulation of branchial arch skeletal pattern and development. *J Anat* **207**, 501-61.

Dongen, S. V. (2006). Fluctuating asymmetry and developmental instability in evolutionary biology: past, present and future. *J Evol Biol* **19**, 1727-43.

Eberhart, J. K., Swartz, M. E., Crump, J. G. and Kimmel, C. B. (2006). Early Hedgehog signaling from neural to oral epithelium organizes anterior craniofacial development. *Development* **133**, 1069-77.

Ekker, M., Wegner, J., Akimenko, M. A. and Westerfield, M. (1992). Coordinate embryonic expression of three zebrafish engrailed genes. *Development* **116**, 1001-10.

Ellies, D. L., Stock, D. W., Hatch, G., Giroux, G., Weiss, K. M. and Ekker, M. (1997). Relationship between the genomic organization and the overlapping embryonic expression patterns of the zebrafish dlx genes. *Genomics* **45**, 580-90.

Fraser, G. R. (1962). Our genetical 'load'. A review of some aspects of genetical variation. *Ann. Hum. Genet.* **25**, 387-415.

Gattuso, J., Patton, M. A. and Baraitser, M. (1987). The clinical spectrum of the Fraser syndrome: report of three new cases and review. *J Med Genet* **24**, 549-55.

Gautier, P., Naranjo-Golborne, C., Taylor, M. S., Jackson, I. J. and Smyth, I. (2008). Expression of the fras1/frem gene family during zebrafish development and fin morphogenesis. *Dev Dyn* **237**, 3295-304.

Ghanem, N., Jarinova, O., Amores, A., Long, Q., Hatch, G., Park, B. K., Rubenstein, J. L. and Ekker, M. (2003). Regulatory roles of conserved intergenic domains in vertebrate Dlx bigene clusters. *Genome Res* **13**, 533-43.

Graham, A., Okabe, M. and Quinlan, R. (2005). The role of the endoderm in the development and evolution of the pharyngeal arches. *J Anat* **207**, 479-87.

Graham, J. H., Raz, S., Hel-Or, H. and Nevo, E. (2010). Fluctuating Asymmetry: Methods, Theory, and Applications. *Symmetry* **2**, 466-540.

Hatta, K., Schilling, T. F., BreMiller, R. A. and Kimmel, C. B. (1990). Specification of jaw muscle identity in zebrafish: correlation with engrailed-homeoprotein expression. *Science* **250**, 802-5.

Jadeja, S., Smyth, I., Pitera, J. E., Taylor, M. S., van Haelst, M., Bentley, E., McGregor, L., Hopkins, J., Chalepakis, G., Philip, N. et al. (2005). Identification of a new gene mutated in Fraser syndrome and mouse myelencephalic blebs. *Nat Genet* **37**, 520-5.

Jeong, J., Li, X., McEvilly, R. J., Rosenfeld, M. G., Lufkin, T. and Rubenstein, J. L. (2008). Dlx genes pattern mammalian jaw primordium by regulating both lower jaw-specific and upper jaw-specific genetic programs. *Development* **135**, 2905-16.

Jowett, T. and Yan, Y. L. (1996). Double fluorescent in situ hybridization to zebrafish embryos. *Trends Genet* **12**, 387-9.
Kaji, T. and Artinger, K. B. (2004). dlx3b and dlx4b function in the development of Rohon-Beard sensory neurons and trigeminal placode in the zebrafish neurula. *Dev Biol* **276**, 523-40.

Kawakami, K., Takeda, H., Kawakami, N., Kobayashi, M., Matsuda, N. and Mishina, M. (2004). A transposon-mediated gene trap approach identifies developmentally regulated genes in zebrafish. *Dev Cell* **7**, 133-44.

Kimmel, C. B., Ballard, W. W., Kimmel, S. R., Ullmann, B. and Schilling, T. F. (1995). Stages of embryonic development of the zebrafish. *Dev Dyn* **203**, 253-310.

Kimmel, C. B., Miller, C. T. and Keynes, R. J. (2001). Neural crest patterning and the evolution of the jaw. *J Anat* **199**, 105-20.

Kimmel, C. B., Miller, C. T., Kruze, G., Ullmann, B., BreMiller, R. A., Larison, K. D. and Snyder, H. C. (1998). The shaping of pharyngeal cartilages during early development of the zebrafish. *Dev Biol* **203**, 245-63.

Kimmel, C. B., Ullmann, B., Walker, M., Miller, C. T. and Crump, J. G. (2003). Endothelin 1-mediated regulation of pharyngeal bone development in zebrafish. *Development* **130**, 1339-51.

Kirby, B. B., Takada, N., Latimer, A. J., Shin, J., Carney, T. J., Kelsh, R. N. and Appel, B. (2006). In vivo time-lapse imaging shows dynamic oligodendrocyte progenitor behavior during zebrafish development. *Nat Neurosci* **9**, 1506-11.

Kiyozumi, D., Osada, A., Sugimoto, N., Weber, C. N., Ono, Y., Imai, T., Okada, A. and Sekiguchi, K. (2005). Identification of a novel cell-adhesive protein spatiotemporally expressed in the basement membrane of mouse developing hair follicle. *Exp Cell Res* **306**, 9-23.

Kiyozumi, D., Sugimoto, N. and Sekiguchi, K. (2006). Breakdown of the reciprocal stabilization of QBRICK/Frem1, Fras1, and Frem2 at the basement membrane provokes Fraser syndrome-like defects. *Proc Natl Acad Sci U S A* **103**, 11981-6.

Knight, R. D. and Schilling, T. F. (2006). Cranial neural crest and development of the head skeleton. *Adv Exp Med Biol* **589**, 120-33.

Kunath, M., Ludecke, H. J. and Vortkamp, A. (2002). Expression of Trps1 during mouse embryonic development. *Mech Dev* **119 Suppl 1**, S117-20.

Leamy, L. J. and Klingenberg, C. P. (2005). The genetics and evolution of fluctuating asymmetry. *Annu Rev Ecol Evol Syst* **36**, 1-21.

Lehman, H. E. (1987). Chordate Development: A practical textbook with atlases and techniques for experimental and descriptive embryology. Winston-Salem, North Carolina: Hunter Textbooks Inc.

Linton, J. M., Martin, G. R. and Reichardt, L. F. (2007). The ECM protein nephronectin promotes kidney development via integrin alpha8beta1-mediated stimulation of Gdnf expression. *Development* **134**, 2501-9.

Liu, D., Chu, H., Maves, L., Yan, Y. L., Morcos, P. A., Postlethwait, J. H. and Westerfield, M. (2003). Fgf3 and Fgf8 dependent and independent transcription factors are required for otic placode specification. *Development* **130**, 2213-24.

McGregor, L., Makela, V., Darling, S. M., Vrontou, S., Chalepakis, G., Roberts, C., Smart, N., Rutland, P., Prescott, N., Hopkins, J. et al. (2003). Fraser syndrome and mouse blebbed phenotype caused by mutations in FRAS1/Fras1 encoding a putative extracellular matrix protein. *Nat Genet* **34**, 203-8.

Miller, C. T. and Kimmel, C. B. (2001). Morpholino phenocopies of endothelin 1 (sucker) and other anterior arch class mutations. *Genesis* **30**, 186-7.

Miller, C. T., Schilling, T. F., Lee, K., Parker, J. and Kimmel, C. B. (2000). sucker encodes a zebrafish Endothelin-1 required for ventral pharyngeal arch development. *Development* **127**, 3815-28.

Miller, C. T., Swartz, M. E., Khuu, P. A., Walker, M. B., Eberhart, J. K. and Kimmel, C. B. (2007). mef2ca is required in cranial neural crest to effect Endothelin1 signaling in zebrafish. *Dev Biol* **308**, 144-57.

Miller, C. T., Yelon, D., Stainier, D. Y. and Kimmel, C. B. (2003). Two endothelin 1 effectors, hand2 and bapx1, pattern ventral pharyngeal cartilage and the jaw joint. *Development* **130**, 1353-65.

Muller, U., Wang, D., Denda, S., Meneses, J. J., Pedersen, R. A. and Reichardt, L. F. (1997). Integrin alpha8beta1 is critically important for epithelial-mesenchymal interactions during kidney morphogenesis. *Cell* **88**, 603-13.

Nair, S., Li, W., Cornell, R. and Schilling, T. F. (2007). Requirements for Endothelin type-A receptors and Endothelin-1 signaling in the facial ectoderm for the patterning of skeletogenic neural crest cells in zebrafish. *Development* **134**, 335-45.

Nusslein-Volhard, C. (2002). Zebrafish: A Practical Approach: Oxford University Press.
Ozeki, H., Kurihara, Y., Tonami, K., Watatani, S. and Kurihara, H. (2004). Endothelin-1 regulates the dorsoventral branchial arch patterning in mice. *Mech Dev* **121**, 387-95.

Panganiban, G. and Rubenstein, J. L. (2002). Developmental functions of the Distal-less/Dlx homeobox genes. *Development* **129**, 4371-86.

Parinov, S., Sevugan, M., Ye, D., Yang, W. C., Kumaran, M. and Sundaresan, V. (1999). Analysis of flanking sequences from dissociation insertion lines: a database for reverse genetics in Arabidopsis. *Plant Cell* **11**, 2263-70.

Park, B. K., Sperber, S. M., Choudhury, A., Ghanem, N., Hatch, G. T., Sharpe, P. T., Thomas, B. L. and Ekker, M. (2004). Intergenic enhancers with distinct activities regulate Dlx gene expression in the mesenchyme of the branchial arches. *Dev Biol* **268**, 532-45.

Pavlakis, E., Chiotaki, R. and Chalepakis, G. (2011). The role of Fras1/Frem proteins in the structure and function of basement membrane. *Int J Biochem Cell Biol* **43**, 487-95.

Petrou, P., Pavlakis, E., Dalezios, Y. and Chalepakis, G. (2007). Basement membrane localization of Frem3 is independent of the Fras1/Frem1/Frem2 protein complex within the sublamina densa. *Matrix Biol* **26**, 652-8.

Petrou, P., Pavlakis, E., Dalezios, Y., Galanopoulos, V. K. and Chalepakis, G. (2005). Basement membrane distortions impair lung lobation and capillary organization in the mouse model for fraser syndrome. *J Biol Chem* **280**, 10350-6.

Pitera, J. E., Scambler, P. J. and Woolf, A. S. (2008). Fras1, a basement membrane-associated protein mutated in Fraser syndrome, mediates both the initiation of the mammalian kidney and the integrity of renal glomeruli. *Hum Mol Genet* **17**, 3953-64.

Polak, M. (2003a). Developmental Instability: Causes and Consequences, (ed., pp. 459. New York, New York: Oxford University Press.

Polak, M. (2003b). Developmental Instability: Causes and Conseuences, (ed., pp. 459. New York, New York: Ohford University Press.

Prasun, P., Pradhan, M. and Goel, H. (2007). Intrafamilial variability in Fraser syndrome. *Prenat Diagn* **27**, 778-82.

Qiu, M., Bulfone, A., Ghattas, I., Meneses, J. J., Christensen, L., Sharpe, P. T., Presley, R., Pedersen, R. A. and Rubenstein, J. L. (1997). Role of the Dlx homeobox genes in proximodistal patterning of the branchial arches: mutations of Dlx-1, Dlx-2, and Dlx-1 and -2 alter morphogenesis of proximal skeletal and soft tissue structures derived from the first and second arches. *Dev Biol* **185**, 165-84.

Rodriguez-Mari, A., Yan, Y. L., Bremiller, R. A., Wilson, C., Canestro, C. and Postlethwait, J. H. (2005). Characterization and expression pattern of zebrafish Anti-Mullerian hormone (Amh) relative to sox9a, sox9b, and cyp19a1a, during gonad development. *Gene Expr Patterns* **5**, 655-67.

Ruest, L. B., Xiang, X., Lim, K. C., Levi, G. and Clouthier, D. E. (2004). Endothelin-A receptor-dependent and -independent signaling pathways in establishing mandibular identity. *Development* **131**, 4413-23.

Sato, T., Kurihara, Y., Asai, R., Kawamura, Y., Tonami, K., Uchijima, Y., Heude, E., Ekker, M., Levi, G. and Kurihara, H. (2008). An endothelin-1 switch specifies maxillomandibular identity. *Proc Natl Acad Sci U S A* **105**, 18806-11.

Schnapp, L. M., Breuss, J. M., Ramos, D. M., Sheppard, D. and Pytela, R. (1995a). Sequence and tissue distribution of the human integrin alpha 8 subunit: a beta 1-associated alpha subunit expressed in smooth muscle cells. *J Cell Sci* **108 (Pt 2)**, 537-44.

Schnapp, L. M., Hatch, N., Ramos, D. M., Klimanskaya, I. V., Sheppard, D. and Pytela, R. (1995b). The human integrin alpha 8 beta 1 functions as a receptor for tenascin, fibronectin, and vitronectin. *J Biol Chem* **270**, 23196-202.

Schulte-Merker, S., Hammerschmidt, M., Beuchle, D., Cho, K. W., De Robertis, E. M. and Nusslein-Volhard, C. (1994). Expression of zebrafish goosecoid and no tail gene products in wild-type and mutant no tail embryos. *Development* **120**, 843-52.

Shafeghati, Y., Kniepert, A., Vakili, G. and Zenker, M. (2008). Fraser syndrome due to homozygosity for a splice site mutation of FREM2. *Am J Med Genet A* **146A**, 529-31.

Short, K., Wiradjaja, F. and Smyth, I. (2007). Let's stick together: the role of the Fras1 and Frem proteins in epidermal adhesion. *IUBMB Life* **59**, 427-35.

Slavotinek, A., Li, C., Sherr, E. H. and Chudley, A. E. (2006). Mutation analysis of the FRAS1 gene demonstrates new mutations in a propositus with Fraser syndrome. *Am J Med Genet A* **140**, 1909-14.

Slavotinek, A. M., Baranzini, S. E., Schanze, D., Labelle-Dumais, C., Short, K. M., Chao, R., Yahyavi, M., Bijlsma, E. K., Chu, C., Musone, S. et al. (2011). Manitoba-oculo-tricho-anal (MOTA) syndrome is caused by mutations in FREM1. *J Med Genet*.

Slavotinek, A. M. and Tifft, C. J. (2002). Fraser syndrome and cryptophthalmos: review of the diagnostic criteria and evidence for phenotypic modules in complex malformation syndromes. *J Med Genet* **39**, 623-33.

Smyth, I., Du, X., Taylor, M. S., Justice, M. J., Beutler, B. and Jackson, I. J. (2004). The extracellular matrix gene Frem1 is essential for the normal adhesion of the embryonic epidermis. *Proc Natl Acad Sci U S A* **101**, 13560-5.

Sperber, S. M., Saxena, V., Hatch, G. and Ekker, M. (2008). Zebrafish dlx2a contributes to hindbrain neural crest survival, is necessary for differentiation of sensory ganglia and functions with dlx1a in maturation of the arch cartilage elements. *Dev Biol* **314**, 59-70.

Stock, D. W., Ellies, D. L., Zhao, Z., Ekker, M., Ruddle, F. H. and Weiss, K. M. (1996). The evolution of the vertebrate Dlx gene family. *Proc Natl Acad Sci U S A* **93**, 10858-63.

Stock, D. W., Jackman, W. R. and Trapani, J. (2006). Developmental genetic mechanisms of evolutionary tooth loss in cypriniform fishes. *Development* **133**, 3127-37.

Streisinger, G., Walker, C., Dower, N., Knauber, D. and Singer, F. (1981). Production of clones of homozygous diploid zebra fish (Brachydanio rerio). *Nature* **291**, 293-6.

Sumiyama, K., Irvine, S. Q. and Ruddle, F. H. (2003). The role of gene duplication in the evolution and function of the vertebrate Dlx/distal-less bigene clusters. *J Struct Funct Genomics* **3**, 151-9.

Tallafuss, A. and Bally-Cuif, L. (2003). Tracing of her5 progeny in zebrafish transgenics reveals the dynamics of midbrain-hindbrain neurogenesis and maintenance. *Development* **130**, 4307-23.

Thevenaz, P., Ruttimann, U. E. and Unser, M. (1998). A pyramid approach to subpixel registration based on intensity. *IEEE Trans Image Process* **7**, 27-41.

Thomas, I. T., Frias, J. L., Felix, V., Sanchez de Leon, L., Hernandez, R. A. and Jones, M. C. (1986). Isolated and syndromic cryptophthalmos. *Am J Med Genet* **25**, 85-98.

van Haelst, M. M., Maiburg, M., Baujat, G., Jadeja, S., Monti, E., Bland, E., Pearce, K., Hennekam, R. C. and Scambler, P. J. (2008). Molecular study of 33 families with Fraser syndrome new data and mutation review. *Am J Med Genet A* **146A**, 2252-7.

van Haelst, M. M., Scambler, P. J. and Hennekam, R. C. (2007). Fraser syndrome: a clinical study of 59 cases and evaluation of diagnostic criteria. *Am J Med Genet A* **143A**, 3194-203.

Verreijdt, L., Debiais-Thibaud, M., Borday-Birraux, V., Van der Heyden, C., Sire, J. Y. and Huysseune, A. (2006). Expression of the dlx gene family during formation of the cranial bones in the zebrafish (Danio rerio): differential involvement in the visceral skeleton and braincase. *Dev Dyn* **235**, 1371-89.

Vrontou, S., Petrou, P., Meyer, B. I., Galanopoulos, V. K., Imai, K., Yanagi, M., Chowdhury, K., Scambler, P. J. and Chalepakis, G. (2003). Fras1 deficiency results in cryptophthalmos, renal agenesis and blebbed phenotype in mice. *Nat Genet* **34**, 209-14.

Walker, M. B. and Kimmel, C. B. (2007). A two-color acid-free cartilage and bone stain for zebrafish larvae. *Biotech Histochem* **82**, 23-8.

Walker, M. B., Miller, C. T., Coffin Talbot, J., Stock, D. W. and Kimmel, C. B. (2006). Zebrafish furin mutants reveal intricacies in regulating Endothelin1 signaling in craniofacial patterning. *Dev Biol* **295**, 194-205.

Walker, M. B., Miller, C. T., Swartz, M. E., Eberhart, J. K. and Kimmel, C. B. (2007). phospholipase C, beta 3 is required for Endothelin1 regulation of pharyngeal arch patterning in zebrafish. *Dev Biol* **304**, 194-207.

Welten, M. C., de Haan, S. B., van den Boogert, N., Noordermeer, J. N., Lamers, G. E., Spaink, H. P., Meijer, A. H. and Verbeek, F. J. (2006). ZebraFISH: fluorescent in situ hybridization protocol and three-dimensional imaging of gene expression patterns. *Zebrafish* **3**, 465-76.

Westerfield, M. (1995). The Zebrafish Book: A guide for the laboratory use of zebrafish (Danio Rerio). Eugene, Oregon: University of Oregon Press.

Westerfield, M. (2007). The Zebrafish Book: A guide for the laboratory use of zebrafish (Danio Rerio). Eugene, Oregon: University of Oregon Press.

Yan, Y. L., Hatta, K., Riggleman, B. and Postlethwait, J. H. (1995). Expression of a type II collagen gene in the zebrafish embryonic axis. *Dev Dyn* **203**, 363-76.

Yan, Y. L., Miller, C. T., Nissen, R. M., Singer, A., Liu, D., Kirn, A., Draper, B., Willoughby, J., Morcos, P. A., Amsterdam, A. et al. (2002). A zebrafish sox9 gene required for cartilage morphogenesis. *Development* **129**, 5065-79.

Yan, Y. L., Willoughby, J., Liu, D., Crump, J. G., Wilson, C., Miller, C. T., Singer, A., Kimmel, C., Westerfield, M. and Postlethwait, J. H. (2005). A pair of Sox: distinct and overlapping functions of zebrafish sox9 co-orthologs in craniofacial and pectoral fin development. *Development* **132**, 1069-83.

Yanagisawa, H., Clouthier, D. E., Richardson, J. A., Charite, J. and Olson, E. N. (2003). Targeted deletion of a branchial arch-specific enhancer reveals a role of dHAND in craniofacial development. *Development* **130**, 1069-78.

Yelon, D., Ticho, B., Halpern, M. E., Ruvinsky, I., Ho, R. K., Silver, L. M. and Stainier, D. Y. (2000). The bHLH transcription factor hand2 plays parallel roles in zebrafish heart and pectoral fin development. *Development* **127**, 2573-82.

Zuniga, E., Stellabotte, F. and Crump, J. G. (2010). Jagged-Notch signaling ensures dorsal skeletal identity in the vertebrate face. *Development* **137**, 1843-52.